Tuesday, October 14, 2003
POSTER SESSION II
7:00 – 9:30 p.m.

Leverington D. W.
Preliminary Results from a Survey of Candidate Permafrost and Periglacial Features on Mars **[#8013]**

Lim D. S. S. Douglas M. S. V.
The Use of Paleolimnology for Tracking Climate Change in the Canadian High Arctic – Analogies for Mars Exploration **[#8004]**

Longhi J.
Some Applications of CO_2-H_2O Phase Equilibria to the Composition and Evolution of the Martian Polar Ice Caps **[#8100]**

Määttänen A. Korhonen H. Lehtinen K. E. J. Vehkamäki H. Kulmala M.
An Investigation of Aerosol Dynamics in the Atmosphere of Mars **[#8045]**

Mangold N.
Distribution and Climatic Control of Small Scale Polygons on Mars **[#8044]**

Mangold N. Maurice S. Feldman W. Costard F. Forget F.
Geographical Relationships Between Small Scale Polygons and Ground Ice Distribution from Neutron Spectrometer on Mars **[#8043]**

Marchant D. R. Head J. W. Kreslavsky M. A.
Tongue-shaped Lobes on Mars: Relation to Rock Glacier Deposits and Long-Term History of Emplacement **[#8106]**

Markiewicz W. J. Kossacki K. J.
CO_2 Ice in Polygonal Troughs in Malea Planum, Mars: Sub-Surface H_2O Ice, MOC Images and TES Surface Temperature **[#8042]**

Matzl M. Schneebeli M.
Combining Micro-Penetrometer and Near-Infrared Photography to Measure Physical Properties in Snow Profiles **[#8062]**

McEwen A. Herkenhoff K. Hansen C. Bridges N. Delamere W. A. Eliason E. Grant J. Gulick V. Keszthelyi L. Kirk R. Mellon M. Smith P. Squyres S. Thomas N. Weitz C.
MRO's High Resolution Imaging Science Experiment (HiRISE): Polar Science Expectations **[#8079]**

Moersch J. E. Drake D. M.
Neutron Detector for Mars Rover Missions **[#8093]**

Moudden Y. Beagley S. R. Fomichec V. McConnell J. C. Akingunola A. Garcia Munioz A.
Development of a Mars General Circulation Model **[#8034]**

Nieto C. E. Stewart R. R.
Geophysical Investigations at a Mars Analog Site: Devon Island, Nunavut **[#8115]**

Ouvarova T. Caldwell J. Atreya S. Wong A. Renno N. James P.
Hubble Space Telescope Search for Localized Outgassing on Mars **[#8065]**

Pathare A. V. Marchant D. R. Head J. W.
Preservation of Ancient Glacial Ice Below Sublimation Till in the Dry Valleys of Antarctica: Implications for Mars **[#8114]**

Pettinelli E. Burghignoli P. Galli A. Pisani A. R. Ticconi F. Del Vento D. Cereti A.
Electromagnetic Propagation Modelling for GPR Exploration of Martian Subsoil **[#8080]**

Portyankina G. Markiewicz W. J.
Model for Formation of Spider Patterns in the Cryptic Region **[#8026]**

Sakimoto S. E. H. Weren S. L.
Martian North Polar Impacts and Volcanoes: Feature Discrimination and Comparisons to Global Trends **[#8094]** **Moved to Print Only**

Schmidt K. G.
Investigation of Exchange Processes in the Martian Water Cycle **[#8008]**

Schmitt B. Mulato L. Douté S.
The Formation and Detectability of CO_2 Clathrate Hydrate on Mars **[#8073]**

Siili T. Määttänen A.
Sublimation and Condensation Flows in Chasma Borealis: A Sensitivity Study Using a 2-D Ensemble Mesoscale Circulation Model **[#8046]**

Simoes S. Trautner R. Grard R.
The Application of the Electric Sounding Technique to the Search for Water at Shallow Depths with Planetary Landers and Rovers: A Survey of the RSSD-ESA Activities **[#8010]**

Tamppari L. K. Smith M. D. Hale A. S. Bass D. S.
Interannual Comparison of Water Vapor in the North Polar Region of Mars **[#8119]**

van Gasselt S. Reiß D. Jaumann R.
Distribution and Morphology of Polygons, South Polar Region, Mars **[#8088]**

Vasavada A. R. Richardson M. I. Byrne S. Ivanov A. B. Christensen P. R. THEMIS Team
Thermophysical Properties of Mars' North Polar Layered Deposits and Related Materials from Mars Odyssey THEMIS **[#8095]**

Wentworth S. J. Gibson E. K. Jr. McKay D. S.
Low-Temperature, Aqueous Alteration of Soil in Wright Valley, Antarctica, Compared with Aqueous Alteration on Mars **[#8128]**

Wilson A. T.
Life in Perennially Ice Covered Lakes on Mars — An Antarctic Analogue **[#8039]**

Woodworth-Lynas C. Guigné J. Y.
Ice Keel Scour Marks and Ice Floe Grounding Structures in Kasei Valles and Echus Chasma **[#8012]**

Wyatt M. B. Tanaka K. L.
Origin of MGS-TES Surface Compositions in the Northern Plains and Polar Region of Mars **[#8118]**

PRELIMINARY RESULTS FROM A SURVEY OF CANDIDATE PERMAFROST AND PERIGLACIAL FEATURES ON MARS. D. W. Leverington[1], [1]Center for Earth and Planetary Studies, Smithsonian Institution, Washington, DC 20560; leveringtond@nasm.si.edu.

Introduction: Several studies have noted that high-resolution images acquired by the Mars Observer Camera (MOC) may be used to identify candidate Martian permafrost and periglacial features at scales more consistent with their terrestrial counterparts. In the present research, a comprehensive survey of Martian candidate features is being conducted.

Background: Typical terrestrial permafrost and periglacial features (where "periglacial" refers here to environments where frost action dominates) include frost mounds, earth hummocks, ice wedges, sorted circles, thermokarst features, and features produced by gelifluction. Terrestrial *frost mounds* are mound-shaped landforms that are produced in a variety of ways by the combined processes of ground freezing and groundwater movement [1]. Although large frost mounds such as pingos [2,3] are greater than 10 m in height and 100 m in horizontal dimension, frost mounds can be as small as several meters across. *Earth hummocks* are hummocks that have a core of silty and clayey mineral soil and show evidence of cryoturbation [1,4]. On the Earth, these features are believed to form only in permafrost regions; individual earth hummocks are typically 50 to 150 cm across, and often occur in dense clusters. *Ice wedges* are formed mainly in zones of continuous permafrost through the combined and repeated processes of thermal contraction cracking and the penetration of surface water into these cracks by water flow and by the formation of hoar frost [5,6]. Terrestrial ice wedges can be about 10 cm to 3 m in width at the surface, tapering to zero width at a depth of 1-20 m. Ice wedges, and their sand wedge counterparts [7], are typically expressed at the surface in plan view as a network of polygons. *Sorted circles* are tightly-spaced circular domains of fine-grained materials surrounded by gravel ridges, and are formed by freeze-thaw action [8]. On the Earth, the circular domains are typically about 2-4 m across, and the gravel ridges are about 20 cm high [9]. *Thermokarst features* are caused by changes in ground thermal regimes that result in ice thaw and ground subsidence [10-12]. *Gelifluction features* are formed by downslope creep of frozen ground; individual terrestrial lobes can be up to tens of meters wide and hundreds of meters long.

Permafrost and Periglacial Features on Mars: Near-surface ice is stable at latitudes poleward of about 40 degrees [13-15]. Features cited in the Viking era as possible indicators of near-surface ice included alas-like flat-floored depressions [16-18], grooved and lobate landslide and valley deposits that implied processes of rock-glacier flow and gelifluction [19-23], crater ejecta blankets with lobate margins and radial flow patterns [16,24-25], and mid-latitude terrain softening [26]. Examples of patterned ground, most notably networks of relatively large polygons, were cited as possible indicators of near-surface ice and the activity of periglacial processes [16,20,24,27-29]. Clusters of small circular to elongated mounds were observed in Gusev crater and hypothesized to be related to terrestrial frost mounds [30].

The availability of high-resolution MOC images over widely-distributed locales on Mars provides an excellent opportunity for identifying possible periglacial and permafrost features on scales comparable to terrestrial features. For example, tongue-shaped lobes on Mars have now been identified as likely near-surface ice-rich sediment bodies within which processes related to terrestrial rock glaciers may be operating [31,32]. A widespread mid-latitude surface unit has been identified as a possible mantle of ice-rich materials [33]. Local-scale polygonal terrains have been identified [34-36] at latitudes consistent with regions where near-surface water may have been detected [37].

A Survey of Small-Scale Hummocky and Polygonal Features on Mars: High-resolution MOC images are being examined for features that have morphological similarities with terrestrial permafrost and periglacial features. To date, over 250 images have been found that show features considered to be good candidates for Martian analogs of terrestrial hummocks, ice-wedge networks, and gelifluction and thermokarst features. Consistent with other studies [36], these features have been found to predominantly exist at latitudes poleward of about 55 degrees.

Both hummocky and polygonal terrains are prevalent in a number of high-latitude regions on Mars. High-latitude hummock features are often found in large groups of uniformly-sized (~10 m across) and spaced (~20 m) hummocks. Local-scale Martian polygonal networks have been found with a wide variety of geometries, including rectangular, random orthogonal, simple polygonal, and radial orthogonal; the dimensions of individual network units vary widely, with apparent sizes as small as ~10 m or less. While

polygonal features are often clearly evident (Fig.1), they are sometimes relatively subtle features due to factors such as stripping or burial of materials (Fig.2). Dark polygonal features are found on a small proportion of polar dunefields (Fig.3), although most or all of these features may simply be the temporary product of aeolian and defrosting processes. Permafrost-related polygons would be useful for constraining the recent mobility of polar dunes and associated materials.

Conclusions: Strong candidates for Martian analogs of terrestrial permafrost and periglacial features exist in high-latitude regions of Mars. Features such as hummock fields, local-scale polygonal networks, and potential gelifluction and thermokarst features continue to be identified and examined.

References: [1] ACGR (1988) NRC, Tech. Mem. 142. [2] Mackay, J.R. (1977*) Can. J. Earth Sci., 14*, 209-222. [3] Mackay, J.R. (1990) *Can. J. Earth Sci., 27*, 1115-1125. [4] Mackay, J.R. (1980) *Can. J. Earth Sci., 17*, 996-1006. [5] Mackay, J.R. (1974) *Can. J. Earth Sci., 11,* 1366-1383. [6] Burn, C.R. (1990) *Perm. Peri. Pro., 1,* 3-14. [7] Murton, J.B., French, H. M. (1993) *J. Quat. Sci., 8,* 185-196. [8] Kessler, M.A., Werner, B.T. (2003) *Science, 299,* 380-383. [9] Hallet, B. (1990) *Can. J. Phys., 68*, 842-852. [10] Mackay, J.R. (1970) *Can. Geotech. J*., *7,* 420-432. [11] French, H.M. (1974) *Can. J. Earth Sci., 11,* 785-794. [12] Burn, C.R., Friele, P.A. (1988) *Arctic, 42,* 31-40. [13] Jakosky, B.M., Farmer, C.B. (1982) *JGR, 87,* 2999-3019. [14] Clifford, S.M., Hillel, D. (1983) *JGR, 88,* 2456-2474. [15] Mellon, M.T. *et al*. (1997) *JGR, 102,* 19,357-19,369. [16] Rossbacher, L.A., Judson, S. (1981) *Icarus, 35,* 39-59. [17] Costard, F.M. (1990) *LPI Tech. Rep. 90-06*, 114-115. [18] Costard, F.M., Dolfus, A. (1987) *LPI Tech. Rep. 87-02,* 16-17. [19] Carr, M.H. (1984) NASA SP-469, 207-263. [20] Lucchitta, B.K. (1981) *Icarus, 45,* 264-303. [21] Squyres, S.W. (1978) *Icarus, 34,* 600-613. [22] Colaprete, A., Jakosky, B.M. (1998) *JGR, 103,* 5897-5909. [23] Mangold, N., Allemand, P. (2001) *Geophys. Res. Lett., 28,* 407-410. [24] Carr, M.H., Schaber, G.G. (1977) *JGR, 82,* 4039-4054. [25] Horner, V.M., Greeley, R. (1987) *LPI Tech. Rep. 87-02*, 25. [26] Squyres, S.W., Carr, M.H. (1986) *Science, 231*, 249-252. [27] Rossbacher, L.A. (1987) *LPI Tech. Rep. 87-02*, 38-39. [28] Mellon, M.T. (1997) *JGR, 102,* 25,617-25,628. [29] Lucchitta, B.K. (1983) *4th Int. Conf. on Permafrost*, 744-449. [30] Cabrol, N.A. *et al*. (2000) *Icarus, 145,* 91-107. [31] Marchant, D.R., Head, J.W. (2003) *6th Int. Conf. on Mars*, #3091. [32] Howard, A.D. (2003) *LPS XXXIV*, #1065. [33] Mustard, J.F. *et al*. (2001) *Nature, 412,* 411-4114. [34] Seibert, N.M., Kargel, J.S. (2001) *GRL*, 28, 899-902. [35] Yoshikawa, K. (2000) *2nd Mars Polar Sci. Conf*., #4045. [36] Kuzmin, R.O. Zabalueva, E.V. (2003) *LPS XXXIV*, #1912. [37] Boynton, W.V. *et al*., (2002) *Science, 297*, 81-85.

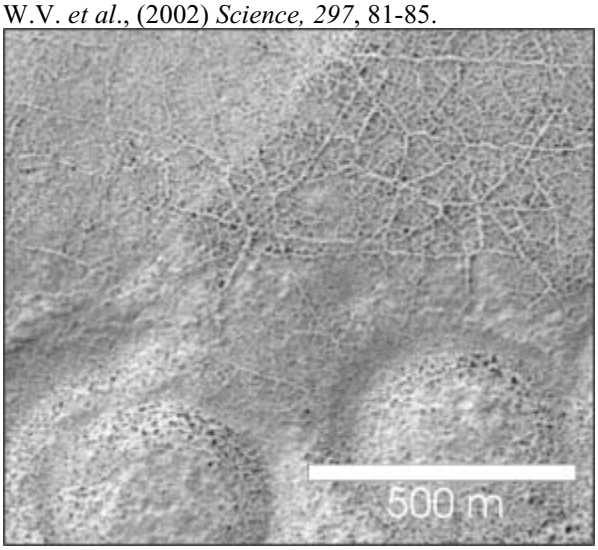

Figure 1 (MOC M0807668)

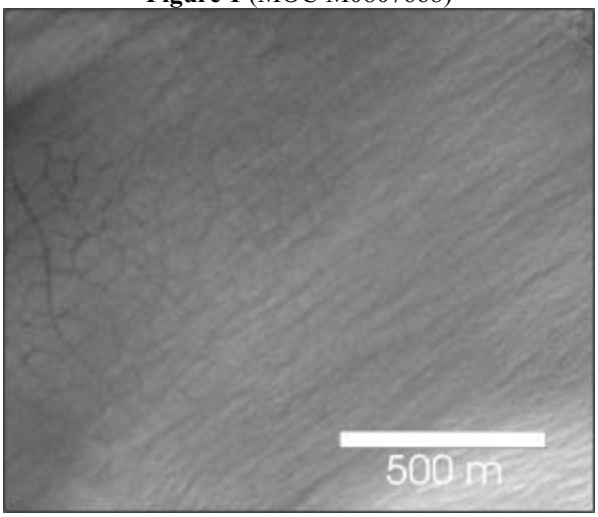

Figure 2 (MOC E1300770)

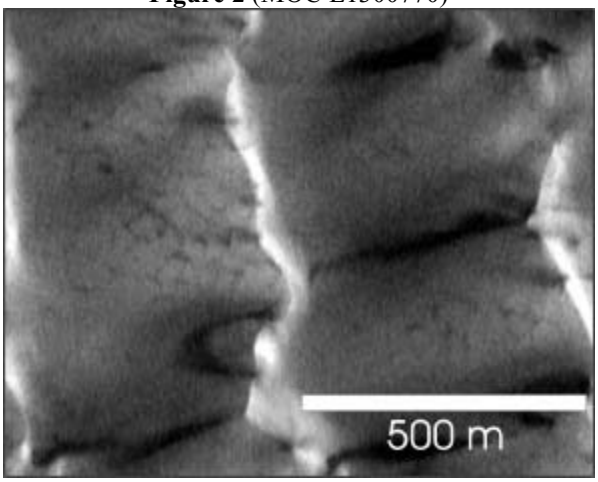

Figure 3 (MOC SP249004)

THE USE OF PALEOLIMNOLOGY FOR TRACKING CLIMATE CHANGE IN THE CANADIAN HIGH ARCTIC – ANALOGIES FOR MARS EXPLORATION. D. S. S. Lim[1] and M. S. V. Douglas[1], [1] Paleoenvironmental Assessment Laboratory (PAL), Dept. of Geology, University of Toronto, Toronto, Ontario, Canada M5S 3B1; lim@geology.utoronto.ca.

Tracking Climate Change in the High Arctic: The Canadian High Arctic is a distinct region of our planet in the way that it supports life, responds to shifts in the climate, and affects the environments of the rest of the globe. High Arctic characteristics such as low incoming radiation, small land mass (one tenth the size of tropical regions), and high-albedo surfaces (as a result of the longevity and high reflectivity of the snow and ice cover) exacerbate the effects of hemispheric temperature trends and contribute to the environmental vulnerability of this area of our globe [1, 2]. Over the last hundred years, an arctic warming trend has been recorded with increases in average arctic temperatures exceeding those recorded for the hemisphere as a whole [3]. High arctic environmental changes are not, however, isolated to this region, since they are strongly tied to general circulation patterns due to its inherent role as an energy sink [4]. For example, changes to the High Arctic's climate, such as increases in river run-off as a result of warming effects, may result in the alteration of global thermohaline circulation patterns and eventually lead to changes in low latitude climate systems [3].

Further investigation of high arctic climate and environmental change is still needed to better understand their widespread effects, which necessitates (a) the acquisition of baseline ecological data and (b) long-term monitoring efforts. A paucity of long-term environmental data exists for the High Arctic, due largely to the logistical difficulties and constraints associated with field expeditions in this remote polar region. The physical, biological and chemical limnological and paleolimnological data from the lakes and shallow ponds that dot the High Arctic tundra can provide a means of efficiently and economically meeting both of these requirements. These water bodies are both sensitive and vulnerable to such environmental influences as global warming [5], increased UV-B penetration [6], and local pollution inputs [7]. Furthermore, these lakes and ponds contain both ecological and genetic information that may help to expand our understanding of such basic biological concepts as speciation, and top-down trophic control, and, as a result, assist in the refinement of eco-management techniques used on temperate lakes [8].

Paleolimnological Investigations in the High Arctic: The Paleoenvironmental Assessment Laboratory (PAL) at the University of Toronto, working in partnership with the Paleoecological Environmental Assessment and Research Laboratory (PEARL) at Queen's University in Kingston, Ontario, focuses on acquiring both baseline and historical limnic data from the High Arctic using paleoenvironmental techniques. Fossilized freshwater algal remains of diatoms (class *Bacillariophyceae*), in particular, are used as bioindicators in our investigations of past physical and chemical limnic conditions. In the oligotrophic lakes and ponds of the High Arctic, diatoms typically form a significant proportion of the algal community [9]. Furthermore, they are ecologically diverse and respond rapidly to changes in environmental conditions, making them robust bioindicators in reconstructing such variables as salinity, pH, nutrient fluxes and lake levels [10]. PAL and PEARL have targeted sites throughout the High Arctic for paleoenvironmental investigations. Sites are found on such High Arctic islands as Banks, Bathurst, Cornwallis, Devon, Ellef Ringnes, Northern Ellesmere, Prince Patrick, and Victoria. Our work continues to expand throughout the High Arctic with the goal of creating both a spatial and temporal map of environmental data from this sensitive region of the world.

Implications for the Exploration of Mars: The application of paleolimnological techniques to climate change issues in the Canadian High Arctic has implications for future geobiological research on Mars. Specifically, ancient lake deposits on Mars have become a strategic focus for geobiological and astrobiological studies on the Red Planet. For example, Cabrol and Grin [11], Grin and Cabrol [12], and Wharton et al. [13] describe observational evidence for martian paleolakes, including in Gusev Crater [12], target site of the 2003 Spirit Mars Exploration Rover Mission. Paleolimnological investigations on Mars may lead to the acquisition of critical historical climate data from this planet, and paleolimnological research in polar settings such as the Canadian High Arctic may act as an analogue for future lacustrine investigations on Mars. Comparability in climate regimes, depositional processes, dearth of long-term environmental data, and other characteristics have led to a growing interest in polar paleolimnological studies as analogues to potential paleolake deposits on Mars. Furthermore, many of the tools and techniques that have been refined over the years for use in high arctic paleolimnological investigations will no doubt play a role in the future development of investigative strategies for the exploration of Mars paleolakes. The interesting physical,

chemical and potentially biological characteristics of high latitude water bodies may be analogous to the paleolakes that the early climate regime on Mars may have supported. Therefore, the lessons and experiences garnered in these remote regions may serve as a foundation for future robotic or human-led geobiological exploration on the Red Planet.

References: [1] Roots E. F. (1990) In *Artic and Global Change, J. A. W. McCulloch (ed.)*, 6-31. [2] Rouse W. R. (1994) In *Canada's Cold Environments*, H. M. French and O. Slaymaker (eds.) 65-92. [3] Overpeck, J. et al. (1997) *Science, 278*, 1251-1256. [4] Ledrew, E. F. (1993) In *Artic and Global Change, J. A. W. McCulloch (ed.)*, 271-290. [5] Smol J. P. et al. (1991) *Verh. Internat. Verein. Limnol,24*, 1240-1246. [6] Vincent W. F. and Pienitz R. (1996) *Geoscience Canada*, *23*, 231-236. [7] Douglas M. S. V. and Smol J. P. (1999) In *The Diatoms: Applications for the Environment and Earth Sciences*, E. Stoermer and J. P. Smol (eds.) 227-244. [8] Hammar J. (1989) *Ambio, 16*, 6-22. [9] Douglas M. S. V. and Smol J. P. (1993) *Nova Hedwigia 57(3-4)*, 511-552. [10] Dixit S. S. et al. (1992) *Environ. Sci. Technol. 26(1),* 23-32. [11] Cabrol N. A. and Grin E. A. (1999) *Icarus*, *142*, 160-172. [12] Grin E. A. and Cabrol N. A. (1997) *Icarus*, *130*, 461-474. [13] Wharton Jr. R. A. et al. (1995) *Journal of Paleolimnology*, *13,* 267-283.

SOME APPLICATIONS OF CO2-H2O PHASE EQUILIBRIA TO THE COMPOSITION AND EVOLUTION OF THE MARTIAN POLAR ICE CAPS. J. Longhi , Lamont-Doherty Earth Observatory, Palisades, NY 10964 (longhi@lamont.ldeo.columbia.edu)

Preferential melting of CO2 ice and clathrate layers within polar ice caps during periods of low obliquity may lead to sequestration of liquid CO2 in the Martian crust.

Fig. 1 is an update of the P-T projection of the CO2-H2O phase diagram [1,2] showing the approximate location of the solid state breakdown of CO2 clathrate (H) to water ice (I) and solid CO2 (S). Because of extremely limited solubility of H2O in CO2 liquid and gas at low temperatures, binary equililibria ***1*** and ***5*** are virtually equivalent to the sublimation and boiling curves for pure CO2, respectively.

Little solubility data are available with which to draw temperature composition diagrams, but some of the extent data [4] are shown in Fig. 2, which is a 2-bar T-X section. This diagram is relevant to putative ancient greenhouse atmospheres [5]. For a calculated surface temperature of 240° K the average atmosphere would have been in equilibrium with ice at saturation, similar to the present. However, the concentration of H2O would have been > 50 times the present average, and because of the higher atmospheric pressure the actual mass of atmospheric water could have been ~ 18,000 times the present amount. The evaporation rate in equatorial regions would have been much higher and Mars would appear more arid than today.

It is widely noted that ground ice is stable poleward of ~ 40° latitude and that night frosts occur even where no ice is present [6]. This implies that the martian atmosphere is on average saturated with ice (or close to it), and that the atmospheric composition (0.0067 wt% H2O) and frost point (198° K) [6] can be employed to construct a diagram analogous to Fig. 2 for martian surface pressure. Fig. 3 illustrates a T-X section drawn for the average surface pressure (6 mb – solid curve). The diagram predicts that water ice will be the first phase to precipitate upon cooling, that ~ 50° additional cooling is needed before the precipitate changes to clathrate, and that an additional 10° cooling is needed before CO2 and clathrate precipitate together (S >> H). Two other curves are also shown for the extremes of surface pressure (10 mb for the north polar regions and 2 mb for the south polar region and the higher portions of Tharsis). In the 10 mb section the atmospheric composition is farther into the gas + ice field (GI); at 2 mb the average atmospheric composition just intersects the ice field; however, water abundances are typically much lower in the southern hemisphere [7], so clathrate is probably the first phase to precipitate in the south polar region, followed by CO2 after ≤ 10 ° cooling. In fact the lowest water contents in the southern hemisphere are stable for months [7], suggesting that atmospheric water may be buffered by the solid-CO2 + clathrate "eutectic". These diagrams are consistent with observations that the northern ice cap is water-rich, whereas the southern ice cap has a residual CO2-rich top layer [8].

Basal melting has been suggested for both ice caps [9,10]. Fig 4 illustrates a schematic polybaric section along the temperature gradients calculated by [10]. Depths are given in km. Because ice is a much better conductor than solid-CO2 or clathrate [10], greater thicknesses are possible for water-rich ice caps before basal melting ensues. It is believed that in periods of low obliquity the polar ice caps tend to thicken with the addition of solid CO2 [11]. Because the dry ice and clathrate are much better insulators than water ice, the thermal gradient would have increased until melting began. The diagram predicts that mixtures of dry ice and clathrate melt at much lower temperature than water ice + clathrate. Therefore, generation of CO2-rich melts is likely, and because liquid CO2 is denser than water or water ice, it is likely to percolate into the crust This process, which sequesters CO2 in the crust, may be a major agent of atmospheric evolution.. Migration of subsurface liquid CO2 toward the equator may have led to explosive encounters with ground water or ice.

REFERENCES: [1] Longhi J. (2000) *Lunar and Planetary Science XXXI,* Abstract #1903, Lunar and Planetary Institute, Houston.. [2] Longhi J. (2001) *Lunar and Planetary Science XXXII,* Abstract #1955. [3] Zureck R.W., Barnes J.R., Haeberle R.M., Pollack J.B., Tillman J.E., and Leovy C.B. (1992) in *MARS*,H. H. Kieffer, B. M. Jakosky, C. W. Snyder, and M. S. Matthews eds., pp. 835-933, Univ. of Arizona Press, Tuscon. [4] Wiebe R. (19390 *J. Am. Chem. Soc. 61*. [5]] Fanale F.P., Postawako S., Pollack J., Carr M.H., and Pepin R.O.

(1992) in *MARS,* pp. 1135-1179. [6] Carr M.H. (1996) *Water on Mars*. Oxford Univ. Press, New York, 229 pp. [7] Jakowsky B.M and Haberle R.M. (1992) in *MARS,* pp. 969-1016. [8] James P.B, Kieffer H.H., and Paige D. A. (1992) in *MARS,* pp. 934-968. [9] Clifford S.M. (1993) *J. Geophys. Res. 98,* 10,973-11,016. [10] Mellon M.T. (1996) *Icarus 124,* 268-279.[11] Kieffer H.H. and Zent A.P. in *MARS,* pp. 1180-1218.

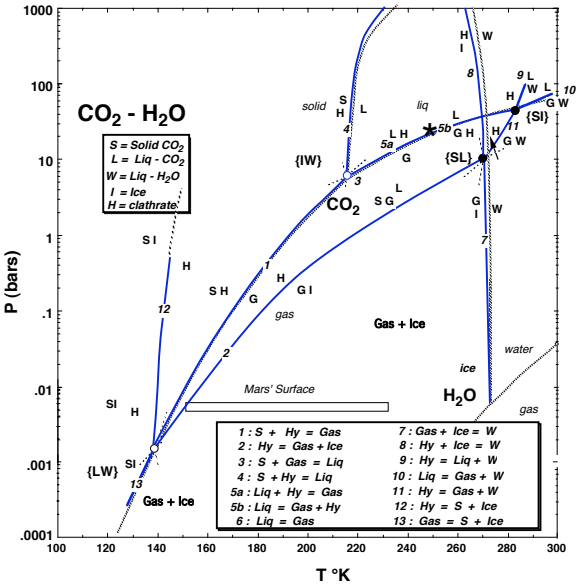

Fig. 1.Low-temperature portion of CO2-H2O phase diagram after [1,2]. Proposed binary invariant points indicated by open circles. Position of low-T stability limit of clathrate (H = S + Ice) is calculated.

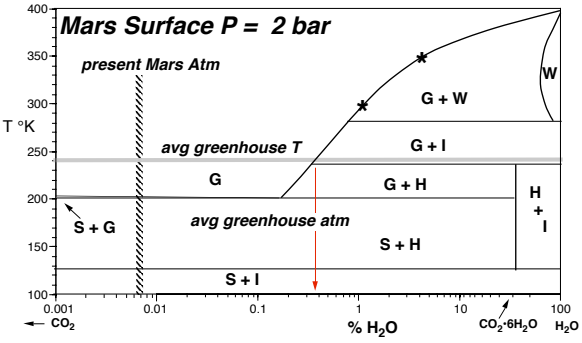

Fig. 2 2-bar isobaric section. Solubility data (*) from [4]. Vertical dashed line indicates present martian atmospheric composition; approx. 240°K greenhouse temperature from [5]. Maximum average H2O in atmosphere would be > 50x present concentration, but > 10000 times present mass.

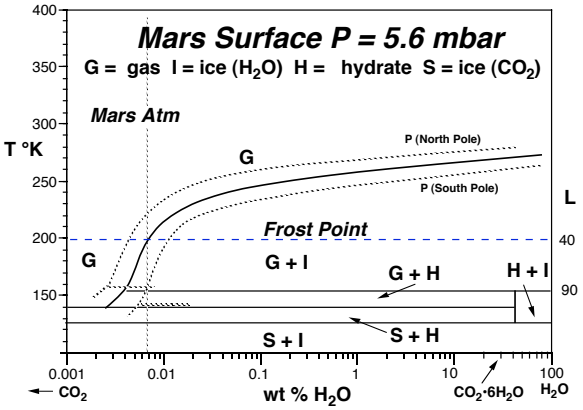

Fig. 3 Schematic isobaric sections based on frost point and atmospheric composition. Ice is first condensate at lower elevations; clathrate may be first at higher elevations

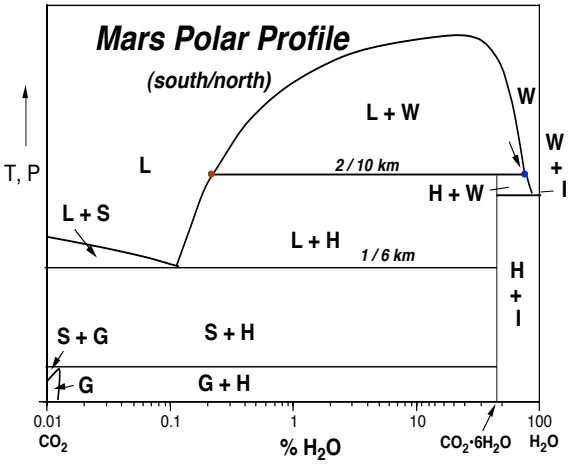

Fig. 4 Schematic profile along polar P-T profiles after [10]. Numbers are depths in km along thermal profiles calculated by [10]: dry ice/water ice.

AN INVESTIGATION OF AEROSOL DYNAMICS IN THE ATMOSPHERE OF MARS. A. Määttänen, H. Korhonen, K. E. J. Lehtinen, H. Vehkamäki, M. Kulmala, *Division of Atmospheric Sciences, FIN-00014 University of Helsinki, FINLAND, (Anni.Maattanen@helsinki.fi)*.

Atmospheric models are developed and used for several purposes. The research of climate change is a hot topic at the moment, and global climate models produce results about past and future climates. Numerical weather prediction models are well-known in the sense that they are used to produce the everyday weather predictions for e.g. television. Both model types can be converted to other planetary atmospheres as well, to describe their weather and climate.

Aerosol models have recently been incorporated as components in atmospheric models; detailed microphysical models describe microscale aerosol size distribution and processes in the atmosphere. When used together with or inside an atmospheric model, e.g. cloud and rain particle formation are defined and described in great detail. Aerosol particles affect radiative transfer in the models because they absorb and scatter radiation thus influencing the net radiative forcing of the atmosphere.

In the Martian atmosphere dust and other types of aerosol particles (most importantly carbon dioxide and water ices) scatter and absorb both short- and longwave radiation. This affects the thermal structure of the atmosphere and flow fields therein. Flow patterns affect the aerosol particle distribution by lifting dust from the surface and advecting dust and ice particles in the atmosphere. This feedback between aerosols and flow patterns may, for example, have a great influence in the onset of global (and also local) dust storms.

In the polar areas atmospheric temperatures are low enough for extensive ice nucleation to occur, since e.g. clouds are regularly observed. Aerosol processes may also have some influence in the formation of the polar layered deposits; the mixture of ice and dust is probable also in the atmosphere (via heterogeneous nucleation) from where it can sedimentate to the surface.

Our goal is to build a microphysical aerosol model for the Martian atmosphere. So far we have studied homogeneous and heterogeneous nucleation of carbon dioxide based on the work by Wood (1999). Homogeneous nucleation of CO_2 is very unlikely to happen in the Martian atmosphere because of the very high supersaturation required (10^8), but instead heterogeneous nucleation seems very probable in temperatures below 178 K. Model simulations have been conducted in average atmospheric near-surface conditions for a 100% CO_2 atmosphere (the Martian atmosphere is 95.3% CO_2). Unary nucleation of H_2O will also be studied in the same way. The binary nucleation of carbon dioxide and water will also be investigated.

Future work includes modelling the growth of the aerosol particles by condensation and coagulation using a box model (spatially 0-dimensional). Eventually, when all the components are together and working, the aerosol model will be incorporated into the Mars atmospheric models of the University of Helsinki (Savijärvi 1995, 1999, Savijärvi and Siili, 1993). Thus the microphysical aerosol model will be improving the atmospheric models by, for example, describing cloud formation and aerosol size distribution more precisely and thus improving the accuracy of the radiation schemes.

This work was supported by the *Academy of Finland*, which is gratefully acknowledged.

References

[Savijärvi, 1995] Savijärvi, H. (1995). Mars boundary layer modeling: diurnal moisture cycle and soil properties at the Viking Lander 1 site. *Icarus*, 117:120–127.

[Savijärvi, 1999] Savijärvi, H. (1999). A model study of the atmospheric boundary layer in the Mars Pathfinder lander conditions *Quarterly Journal of the Royal Meteorological Society*, 125:483–493

[Savijärvi and Siili, 1993] Savijärvi, H. and Siili, T. (1993). The Martian slope winds and the nocturnal PBL jet. *Journal of Atmospheric Sciences*, 50:77–88.

[Wood, 1999] Wood, S. E. (1999). Nucleation and growth of CO_2 ice crystals in the Martian atmosphere. Ph.D. thesis

DISTRIBUTION AND CLIMATIC CONTROL OF SMALL SCALE POLYGONS ON MARS N. Mangold, Orsay-Terre, Equipe Planétologie, UMR 8616, CNRS et Université Paris-Sud, Bat. 509, 91405 ORSAY Cedex, France, mangold@geol.u-psud.fr

Introduction:
On the Earth, the formation of patterned ground occurs in periglacial or alpine regions submitted to permanent or transient freezing temperatures. Two climatic effects control their formation: (1) Freeze-thaw cycles which form sorted polygons, hummocks or stripes from ice segregation in lenses and concentration of stones or pebbles and (2) thermal contraction which forms crack networks by volume decrease of the ground during winter (Fig. 1). Ice-wedge polygons are due to a combination of thermal contraction and seasonal melting because meltwater freezes in the cracks in winter and creates a weakness that is reused for cracking [e.g. 1]. The occurrence of polygons on Mars similar to those found on Earth in periglacial regions is thus interesting to study recent modifications of ice distribution and climate. Here, I detail the classification of polygons on Mars and focus on one type of the polygons located close to the south ice cap.

Classification of different type of polygons:
The systematic study of patterned ground on the whole planet Mars has been done using MOC images M01 to E06. Large crack networks observed in NW Elysium and Utopia regions [2,3] as well as those from Athabasca Valles, are not taken in account in the study for a reason of chronology. Indeed, these polygons, although sparsely cratered, show 100 m large craters on about all MOC images [see example on fig.2 of 2]. Despite being Late Amazonian, they are significantly older than the polygons of this study which are almost completely devoid of craters.
We classed patterned grounds using 4 criteria: *(1) Homogeneous or various width*: Polygons are listed as "homogeneous" polygons if they have a regular width and as "various " in the contrary case. (2) *Small or large polygons*: In the case of homogeneous width, polygons are listed as "large" if they are more than 40 m wide and as "small" if they are less than 40 m wide. (3) *Identification of cracks*: The presence of cracks indicates processes involving volume contraction either by freezing, desiccation or tectonic stress. (4) *Topographic control*: We observe that patterned ground are sometimes systematically associated to topography such as crater interior or hillslopes.
Using these criteria we find that polygons of more than 500 images can be listed in 4 main types and 8 subtypes (see whole map of polygons in companion paper, Mangold et al, Geographical relationships between small scale polygons and ground ice distribution from Neutron Spectrometer on Mars). Images with small crack networks (S1) are in very low number (33) compared to the 151 images containing (S2) regular polygons devoid of cracks (Fig. 2A) and 250 images of (S3) regular pattern of hummocks. Large polygons are all formed by cracks identified by their straight shape. There are only two classes of large and homogeneous polygons among which one (Fig. 2B) is found in connection to topography (LT) and the other one (Fig. 2C) in connection to the south polar cap (LPC). The polygons of various sizes (V), divided in complex, fractal and random, consist of a total number of 38 images which are strictly restricted to the southern hemisphere at latitudes from 55 to 80° with a maximum near 70°. 4 subtypes of polygons are found in both hemispheres at the same latitudes. Their distribution thus likely corresponds to climatic effects. Different interpretations of these networks can be given in terms of climate control involving thermal contraction or freeze-thaw cycle like on Earth. Here, I detail the case of polygons (LPC) that are only observed around the south CO_2 cap (Fig. 3).

Interpretation of polygons around the south CO_2 cap by recent variations of the polar cap extend:
Polygons (LPC) have size of 50 to 300 m and they are exclusively at more than 80° of latitude south. Cracks have not the typical morphology of ice-wedge cracks because they are very straight and thin compared to the width of polygons and they are often longer than 1 km. Such regular geometry is more typical of polygons formed by a single and strong episode of contraction. I propose to explain such large and narrow cracks by thermal contraction due to variations in the extent of the CO_2 permanent cap. Indeed, cracking of the ground occurs during the decrease of temperature. Such decrease could be related to the blanketing of the polar deposits by the CO_2 cap. In that case, the surface blanketed by CO_2 is no more heated by the sun in summer and the surface freezes at the temperature of CO_2 around -125°C. A cold thermal wave can propagate even deeper as the duration of the blanketing is long. After that period of expansion, the polar cap would retreat and cracks would become visible at the surface without being completely closed by the thermal expansion. The retreat of the polar cap could correspond to what may be currently observed over MOC images [4]. This scenario is consistent with the lack of similar features in the polar deposits of the North hemisphere because there is no permanent CO_2 polar cap in the North pole. Thus, if this scenario is true, a better understanding of the distribution and formation of these cracks could permit to reconstruct past extent of the CO_2 cap and to identify regions of terrains containing water ice versus those containing CO_2.

References: [1] French, H. M., The periglacial environment, 2nd ed., Longman, 1996 [2] Seibert, N. M. and J. S. Kargel, *Geophys. Research Let.*, 28 (5), 899-902, 2001. [3] Kuzmin, R. O., E. D. Ershow, I. A. Komarow, A. H. Kozlov and V. S. Isaev, *LPSC 33th*, abstract #2030, 2002. [4] Malin et al., *Science*, 2001.

Acknowledgement: The author acknowledges the use of Mars Orbiter Camera images processed by Malin Space Science Systems that are available at http://www.msss.com/moc_gallery/ and the USGS MOC images web graphical assistant available at http://ida.wr.usgs.gov/. This study is supported by the Programme National de Planétologie (PNP) of Institut National des Sciences de l'Univers (INSU), France.

Fig. 1: Patterned ground on Earth (a) About 1 m large sorted polygons in Greenland (photo J.-P. Peulvast) (b) About 30 m large ice wedges polygons (Canada, GSC photograph).

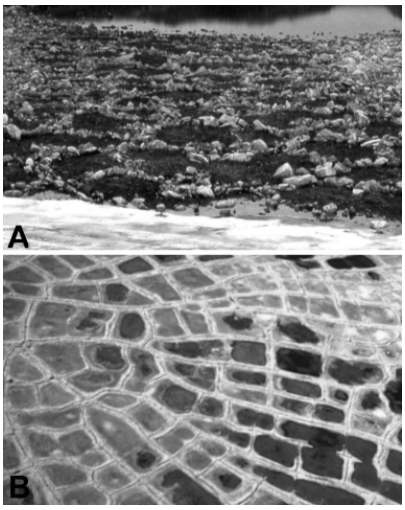

Fig. 3: MOC image of the front of the south polar cap of CO2 with swiss cheese features. Polygons LPC are observed below these swiss-cheese terrains in what is likely ice-rich terrains devoid of permanent CO2 ice.

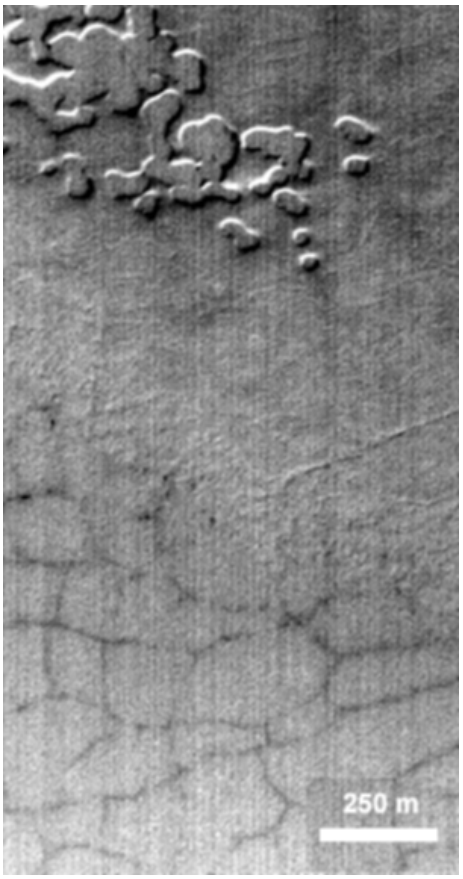

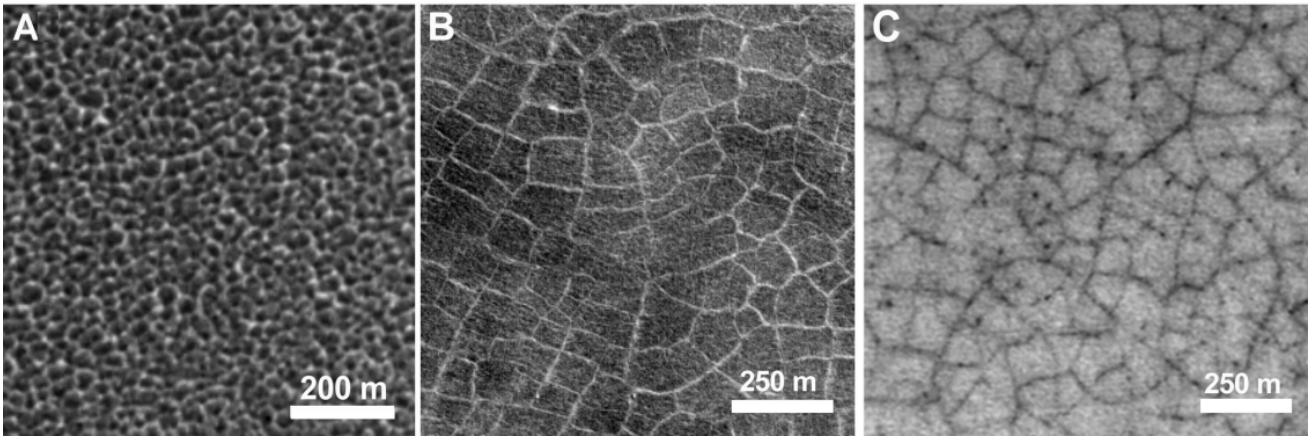

Fig. 2: MOC images of small polygons (S2), large homogeneous polygons (LT) and polygons closed to CO_2 cap (C).

GEOGRAPHICAL RELATIONSHIPS BETWEEN SMALL SCALE POLYGONS AND GROUND ICE DISTRIBUTION FROM NEUTRON SPECTROMETER ON MARS. N. Mangold[1], S. Maurice[2], W. Feldman[3], F. Costard[1], F. Forget[4], [1] Orsay-Terre, Equipe Planétologie, UMR 8616, CNRS et Université Paris-Sud, Bat. 509, 91405 ORSAY Cedex, France, mangold@geol.u-psud.fr, [2] Observatoire Midi-Pyrénées, Toulouse, [3] Los Alamos National Laboratory, New Mexico, USA, [4] Lab. Météorologie Dynamique, Jussieu, Paris.

Introduction:
The occurrence of polygons on Mars similar to those found on Earth in periglacial regions is the subject of debates since three decades. Large polygonal systems have been identified on Viking images of the Northern plains [1]. New high resolution images of the Mars Observer Camera MOC of Mars Global Surveyor (MGS) show small-scale polygons much more similar in size to terrestrial patterned ground [2-5]. The necessary element to the formation of polygons, either by thermal contraction or by freeze-thaw cycles, is the presence of ice in the ground [6]. Our study shows that the global distribution of small-scale polygons on Mars is correlated with the distribution of near-surface ice obtained from the Neutron Spectrometer (NS), one of the component of the Gamma Ray Spectrometer (GRS) aboard Mars Odyssey. This correlation favors the periglacial origin of these polygons which can thus be used as indicators of ground ice and climate variations.

Distribution of polygons on Mars:
The classification of polygons is detailed in the companion abstract (Mangold, Distribution and climatic control of polygons on Mars). These polygons are similar in shape to polygons formed on the Earth by thermal contraction, with seasonal thaw possible in addition. They are classed in polygons smaller than 40 m (S) apparently devoid of cracks (Fig. 1), homogeneous polygons formed by crack networks larger than 40 m (L) and polygons formed by crack networks of heterogeneous size (V). All of these polygons are located in regions of high latitudes poleward of 55° in both hemispheres (Fig. 2). Small polygons (S) and most homogeneous large polygons (L) are found symmetrically in both hemispheres making a climatic control in their formation likely. Nevertheless, the subtype of large homogeneous polygons (LPC) is observed specifically around the polar cap (see companion abstract for explanation). The complex polygons of heterogeneous sizes (V) are located in the southern hemisphere only in the latitude of 65-80 with a gap between 120-220°E. There is no relationship between the distribution of polygons and the Martian stratigraphy: polygons exist in Noachian, Hesperian or Amazonian units. The reason is that the youthful deposits in which they are found is also independent of the stratigraphy established at Viking scale. This young layer is likely composed by a mantling of smooth deposits of dusty, loess like material, containing ice in large amount [7].

Correlation with Neutron Spectrometer data:
The new data from the Gamma Ray Spectrometer (GRS) onboard Mars Odyssey shows that the ground is strongly enriched in ice in polar regions [8]. The ground poleward of 60° may contain proportions of ice of more than 50% in volume whereas the top 10 or 20 cm remains desiccated [8,9]. The Neutron Spectrometer (NS) measures the distribution of hydrogen, supposed to be in the form of ground ice in the latitudes poleward of about 50-60° (Fig. 2). There is a correlation between the distribution of polygons and the distribution of ground ice from NS. Such correlation confirms a periglacial origin for the patterned grounds observed. Looking more in details, small polygons (S) and homogeneous large polygons (L) follow accurately the limit at 55-60° like if they were directly dependent on the occurrence of near-surface ice at these latitudes. The limit is much more equivalent in the south hemisphere than in the northern. Regional differences exist locally. On the NW of Tharsis volcanoes the NS detects near-surface ice down to 45° of latitude whereas polygons seems to exist only at 55° of latitude. By contrast, polygons are found in the latitudes 50-60°N at longitudes of 80-100°E whereas the NS data indicate a limit of ice around 60°.

Interpretation:
The two processes able to produce polygons on the Earth, thermal contraction or freeze-thaw cycles, affect both only the top few meters of the ground because they are the consequence of the propagation of seasonal or diurnal thermal waves. Daily temperature changes produce polygonal features but the maximum propagation depth of the thermal wave is limited to the top 10 cm [10]. In the case of seasonal thaw, the layer which thaws each summer is typically of 1 m thick on the Earth. Seasonal thaw is not possible on Mars currently but obliquity variations may have permitted to thaw the ground down to several tens of centimeters in the recent past [11]. On the other hand, thermal contraction produces crack networks by seasonal changes of temperatures. Seasonal temperature changes induce cracking down to 1 or 2 meters depending on thermal properties of the ground [10]. These depths are similar to the depth of hydrogen possible to be detected by NS which is of about 2 m at maximum. Ground ice may exist deeper than 2 m in regions equatorward to 60° of latitudes without being detected by NS data. However, polygons may not exist at these latitudes because the

depth of this ground ice is not reached by the seasonal thermal waves. Polygons thus correlate to the presence of near-surface ground ice detected by NS probably because periglacial processes like seasonal thermal contraction exist only if water ice is present in the top 1 or 2 m of the ground as detected by Neutron Spectrometer.

Fig; 1: (left) MOC images of small polygons (S). Cracks are not visible but scale limits the identification of geomorphic parameters. (right) MOC image of large polygons (L) very similar to such of high latitudes region of Earth.

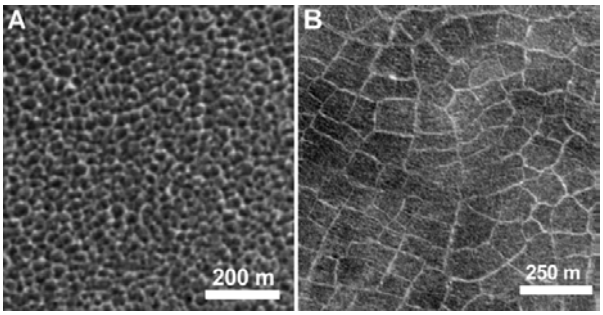

References: [1] Pechmann, *Icarus*, 42, 185-210, 1980. [2] Malin M. C. and K. S. Edgett, *J. Geophys. Res*., 106, E10, 23,429-23,570, 2001. [3] Seibert, N. M. and J. S. Kargel, *Geophys. Research Let.*, 28 (5), 899-902, 2001. [4] Kuzmin, R. O., E. D. Ershow, I. A. Komarow, A. H. Kozlov and V. S. Isaev*, LPSC 33th*, abstract #2030, 2002. [5] Mangold, N., F. Forget, F. Costard et J.-Peulvast, *LPSC*, *33th*, #1912, Houston, USA, 2002. [6] French, H. M., The periglacial environment, 2nd ed., Longman, 1996. [7] Tokar, R. L., W. C. Feldman, T. H. Prettyman, K. R. Moore, D. J. Lawrence, R. C. Elphic, M. A. Kresvalsky, J. W. Head III, J. F. Mustard, W. V. Boynton, *Geophys. Res. Let*., 29, 19, doi10.1029/2002GL015691, 2002. [8] Boynton, W. V. and the GRS team, *Science*, 297, 71-75, 2002. [9] Feldman, W. C., and the GRS Team, *Science*, 297, 76-80, 2002. [10] Mellon, M. T., *J. Geophys. Res*., 102 (E11), 25,617-25,628, 1997.[11] Costard F., Forget F., Mangold N. and J.-P. Peulvast. *Science*, 295, 110-113, 2002.

Acknowledgements: The authors acknowledge the use of Mars Orbiter Camera images processed by Malin Space Science Systems that are available at http://www.msss.com/moc_gallery/ and the USGS MOC images web graphical assistant available at http://ida.wr.usgs.gov/. This study is supported by the Programme National de Planétologie (PNP) of Institut National des Sciences de l'Univers (INSU), France.

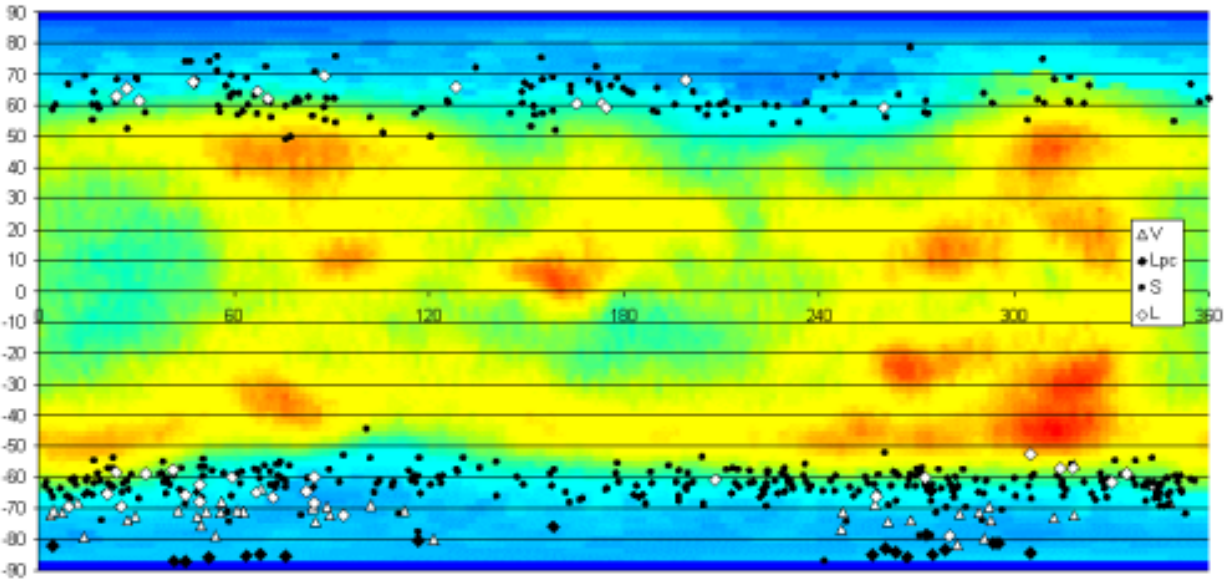

Fig. 2: Distribution of polygons over map of ground ice distribution by the Neutron Spectrometer of GRS onboard Mars Odyssey (Arabia is at left). Most polygons of all types are found in regions where hydrogen is detected at depth of less than 1-2 meters. Equatorial regions with detection of hydrogen have been interpreted as clay rich regions by recent studies.

TONGUE-SHAPED LOBES ON MARS: RELATION TO ROCK GLACIER DEPOSITS AND LONG-TERM HISTORY OF EMPLACEMENT. D. R. Marchant[1], J. W. Head[2], and M. A. Kreslavsky[2,3]. [1]Department of Earth Sciences, Boston University, Boston, MA 02215 marchant@bu.edu; [2]Department of Geological Sciences, Brown University, Providence, RI 02912; [3]Kharkov National University, Kharkov, Ukraine.

Introduction: Recent work based upon Mars Global Surveyor (MGS) data [1,2], in conjunction with previous analyses of Viking data [3], suggests that rock glaciers, similar in form to those found in polar climates on Earth, have been an active erosional feature in the recent geologic history of Mars. A wide range of literature exists describing rock glacier characteristics, form, and distribution, but diversity of opinion exists on rock glacier nomenclature and genesis.

We previously outlined the two-fold genetic classification of *Benn and Evans* [4] for terrestrial rock glaciers, and then proposed a non-genetic descriptive set of terms to be applied to martian features [5] (Fig. 1,2).

Different processes and environments could produce similar or gradational landforms and thus the landforms themselves might not be unequivocal indicators of a specific origin. Thus, we follow *Whalley and Azizi* [1] and suggest that non-genetic descriptive terms be used for the martian features.

We call on established anatomical morphology for nomenclature (Fig. 1,2). The tongue-shaped lobe can be divided into the tip, or *apex*, the *blade* (the flat surface just behind the tip), the body and its rear part (the *dorsum*), and the tongue *root*. Ridges along the edges are called marginal ridges and those concave outward ones at the tongue apex are called *apical ridges*. Within the tongue body and in the dorsum area occur a series of *chevron-shaped ridges* with the apex of the chevrons pointing toward the tongue apex. The central part of the tongue is depressed. The tongue root zones occur in the upper parts of crater walls in subdued alcoves. The tongue width narrows by at least a factor of two from the root zone toward the tongue body. Chevron ridges occur primarily within this transition zone. Surrounding the tongue-shaped lobes are linear to elongate smoothed and subdued ridges and mounds, some with scalloped margins. The scalloped margins occur on the inside and the broad structure often mimics the tongue shape. In Fig. 1, subdued channels emerge from the apices of these broad features. We interpret these broad features to be remnants of earlier larger and more extensive lobes.

On the basis of the characteristics of the tongue-shaped lobes on Mars, their associated features, and comparison to features in the Antarctic Dry Valleys of known origin, we can reach the following conclusions: 1) A variety of features on Mars are very similar to features on Earth that form in glacial and periglacial environments; 2) Confusing nomenclature, genetic classifications, possible form convergence or equifinality, and uncertain origins of many of the terrestrial examples all make direct application of general Earth morphological comparisons to Mars difficult; 3) We therefore have developed a descriptive and non-genetic nomenclature for these features; 4) Careful comparison of the Mars features to well-studied Earth analogs in the Mars-like environment of the Antarctic Dry Valleys can lead to insights into the origin of these features on Mars; 5) The morphology and characteristics of the Mars features examined in this study have been carefully compared to three types of features in the Antarctic Dry Valleys: a) gelifluciton lobes, b) rock glaciers, and c) alpine glaciers; 6) The tongue-like lobate, concave nature of these features is very similar to alpine glaciers and debris-covered glacier deposits. In these cases, the percentage of ice in the original deposit was very high, and sublimation and melting led to retreat, and subsidence and downwasting of any debris cover, leaving marginal morainal ridges as a main feature; 7) The presence of fainter, broad lobe-like features with scalloped margins of similar orientation suggest the former wider extent of such activity; 8) The lack of cross-sectional convexity in these tongue-shaped lobes and related deposits suggests that the ice involved in their formation is now largely gone. This suggests that conditions in the past favored the formation of active glaciers and glacial landforms, and that the present time is more equivalent to an interglacial period; 9) The presence of these features on pole-facing interior crater walls suggests that this micro-environment is very favorable for the accumulation of snow and the initiation of local glaciation; 10) This type of glaciation appears to be a significant process in the modification of crater walls and floors.

We now turn to an analysis of the interior of a crater wall located at 44.4S, 195.3W and illustrating a longer-term evolution than those in Figures 1 and 2. This region lies on the north (pole-facing) wall of a crater in the southern hemisphere and shows a variety of features that contrast radically with the features seen on the southern (equator-facing) wall. Average slopes on the northern wall are ~16° and the floor of the crater slopes about 2-3° to the south.

Figure 3 illustrates the features and facies that have been mapped in this area. First the floor of the crater is marked by extensive dune deposits that cover broad ridges that partly mimic the wall-facing scarp that is seen at point 1. Secondly, the scarp along point 1 is broadly cuspate and separates the south-tilting floor from the base of the wall. Inward of this are observed more arcuate patterns (2) that are very similar to the apical ridges and scalloped margins seen in Figure 1 and 2. Northward of this (3) are much more continuous apical ridges and marginal ridges that appear to be very similar to those seen in Figures 1 and 2. Separating these are broader scalloped margins comparable to those in Figure 1 and 2. The characteristics of these deposits and structures, and their location on pole-facing slopes is consistent with many observations of similar features related to ice-rich features and accumulations [6-10]. We interpret these to be related to a former period of ice accumulation and downslope flow onto the crater floor to produce the asymmetric crater interior slopes and southward-tilting floor. Note the differences between the features and structures in Figures 1 and 2 interpreted to be related to the formation of rock and debris covered glaciers. In the case of Figure 1 we concluded that although morphologically fresh, the morphology of these lobate tongues suggested that they were in a state of wasting and retreat, rather than accumulation and advance.

In contrast to the features seen in Figures 1 and 2, the area in Figure 3 is characterized by fan-shaped deposits superposed on the lobate deposits (4). The apices of these fan-shaped deposits extend up into discrete and rough-textured alcoves on the upper parts of the crater walls. These deposits are interpreted to be talus cones that are derived from erosion of debris from the alcove, and channeling of the debris to form talus cones below the alcoves. Note their clear superposition on the underlying units and features related to rock and debris covered glacial emplacement. The superposition of these features strongly suggests that the environment characteristic of this crater wall in earlier history was climatically capable of supporting sufficiently continuous snow accumulation to create an accumulation zone and produce rock and debris covered glaciers. A summary of these conditions is shown in Figure 3 (right). With time, these conditions changed sufficiently to cause retreat of the glacier, localization into discrete tongue-shaped lobes, and then ultimately to loss of most of the volatiles and topography typical of these lobes elsewhere (compare Figure 3 to Figures 1 and 2). These changing conditions then resulted in the formation of discrete chutes and gullies that fed the

large talus aprons that characterize the most recently detectable geological activity at this scale.

In conclusion, this mapping, superposition relationships, and correlation between different examples of comparable crater wall settings strongly suggest that there is a record of changing climate conditions and microenvironments. We have mapped multiple examples of these deposits and are currently assessing variations in space and time to help map out the recent climate history of Mars, and to distinguish long-term climate change from microenvironments.

References: **[1]** Whalley, W. B. and Azizi F. (2003) *JGR, 104 (E4),*8032, doi: 10.1029/2002JE001864. **[2]** Head J. W. and Marchant, D.R. (2003) *Geology, 31*, 641. **[3]** Lucchitta, B. K. (1981) *Icarus,* 45 (2), 264-303. **[4]** Benn, D.I. and Evans, D.J.A. (1998) *Glaciers and Glaciation*, Arnold Publishers, London. **[5]** Marchant, D. R. and Head, J. W., Mars 6, #3091, 2003. **[6]** Malin, M. and Edgett, K, JGR, 106. 23429, 2001. **[7]** Milliken, R. et al., JGR, in press, 2003. **[8]** Howard, A., LPSC 34, #1065, 2003. **[9]** Reiss, D. and Jaumann, R. LPSC 34, #1821, 2003. **[10]** Kargel, J. et al., LPSC 34, #2092, 2003.

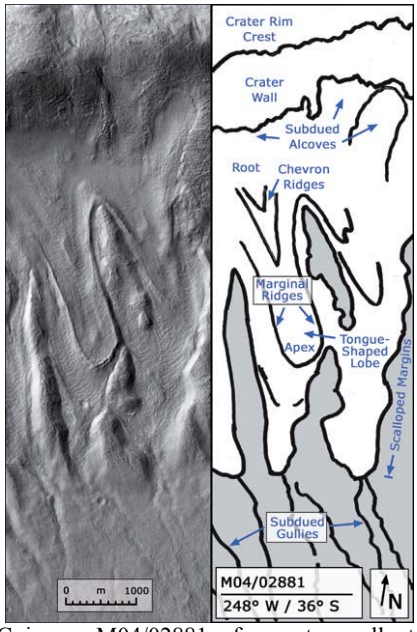

Figure 1. MOC image M04/02881 of a crater wall at 248°W/36°S, Mars. North is at the top of the image, and illumination is from the northwest.

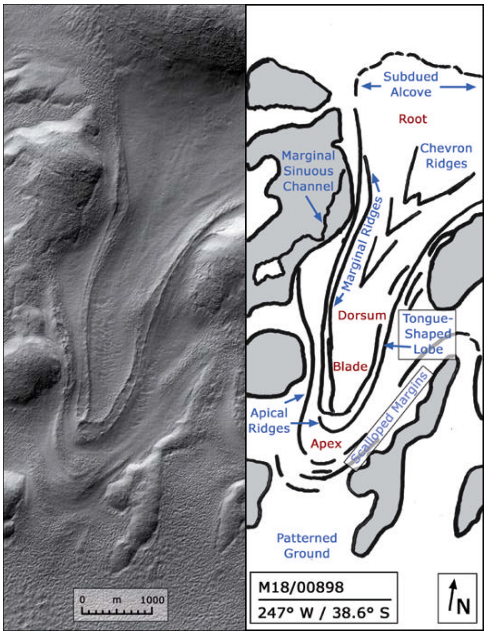

Figure 2. MOC image M18/00898 of a crater wall at 247°W/38.6°S, Mars. North is at the top of the image, and illumination is from the northwest.

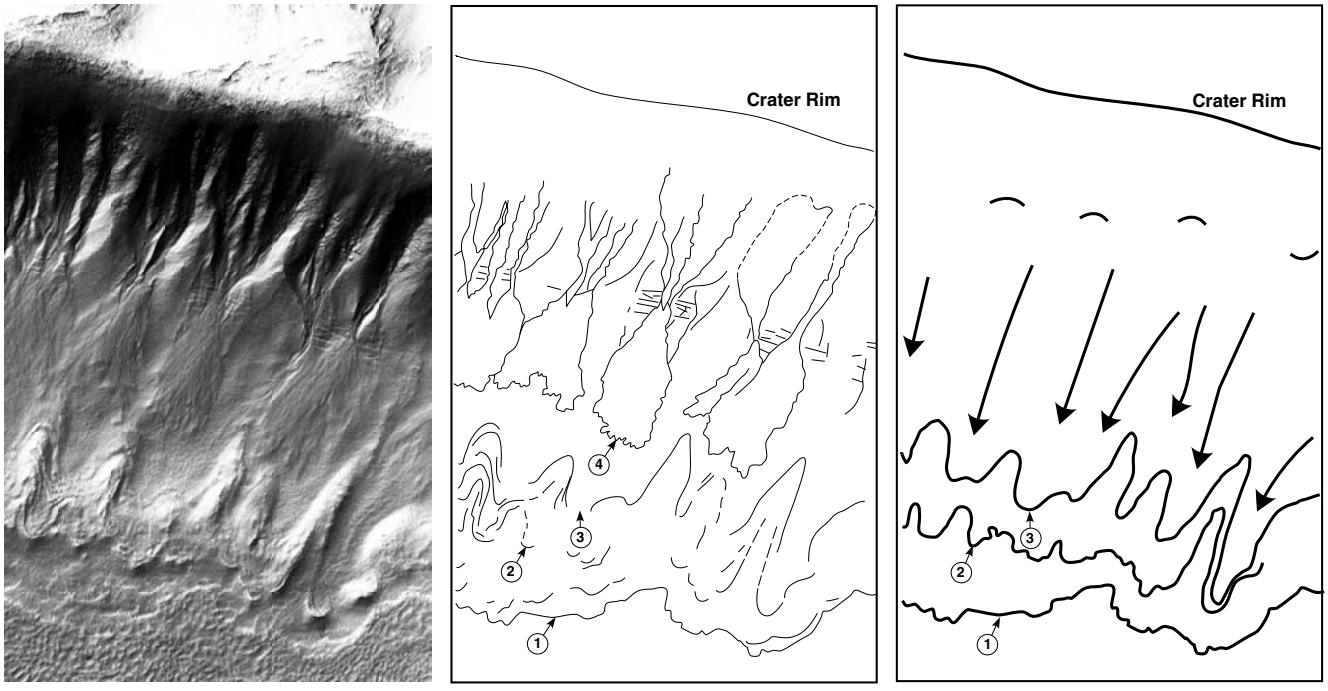

Figure 3. Portion of north (pole-facing) slope of impact crater at 44.45, 195.3W. Left, MOC Image E14 101929. Image is ~3 km in width. Middle, sketch map of features in MOC image. Right, interpreted directions and sequence of glacial advances represented by the deposits and structures.

CO_2 Ice in Polygonal Troughs in Malea Planum, Mars: Sub-Surface H_2O Ice, MOC Images and TES Surface Temperature. W.J. Markiewicz[1] and K.J. Kossacki[2], [1]Max-Planck-Institute for Aeronomy, Max-Planck-Str 2, D-37191 Katlenburg-Lindau, Germany, markiewicz@linmpi.mpg.de, [2]Institute of Geophysics of Warsaw University, Pasteura 7, 02-093 Warsaw, Poland.

Introduction: In this work we analyse the diurnal and seasonal changes of the surface temperature in the south polar region of Mars. This work is a continuation of that presented in [1] were we have modelled the seasonal cycle of CO_2 surface ice within the polygonal features in the Malea Planum region. Our present goal is to investigate the influence of the physical and topographical properties of the polygonal features and the subsurface permafrost on the spatially averaged regolith (surface) temperature. We compare the results of simulations to the seasonal profile of surface temperature derived from the data obtained with the Thermal Emission Spectrometer (TES) on board of the Mars Global Surveyor (MGS). Polygonal patterns were observed with the Mars Orbiter Camera (MOC) also on board of the MGS. An example of such an image, together with the wide angle MOC context image is shown in Fig. 1. The image was taken during early southern spring, L_s=224.96º, the image is centred on 67.71º S and 303.77º W. The high albedo material within the polygonal troughs is interpreted as remnant seasonal CO_2 ice. Formation of the troughs on Mars was analysed in [2].

Surface temperature: The influence of the polygonal features on the average surface temperature can be due to the shadowing of the troughs, but it is also due to the delayed spring sublimation of CO_2 ice deposited within the troughs. Wherever the CO_2 ice is present, the temperature remains close to that of the phase equilibrium of about 145º, significantly lower than the temperature of the surface not covered by the CO_2 ice. During spring the average surface temperature in regions covered by the polygonal patterns will rapidly increase when the surface CO_2 ice disappears. This will be followed by an additional increase starting when the bottoms of the troughs become partially free of the CO_2 ice and continuing until all of the CO_2 ice sublimes away. The magnitude of this secondary increase is most directly dependent on the fraction of the surface covered by the troughs which is in the considered region up to about 10%. This evolution of temperature is seen in the TES data shown in Figure 2. The initial rapid increase at about L_s=220º marks when surface CO_2 is sublimated away. The secondary increase appears around L_s=245º, and can be clearly seen in the detailed plot in Figure 4.

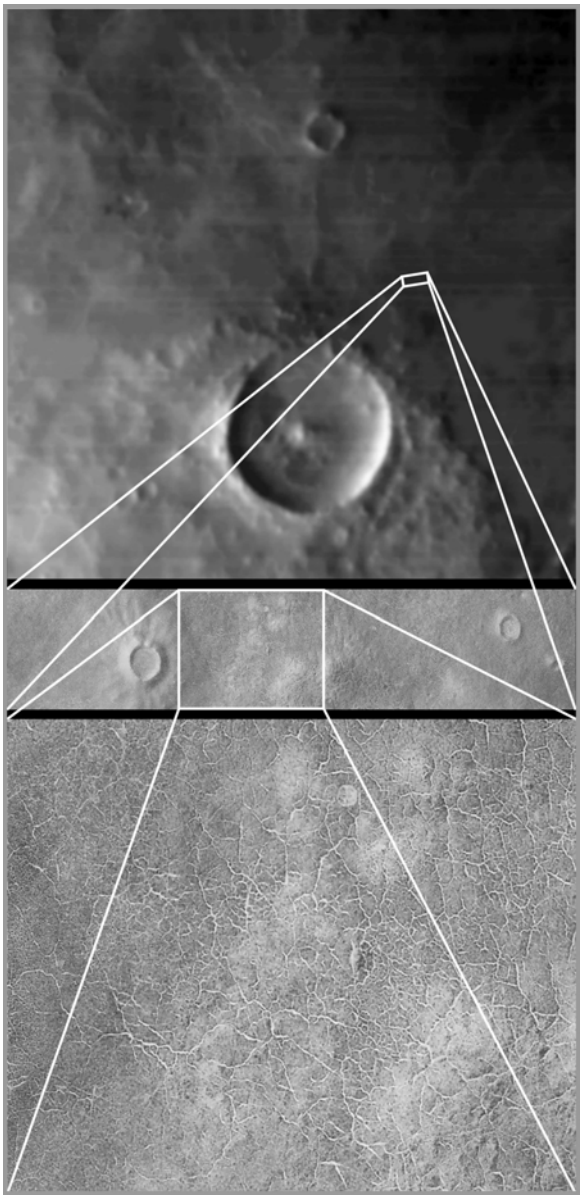

Figure 1 MOC image of the polygonal features with a context image (top). The middle image is 1.5 km across (short side). Resolution is 3 m px^{-1}.

Model: The model used in this work is almost the same as in [1], where the interested reader can also find its full mathematical description. Here we just underline the main features of the model. We analyse heat transport and evolution of water ice distribution in the subsurface vicinity of a trough in the Martian soil.

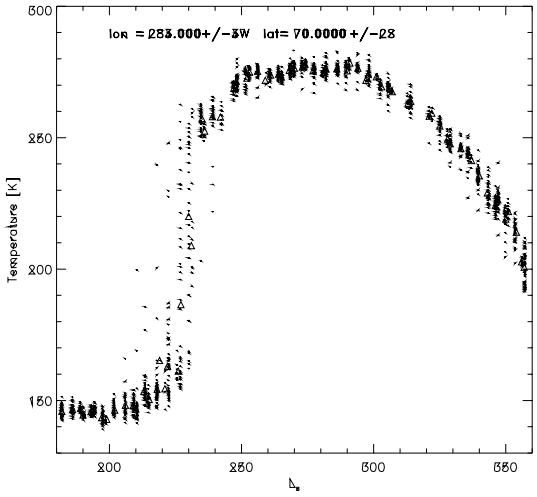

Figure 2 Surface temperature derived from the Thermal Emission Spectrometer data. Dots mark the individual TES footprints and triangles are sol averaged values.

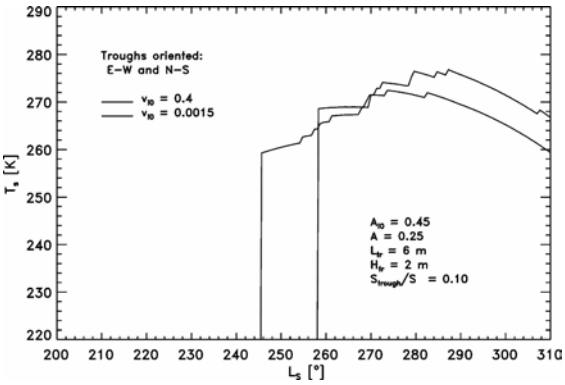

Figure 3 Influence of the content of the subsurface H_2O ice on the average surface temperature. The solid line corresponds to the model with water ice rich regolith, and the dashed line to the model with water free regolith.

The model also includes seasonal variations of the zenith angle of the Sun as well as seasonal variations of atmospheric pressure and composition. We also include sublimation and condensation of CO_2 ice in the trough. The topography considered has spatial scale of meters. This is small enough to assume that the presence of a trough does not have an effect on the diurnal, nor seasonal evolution of atmospheric density and composition which are taken from results of GCM [3]. Most importantly we have looked at two different models of the initial subsurface water ice distribution. One with water rich permafrost and one with effectively dry regolith. Our 2-D model includes condensation and sublimation of the CO_2 ice and a self consistent treatment of variations of the thermal properties of the regolith.

Results: Our primary interest is the amount of water ice that is present in the regolith. In Fig. 3 the surface temperature profiles are plotted for two models of the water ice content in the regolith. One model has volume ice content, v_{i0}=0.4 and the other assumes a dry regolith. When the regolith is rich with water ice, growth of the surface temperature following recession of the seasonal ice cap starts at L_s=245°, about 25 sols earlier than predicted by simulations assuming regolith free of water ice. This is due to the relation between winter condensation rate of CO_2 and the saturation of regolith with water ice. When the concentration of water ice is high, heat flux from regolith reduces winter

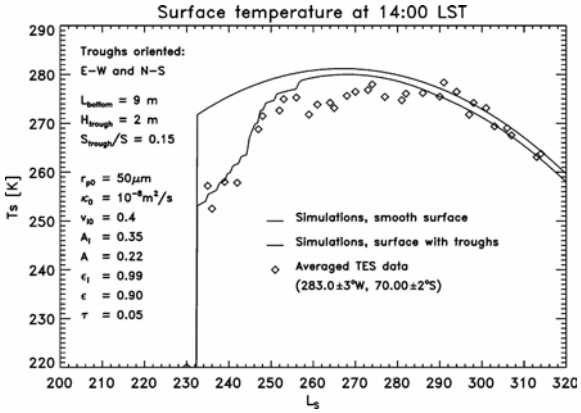

Figure 4 Comparison of the spatially averaged surface temperature from TES data with simulation.

condensation of CO_2 [1] . Resultant thinner deposit of CO_2 ice sublimes away earlier. Subsurface water ice also reduces significantly the maximum summer surface temperatures. This is because the water ice increases the thermal conductivity of the regolith, increasing the inward heat flux and in turn cooling the surface. Clearly only the model with water ice rich regolith can be fitted to the data as finally shown in Figure 4. Further details can be found in [4].

References: [1] Kossacki K.J. and Markiewicz W.J. (2002) *Icarus*, **160**, 73-85. [2] Mellon, M.T. (1997) *JGR*, **102**, 24,177-24,194. [3] Forget F. et al. (1999) *JGR*, **104**, 24,155-24,176. [4] Kossacki K.J. et al. (2003) *Planet. Space Sci.*, **51**, 569-580.

COMBINING MICRO-PENETROMETER AND NEAR-INFRARED PHOTOGRAPHY TO MEASURE PHYSICAL PROPERTIES IN SNOW PROFILES. M. Matzl[1] and M. Schneebeli, [1] WSL Swiss Federal Institute for Snow and Avalanche Research (SLF), Flüelastr. 11, CH-7260 Davos Dorf, Switzerland, matzl@slf.ch

Introduction: The description of layered snow profiles bases mostly on morphological methods. Physical properties are then correlated to the morphology and density of the snow. Different layers and horizons in the snowprofile are classified according to a set of features, most of them by manual and visual inspection [1]. Basic physical parameters, as density, are measured within the layer, assuming no spatial variability within the classified layer. Planar vertical sections allow for higher resolution, but are only feasible for small areas (up to 0.07 m vertical extension). This type of snowprofile has several drawbacks: the features (e.g. hand hardness, grain size, snow type) are measured at discrete locations, the description is one-dimensional and the level of discrimination of layers is subjective. A notable exception is the translucent profile, which is used sometimes for illustration. A quantitative analysis of this type of profile is difficult because transmittance of light is not only dependent on density, but also on grain size. The correlation of physical properties of the snow to density and grain type is incomplete, as is shown by the extensive field measurements of thermal conductivity by Sturm et al. [2]. We developed two new methods, which measure directly with high spatial resolution physical and mechanical properties of a snowpack. The micro-penetrometer measures the strength of bonds between structural elements ("grains") [3]. Near-infrared photography [4] maps the distribution of the specific surface area of a snowprofile with a resolution of about 4 x 10^{-6} m^2. Here we try to combine the signals of these complementary methods.

Methods: The micro-penetrometer (SnowMicroPen) measures the penetration resistance with a sampling distance of 4 µm and a layer resolution of about 1 mm (no thinner layers of snow were observed until now). Based on a mechanical model compressive strength can be calculated directly from the signal [5]. Density and textural information are derived by statistical models. The horizontal spacing of the measurements in the field is for practical reasons about 0.5 m, in the laboratory 0.05 m, each measurement takes about 3-4 minutes. For the near-infrared photography we used a modified digital camera with a CCD sensible in the near infrared. The pitwall is resolved with a resolution of about 1 mm / pixel, effective spatial resolution is about 4 mm^2. Targets of barium-sulphate paper or Teflon were inserted in the profile wall to rectify and calibrate the image. The micro-penetrometer measurements were about 0.05 m behind the profile wall. Details of the methods are described in [6] for the micro-penetrometer and [4] for the NIR-photography.

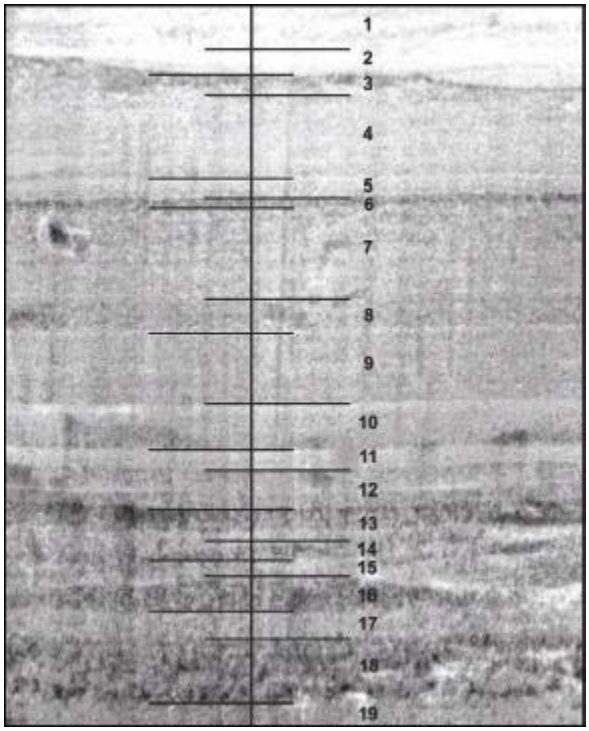

Fig. 1 Corrected near-infrared photography.

Results: A snow profile on a flat area was photographed, rectified and radiometrically corrected. Layers are visually determined and the position of the micro-penetrometer measurement is indicated with a black line (Fig. 1). Similar patterns of change are observed at horizon boundaries for the micro-penetrometer signal and the near-infrared reflectivity (Fig. 2). This shows that similar boundaries are represented in both methods. However, the two signals are not correlated, and are thus representing different properties of the snowpack. Both methods show substantial variability within one horizon.

Discussion: Near-infrared reflectivity, expressed as specific surface area, and penetration resistance measure at high spatial resolution mechanical and physical parameters in a snowpack. The two methods are supplementary. Snowpacks observed with these methods show much more complexity than observed in a classical snow profile, and have the advantage that an objective and persistent record of the snow profile can be

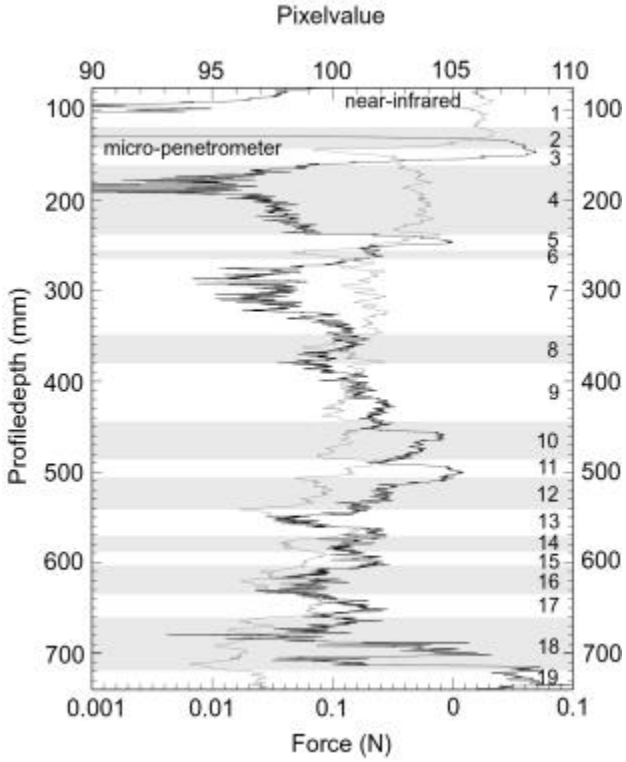

Fig. 2 Comparison of micro-penetrometer resistance and near-infrared reflectivity. Visually determined layers are indicated as grey and white bars.

kept. Additional research has to go in the physical interpretation of the signals and the statistical evaluation of the data. This will be done also by the use of geostatistical methods. The method has a large potential for calibrating radar spectra in the snow cover and to improve correlating chemical and physical and climatologically relevant properties of the snowpack.

References: [1] Colbeck, S. C. et al. (1990) *IAHS-ICSI Publ.* [2] Sturm, M. et al. (1997) *J. Glac. 26*, 209-216. [3] Schneebeli, M. et al. (1999) *Cold Reg. Sci. Technol. 30*, 101-114. [4] Schneebeli, M. and Matzl, M. (2003) *Geophysical Research Letters, submitted*. [5] Johnson, J. B. and Schneebeli, M. (1999) *Cold Reg. Sci. Techno. 30*, 91-100. [6] Pielmeier, C. and Schneebeli, M. (2003) *Cold Reg. Sci. Technol, in press*.

MRO's HIGH RESOLUTION IMAGING SCIENCE EXPERIMENT (HiRISE): POLAR SCIENCE EXPECTATIONS. A. McEwen[1], K. Herkenhoff[4], C. Hansen[2], N. Bridges[2], W.A. Delamere[3], E. Eliason[4], J. Grant[5], V. Gulick[6], L. Keszthelyi[4], R. Kirk[4], M. Mellon[7], P. Smith[1], S. Squyres[8], N. Thomas[9], and C. Weitz[10]. [1]LPL, University of Arizona, [2]JPL, [3]Ball Aerospace and Tech. Corp., [4]USGS, [5]CEPS, Smithsonian Ins., [6]NASA Ames/SETI, [7]University of Colorado, [8]Cornell University, [9]University of Bern, Switzerland, [10]PSI/NASA HQ.

Introduction: The Mars Reconnaissance Orbiter (MRO) is expected to launch in August 2005, arrive at Mars in March 2006, and begin the primary science phase in November 2006. MRO will carry a suite of remote-sensing instruments and is designed to routinely point off-nadir to precisely target locations on Mars for high-resolution observations. The mission will have a much higher data return than any previous planetary mission, with 34 Tbits of returned data expected in the first Mars year in the mapping orbit (255 x 320 km).

The HiRISE camera [1] features a 0.5 m telescope, 12 m focal length, and 14 CCDs (Table 1).

Table 1. HiRISE Capabilities

Ground Sampling Dimension (GSD)	30 cm/pixel (at 300 km altitude)
Swath width (Red bandpass)	6 km (at 300 km altitude)
3-Color swath width	1.2 km (at 300 km)
Maximum image size	20,000 x 65,000 pixels
Signal:Noise Ratio (SNR)	>100:1
Color Bandpasses	Red: 550-850 nm Blue-Green: 400-600 nm NIR: 800-1000 nm
Stereo topographic precision	~20 cm vertical precision over ~1.5 m^2 areas
Pixel binning	None, 2x2, 3x3, 4x4, 8x8, 16x16; each CCD separately commanded.
Compression	Fast and Efficient Lossless Image Compression System (FELICS)

We expect to acquire ~10,000 observations in the primary science phase (~1 Mars year), including ~2,000 images for 1,000 stereo targets [2]. Each observation will be accompanied by a ~6 m/pixel image over a 30 x 45 km region acquired by MRO's context imager. Many HiRISE images will be full resolution in the center portion of the swath width and binned (typically 4x4) on the sides. This provides two levels of context, so we step out from 0.3 m/pixel to 1.2 m/pixel to 6 m/pixel (at 300 km altitude). We expect to cover ~1% of Mars at better than 1.2 m/pixel, ~0.1% at 0.3 m/pixel, ~0.1% in 3 colors, and ~0.05% in stereo. Our major challenge is to find the key contacts, exposures, and type morphologies to observe.

Landing Site Safety and Trafficability. A prime objective of HiRISE is to characterize landing sites and identify potential hazards to landed missions. The size and shape of boulders and other topographic obstacles considered dangerous varies from mission to mission, but, for example, 0.5-meter high boulders were considered potentially fatal to the 2001 lander (which may land in the north polar region via the Mars Scout mission called Phoenix [3]). MOC is able to detect giant boulders or detached chunks of bedrock larger than ~5 m diameter, but boulder counts are probably incomplete for objects smaller than ~10 m. Such large objects only occur in limited geologic settings such as near the base of steep slopes that are less than a few km high or near the rims of impact craters. For MER landing site studies it has been necessary to rely on extrapolations based on observed giant boulders using the size-frequency distribution of boulders at previous Mars landing sites and at Earth analog terrains, along with estimates of rock abundance from thermal models [4]. HiRISE will directly map out the distribution of boulders larger than 1 m diameter (typically 0.5 m high).

Mars Polar Science Issues. HiRISE will address many important polar science issues; a few examples are given below.

How recently did the mid-latitude gullies form?
Malin and Edgett [5] proposed that the gullies are young (probably less than 10^6 yrs) because there are usually no superimposed impact craters and because gully materials are superimposed over dunes and polygonally-patterned ground, which are young features on Earth (10^3 to 10^6 yrs for patterned ground [6]). This leaves open the possibility that gullies are forming today, and that liquid water may exist very near the surface. HiRISE can search for changes in the surface topography (compared with previous MOC or HiRISE images) that would indicate current activity of gullies. Evidence for current formation of dunes (possible) or patterned ground (less likely) would also help address this issue.

How can we use small craters for age constraints? There are almost no resolved craters on some polar deposits and high-latitude units such as gullies and debris flows, suggesting that they are extremely young. However, there are several major problems with the statistics of small craters: (1) primary craters may be confused with secondary craters [7]; (2) small craters are easily eroded or buried by eolian processes; (3) small craters may have endogenic origins, and (4) the atmosphere must screen out small and/or low-density bodies and affect the crater distribution. The improved spatial resolution and topographic capability of HiRISE will help address these issues via better discrimination between primaries and secondaries, improved understanding of eolian processes, and improved ability to discriminate between impact and endogenic craters. Extending crater counts to smaller diameters may also reveal clear evidence for atmospheric screening of small bodies, perhaps varying with surface elevation or time (e.g., climate change).

Were there vast ice sheets? Kargel and Strom [8] first proposed that thick, continent-sized ice sheets were present over the polar regions of Mars. If correct, this hypothesis has major implications for paleoclimates. Glacial moraines are characterized by poorly-sorted mixtures of particle sizes up to large boulders, so HiRISE should see clear evidence for this type of deposit, as well as the rich suite of other meter-scale morphologies associated with glaciers.

What was the origin of the Vastitas Borealis Formation? The northern plains are covered by poorly-understood materials; one interpretation is that these are ocean sediments [e.g., 9]. If correct, the sediments should have fine grain sizes except for widely scattered ice-rafted boulders. The detection of abundant boulders in these deposits might favor direct deposition from floods or mudflow deposits. HiRISE will certainly provide a rich set of observations on periglacial processes in the northern plains [10]. It may be possible to correlate morphologies to surface ice abundances mapped by other experiments.

What is the recent climate history recorded in polar layered deposits? MOC images resolve beds in the polar layered deposits (PLD) down to the resolution limit of the camera [11]. HiRISE images of the PLD are therefore likely to show stratigraphy at finer scales than previously observed, potentially addressing the major uncertainty in the timescales of layer formation. Similarly, higher-resolution images of the PLD will be useful in studying the deformation (faulting and folding) of the PLD [12]. Brightness variations in polar ice could be due to dust load or ice-grain size variations, which the color imaging should distinguish.

What is the efficacy of current eolian activity? Dune migration has not been seen in MOC-Mariner 9 comparisons over several decades [13] nor in MOC-MOC comparisons over a few years [14]. Failure of slip faces of the dunes has been noted [11]. With higher resolution, we might very well see dune motion, thereby providing calibration of the efficacy of eolian processes on Mars in the present day.

What is the polar CO_2 inventory? The "swiss cheese" terrain on the residual south polar ice cap has been observed to retreat 1 to 3 meters in 1 Mars year, apparently via sublimation of CO_2 ice [15]. Continued monitoring of these changes and high-resolution topographic measurements will enable us to better quantify rates of CO_2 loss and the total CO_2 inventory available to facilitate periodic climate change.

Monitoring seasonal change. HiRISE has the ability to image in very low light levels. With pixel binning up to 16x16 combined with 128 lines of Time Delay Integration (TDI), HiRISE can acquire good images under twilight conditions, thus better monitoring the polar regions during their winters.

References. [1] Delamere, W.A. et al. (2003), 6th Int. Mars Conf. [2] Eliason, E.M. et al. (2003), 6th Int. Mars Conf. [3] Smith, P.H. (2003) LPSC abstract 1855. [4] Golombek. M.P. et al (2003) LPSC abstract 1778. [5] Malin. M.C., and K.E. Edgett (2000) Science 288, 2330-2334. [6] Sletten, R.S., et al. (2003) JGR-Planets 108, No. E4, paper GDS25. [7] McEwen A.S. (2003), 6th Int. Conf. Mars. [8] Kargel, J.S., and Strom, R.G. (1992) Geology 20, 3-7. [9] Kreslavsky, M.A., and Head, J.W. (2003) JGR-Planets 107, paper 4. [10] Mellon, M.T. (1997) JGR-Planets 102, 25617-25628. [11] Malin, M.C. and Edgett K.S. (2001), J. Geophys. Res. 106, 23,429-23,570, 2001. [12] Murray, B. C. et al. (2002). *Icarus* **154**, 80. [13] Zimbelman, J.R., Geophys. Res. Lett., 27, 1069-1072, 2000. [14] Williams, K.K. et al., in press at Geophys. Res. Lett., 2003. [15] Malin, M.C., et al. (2001) Science 294, 2146-2148.

NEUTRON DETECTOR FOR MARS ROVER MISSIONS. J.E. Moersch[1] and D.M. Drake[2], [1]Department of Earth and Planetary Sciences, University of Tennessee, Knoxville, TN 37996, [2]221 LA Cruz Rd., Santa Fe, NM 87501, ddrake@cybermesa.com.

Introduction: Recent results from the Mars Odyssey orbiter mission have added immensely to our understanding of the distribution of water ice in the Martian polar deposits. Regional-scale mapping (~300-km resolution) by Odyssey's Gamma Ray Spectrometer [1] and its two neutron detector subsystems [2,3] has revealed shallow (~1m deep) subsurface deposits of water ice in concentrations ranging from 35-100% in the south polar region [4] and 50-75% in the north [5]. Odyssey's Thermal Emission Imaging System has also found thermal evidence for water ice exposed at the surface of the permanent southern cap, mapable at the 100-meter scale [6]. The next step in studying ice deposits in the polar regions of Mars will be to visit them on the surface with mobile robotic explorers. Rover missions offer the opportunity to map the small-scale distribution of water ice, study its mode(s) of deposition and removal, and perhaps gain insight into the climatic history of Mars.

When galactic cosmic rays interact with planetary material nuclei, a variety of particles are produced, including neutrons. Most of the neutrons produced in these interactions are characterized by energies in the 0.5-6 MeV ("fast") range. These neutrons lose energy by scattering from the nuclei in the surrounding medium. In general, neutrons lose more energy in collisions with lighter nuclei. Thus, the energy of neutrons that leak out of the surface is very sensitive to the presence or absence of hydrogen. The most likely reservoir of hydrogen in the Martian surface is water or water ice, although hydrated minerals (e.g. clays) may also account for some Martian H.

The primary signature of the presence of hydrogen in the regolith is carried by epithermal (0.3 eV-0.5 MeV) neutrons, because in this energy region a small amount of hydrogen is extremely effective on moderating the energy of the neutrons. The thermal neutron (<0.3 eV) flux is also related to the hydrogen content in that the neutrons that leave the epithermal flux end up becoming thermal neutrons. Thus, the ratio of thermal to epithermal neutrons leaking out of the Martian surface provides the best indicator of hydrogen content. Monte Carlo simulations suggest that in typical Martian soil, a range of water concentration from 0-5% (by mass) gives rise to ratios of thermal/epithermal neutron counting rates that vary by a factor of ~6.

Instrument Design: We have been funded by the Mars Instrument Development Program to adapt and optimize existing neutron detector designs that have flown on orbiter missions for use on future Mars rover missions. We have recently finished building our first prototype instrument. The instrument design we have selected is based on dual ^{3}He proportional counter tubes, an approach that has heritage from Lunar Prospector [7] and other orbiter missions. One tube is covered in a cadmium jacket, which absorbs incident thermal neutrons, blocking them from being counted. The other tube is left bare, making it sensitive to both thermal and epithermal neutrons. The difference in count rate between the two tubes gives the thermal count rate. The ratio of this rate to the count rate from the Cd-covered tube is the desired thermal/epithermal ratio. This type of instrument is uncollimated, so its effective sensing footprint is determined by the height of the instrument above the surface. Mounted on a rover, the instrument would be able to map subsurface ice abundances at the ~1-meter scale.

The active volume of each counter tube in our design is 20-cm long by 2.5-cm in diameter, a size chosen to balance the trade between keeping instrument mass and volume low versus minimizing the integration time needed to determine hydrogen abundance. Our calculations indicate that a 1-minute integration time on the Martian surface with this size tube gives an error in the thermal/epithermal ratio of about 4%, which gives a corresponding error in the determination of H-abundance of less than one percent.

The signals from each counter tube are fed to pulse-shaping electronics and then to a multichannel analyzer (MCA), which facilitates rejection of higher-energy pulses from gamma rays. The MCAs bin counts from each tube for a user-specified integration time. The MCAs are controlled and read via serial port connection to a laptop computer. In current form, all of the support electronics for the instrument fit in a volume about half the size of a shoe box, although this size could be greatly reduced using custom electronics.

Preliminary Tests: We are currently executing a series of tests with our instrument at Los Alamos National Laboratory to verify it performs as expected (Figure 1). On Earth, the thick atmosphere shields the surface from galactic cosmic rays, so a ^{252}Cf fast neutron source is used to simulate Martian fast neu-

tron production. Dry Martian soil is simulated with glass bricks. In some experiments, glass pans filled with liquid water were used to measure instrument sensitivity to hydrogen. In other experiments, slabs of polyethylene were used; polyethylene has about the same density of hydrogen as water and is easier to work with because it is solid.

Figures 1 and 2 show results from two sets of initial instrument evaluation experiment runs. The points in Figue 1 were obtained by measuring thermal/epithermal count ratios with varying amounts of liquid water at the surface of our soil simulant. As expected, the thermal/epithermal ratio increases as more water is available to moderate high energy neutrons from the source. The points in Figure 2 were obtained by burying different amounts of polyethylene under soil simulant. Once again, the thermal/epithermal ratio increases as more hydrogen is added.

In the near-future, additional lab tests will be performed to further characterize and quantify instrument performance. We will also experiment with different types of shielding (which would be used to block the signal from hydrogen sources on board the rover), instrument placement, and detector tube size.

Field Tests: After we are satisfied with our instrument design based on laboratory evaluations, we will subject it to a series of field tests intended to help us further refine the design and learn how to most effectively work with data from the instrument. In late 2003, we plan to install the instrument on the NASA Ames K-9 rover and perform simple tests with it using buried polyethylene slabs in the new outdoor "Marscape" test facility at Ames. In 2004, our instrument will be fully-integrated into the K-9 rover instrument suite for full-up Mars mission simulations with a "blind" science team remotely directing the rover and interpreting the data it returns. Our hope is that these simulations will demonstrate the utility our instrument would have for upcoming Mars rover missions.

References: [1] Boynton, W.V. et al. (2002) *Science, 297*, 81-85. [2] Mitrofanov, I. et al. (2002) *Science, 297,* 78-81. [3] Feldman, W.C. et al. (2002) *Science, 297,* 75-78. [4] Tokar, R.L. et al. (2002) *Geophys Res. Let., 29*, art. no. 1904. [5] Mitrofanov, I. et al. (2003) *Science, 300*, 2081-2084. [6] Titus, T.N. et al. (2003) *Science, 299*, 1048-1051. [7] Feldman, W.C. et al. (1999) *Nucl. Inst. Meth. Phys Res., 422*, 562-566.

Figure 1: Prototype instrument undergoing first tests. The two 20-cm long ^{3}He detector tubes are visible near the top of the image, held in place on vertical posts. Between the two tubes is a ^{252}Cf fast neutron source. Three layers of glass bricks under the tubes simulate martian soil. In this particular experiment, two glass pans containing water were placed between the first and second layer of glass bricks.

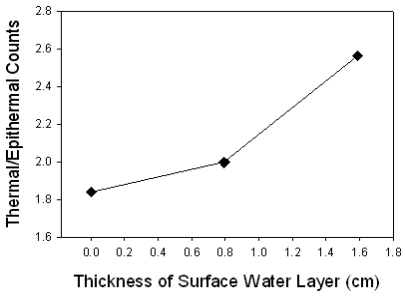

Figure 2: Ratio of thermal to epithermal neutron counts for different depths of water at the surface of our soil simulant. Integration times of 200s were used. As expected, the thermal/epithermal ratio increases with increasing water abundance. These counts are raw (not background-subtracted) and no error bars have yet been assigned.

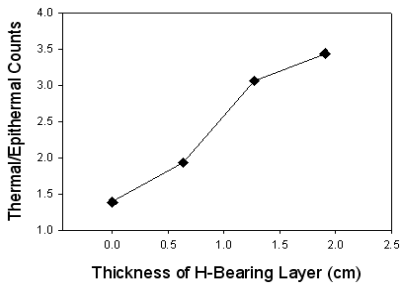

Figure 3: Ratio of thermal to epithermal neutron counts for varying amounts of polyethylene buried under 7.3 cm of soil simulant (which is equivalent to at least 15 cm of real soil because of the difference in density). Integration times of 200s were used. As expected, the thermal/epithermal ratio increases with increasing abundance of buried hydrogen. These counts are raw (not background-subtracted) and no error bars have yet been assigned.

DEVELOPMENT OF A MARS GENERAL CIRCULATION MODEL. Y. Moudden[1], S. R. Beagley, V. Fomichec, J. C. McConnell, A. Akingunola, A. Garcia Munioz. [1]York University Petrie Bldg 4700 Keele St, Toronto ON M3J 1P3 Canada (youssef@numbus.yorku.ca).

Efforts are underway in the Department of Earth and Atmospheric Science at York University to develop a General Circulation Model for Mars. The model, which we call MGEM, is based on the dynamic core of the Meteorological Service of Canada's weather forcast model GEM (Global Environmental Multiscale Model) and is a multiscale grid point semi-Lagrangian semi-implicit model, with a non-hydrostatic option. The multiscale option allows for a horizontal resolution that will enable us to address the mesoscale issues in the Mars atmosphere such as dust lifting mechanisms. The dynamical core has already been tested using TES temperature and surface pressure fields and MOLA topography from MGS. Appropriate changes to the physics parameterizations are being made to deal with the major components of Mars climate. These consist of solar and IR radiative scheme including a non-LTE package, a large scale carbon dioxide condensation scheme and its interaction with the total mass, a dust lifting and transport scheme with its effect on the energy budget. A comprehensive description of the water cycle including the subsurface transport in the regolith, the surface fluxes and the atmosphere transport and condensation is also being developed. The model also is capable of transporting species and chemical and aerosol packages will be added. Other groups within Canada, viz. at Dalhousie University, University of Toronto, University of Western Ontario and University of British Columbia, are planning to contribute to the effort.

We believe that MGEM will be a useful tool for the Martian scientific community, and with the increasing interest in the Mars exploration, MGEM will be useful for instrument design and planning for the future missions.

GEOPHYSICAL INVESTIGATIONS AT A MARS ANALOG SITE: DEVON ISLAND, NUNAVUT. Nieto, C.E.[1] and Stewart, R.R.[1], [1]Dept. of Geology and Geophysics, The University of Calgary (GLGP, 2500 University Dr., N.W., Calgary, Alberta, Canada T2N 1N4. cenieto@ucalgary.ca, stewart@ucalgary.ca).

Abstract

The Haughton meteorite impact structure, located on Devon Island, Nunavut is one of the most Mars-like places on Earth. The Haughton crater is cold (average temperature –17°C), dry, rocky, dusty, and windy. As part of the effort at NASA SETI Institute Haughton Mars Project (HMP), the University of Calgary Applied Geophysics Group conducted geophysical surveys, both ground-penetrating radar (GPR) and high-resolution seismic, in the summer of 2002. Objectives of the geophysical work were to image the permafrost layer as well as assess deeper geologic horizons.

GPR data were acquired using Sensors & Software NOGGIN 250 MHz system and PulseEKKO devices with 50 and 100 MHz antennae. These surveys imaged depths from about 0.5m to 3 m and indicate layering and permafrost events. High-resolution seismic results, recorded with a Geometrics 60-channel recording system and accompanying 28 Hz omni-directional geophones, also show the permafrost layer.

Shallow excavations, seismic refractions, and GPR reflections at the site all proved useful and indicate that the permafrost layer is at a depth of about 60cm. We also tested geophysical operations in prototype spacesuits and found the suits to be manageable although cumbersome. We plan on returning to the Haughton crater in the summer of 2003 for further geophysical surveying and system testing.

Introduction

The Haughton meteorite impact structure on Devon Island, Nunavut in the high Canadian Arctic is one of the most Mars-like places on Earth. The Haughton structure, at 75°22'N longitude and 89°41'W latitude, is a 23 Ma old impact crater about 20 km in diameter [1], [2]. Host rocks of the structure are of Ordovician and Silurian age, mostly of the Allen Bay formation [3]. The impact has left a very impressive scar on the landscape as seen from an airborne radar image.

The northwest region of the outer middle rim hosts the base camp for the Haughton Mars Project [4], [5], [6], [7]. Geophysical surveying can be difficult, even in the summer on Devon Island, due to the high winds of the polar area (up to 70 km/hr during this field survey), low summer temperatures (-5°C to +5°C), sleet, rain, snow - even though this is characterized as a desert [8], and significant ultraviolet radiation [9].

The site chosen for the GPR and seismic surveys was located near the base camp in the "Von Braun Valley" (VBV). We conducted another series of surveys several kilometres away at the "Gemini Hills", but only the VBV surveys will be discussed here. We dug several test pits near the base camp to investigate the composition of the near surface. We found a tan-coloured, saturated silt with small clasts down to depths of about 45 – 65 cm. We then encountered solid and uniform permafrost with the appearance of frozen silt.

Seismic and GPR surveys

We used a Geometrics Strata View 60-channel seismic recorder with 28Hz omni-geophones (planted in vertical and horizontal configurations). One of the seismic micro-spreads is shown in Figure 1. A small sledgehammer was employed as a source striking a base plate in either a vertical or horizontal direction.

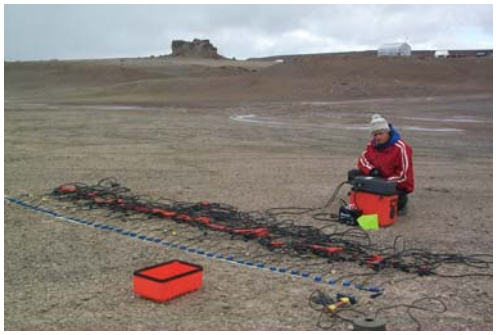

FIG. 1 Photograph the 3-C micro-seismic line in the "Von Braun Valley" at the HMP base camp.

We conducted a number of surveys using a variety of source-receiver combinations. That is, vertical source strikes and vertical receivers, horizontal hammer blows and transverse receivers, etc. A data example for a vertical hammer strike with horizontal, inline receivers (the P-S configuration) is shown in Figure 2.

We are still analysing the seismic data, but have determined very low preliminary P and S velocities in the near-surface silts (260m/s and 168m/s, respectively) with very high velocities in the permafrost (P-wave velocity = 3100m/s, S-wave velocity = 2060m/s).

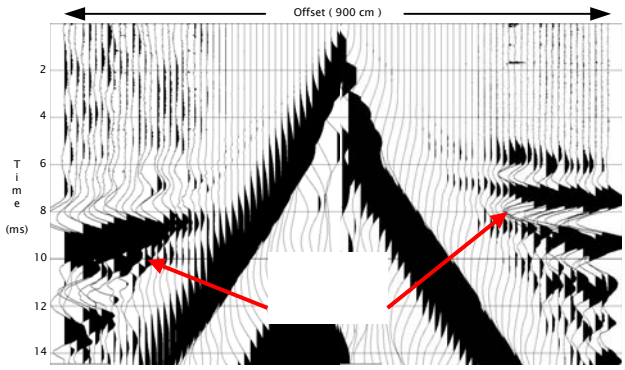

FIG. 2 Vertical hammer blow with inline (horizontal) receivers showing a high amplitude PSS refracted at the top of permafrost.

We processed the PP and PSS refracted data (as it has very high amplitude) into stacked sections that are shown in Figure 3. Since the velocity contrast between the permafrost and silt layer is so high the obtained sections correspond to a zero – offset stacked section. We interpret the dominant event on both sections to be the top of the permafrost [10].

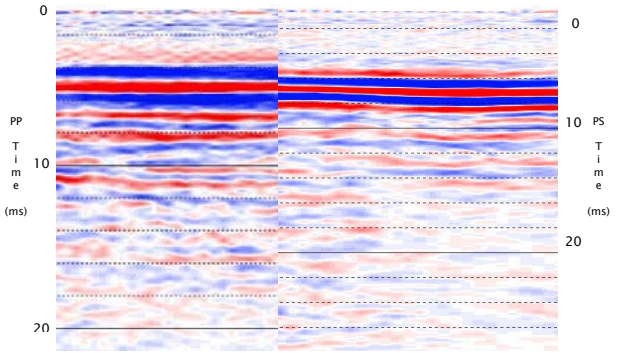

FIG. 3 Vertical hammer blow with inline (horizontal) receivers showing a high amplitude PSS refracted at the top of permafrost.

We also acquired a number of GPR lines in the Von Braun Valley. Use of the Sensors and Software NOGGIN SmartCart greatly simplified acquisition as one just rolls it across the surface and provides a real-time display of the radar arrivals. Having a similar acoustic system would be a great stride forward in subsurface imaging.

We also used a Sensors and Software 250 pulse EKKO system with 50 MHz and 100 MHz antennae in a walk-apart manner to determine radar velocity values. To assist with interpretation of the GPR data, we dug a trench down to the permafrost and pounded a 1m length of rebar into the end of the trench on top of the permafrost. We then surveyed orthogonally across the undisturbed ground above the rebar. This gave a strong diffraction from the rebar and helped determine which event to interpret as the permafrost top (Figure 4). We have experimented with a number of processing flows to find optimal filter, deconvolution, and migration parameters for the GPR data.

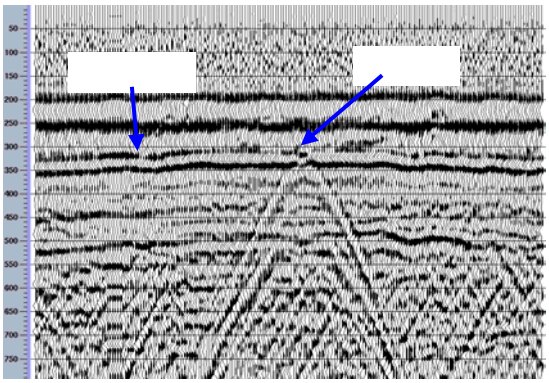

FIG. 4 GPR line from the NOGGIN 250 MHz System in the Von Braun Valley.

Conclusions

This paper provides a preliminary report of some of the geophysical findings of the HMP-2002 field surveys. Both seismic and GPR systems worked well in the field, under some harsh conditions, and provided useful information. Using test pits, reflected GPR data, and refracted seismic energy, we found the permafrost layer to be at about a 60 cm depth. Conducting field operations in prototype spacesuits was cumbersome, but manageable. We plan to return to HMP in the summer of 2003 for further surveys and analysis.

References

[1] Osinski, G.R. and Spray, J.G. (2001) *Eath and Planetary Science Letters, 194, 17-29.* [2] Osinski, G.R., Spray, J.G., and Lee, P. (2001) *Meteoritics and Planetary Science, 36, 731-745.* [3] Scott, D. and Hajnal, Z. (1988) *Meteoritics, 23, 239-247.* . [4] Lee, P. (2002a) *National Space Society, 14, 12-17.* [5] Lee, P. (2002b) *The Planetary Report, v. 1.* [6] Lee, P. (2002c) *The Planetary Report, v. 1.* [7] Long, M.E. (1999) *National Geographic, 196, 34-51.* [8] Cockell, C.S., Lee, P., Schuerger, A.C., Hidalgo, L., Jones, J.A., and Stokes, M.D. (2001) *Arctic, Antarctic, and Alpine Research: 33, 306-318.* [9] Cockell, C.S., Scherer, K., Horneck, P., Rettberg, P., Facius, R., Gugg-Helminger, A., Driscoll, C., and Lee, P. *(2002) Photochemistry and Photobiology, 74, 570-578* [10] Nieto, C. and Stewart, R.R. (2003) *2003 CSPG/CSEG Annual Meeting.*

Acknowledgements

We express our appreciation to the NASA Haughton-Mars Project and especially its principal investigator, Dr. Pascal Lee of NASA Ames. Thank you to Sensors and Software Inc. for GPR support. Many thanks to Mssrs. Eric Gallant and Henry Bland of the CREWES Project at the University of Calgary who provided logistical help. We thank the University of Calgary (especially former Department Head, Dr. Don Lawton) for equipment support. We are grateful to NSERC for providing financial assistance for University of Calgary student, Mr. Robert Birch, via a summer fellowship. University of Calgary graduate students Ms. Julie Aitken and Ms. Monica Moldoveanu have capably assisted in the analysis of these data. Geo-X Systems Ltd. of Calgary has generously provided further processing of the HMP GPR data.

HUBBLE SPACE TELESCOPE SEARCH FOR LOCALIZED OUTGASSING ON MARS

T. Ouvarova and J. Caldwell[1]; S. Atreya, A. Wong, and N. Renno[2]; P. James[3]
[1] York University (Earth and Space Science), 4700 Keele St.,Toronto, ON, Canada, M3J 1P3
[2] University of Michigan, Ann Arbor, MI, USA
[3] University of Toledo, OH, USA

Introduction: Evidence of recent groundwater seepage and surface runoff [1] (at mid and high latitudes) may suggest that current outgassing from small, localized sources on Mars is possible. Further, formaldehyde (CH_2O) has been tentatively detected in the equatorial region of Mars [2]. If this detection is confirmed with future observations, it would give more evidence to support the possibility of present-day localized outgassing occurring on Mars.

Photochemical models [3], based on terrestrial analogues, have identified methane (CH_4), sulfur dioxide (SO_2), and hydrogen sulfide (H_2S) as plausible outgassing products on Mars. Two of these gases have strong bands in the UV (SO_2) and near IR (CH_4) in the range of Hubble Space Telescope's (HST) detectors, however H_2S does not.

HST has obtained spectra of Mars from the UV (with its STIS – Space Telescope Imaging Spectrograph – instrument) to the near IR (by NICMOS – Near Infrared Camera and Multi-Object Spectrometer) in 1997 and 2001. We will analyze the archived data to search for evidence of these outgassing products.

Improving Detection Limits: Although these minor constituents have not been detected in global observations so far, localized outgassing sources concentrations may have been diluted in global averages, by as much as a factor of 10^8. To date, the current global average upper limits, obtained by the IRIS instrument on Mariner 9[4], are 0.02ppm (CH_4) and 0.1ppm (SO_2) at the surface. HST's high spatial resolution may help to detect these gases in local concentrations higher than their global average upper limits.

We are first analyzing STIS spectral data of Mars, to be followed with NICMOS data analysis. The angular resolution of the STIS CCD spectra of Mars is set the by the CCD's pixel size (0.05 arcseconds on the sky) and telescope's point-spread-function (0.1 arcsecond radius for 70% energy inclusion from a 'point source'). The spatial resolution (linear dimensions) is dependent on the distance of HST to Mars at the time of observation and the spectrograph slit width (4 or 10 pixels). For the data from 1997 and 2001, distance to Mars varied from 0.58AU to 1.79AU. This results in HST resolving regions on Mars from 14,000km² to 840,000km², or a 'resolved fraction' of 0.0004 to 0.024 of Mars' cross-section (global average), significantly improving upon the detection thresholds set by Mariner 9.

Data Characteristics: In the UV range of STIS, there is a significant grating scatter effect in the wavelength region below 2,200A. This instrumental effect causes the spectrum to appear to increase towards the lower-wavelengths (see Figure 1), compromising the data below 2,200A.

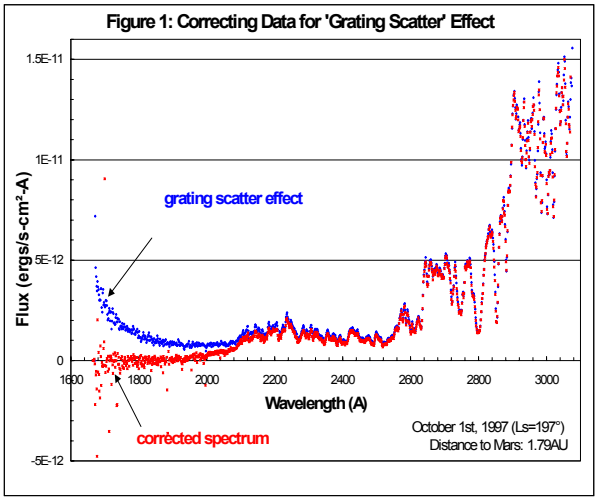

Complementary Images: With each set of spectral observation sets by STIS or NICMOS, typically HST's WFPC2 (Wide Field Planetary Camera 2) obtained images of Mars, within 2-3 hours of the spectral observations. Figure 2 shows one such image taken on October 1st, 1997, when Mars was 1.79AU from the HST, and the planetary disc spanned about 5.2 arcseconds in diameter.

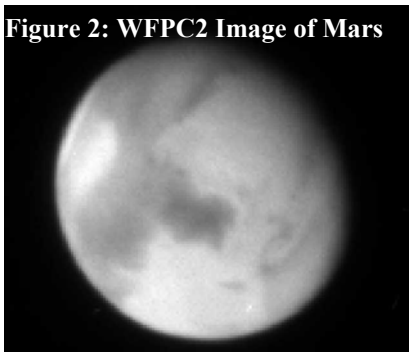

Mars Brightness Profile: STIS has the advantage of observing Mars simultaneously with spectral resolution (across the slit width) and spatial resolution (along the slit length). The disk of Mars, from pole to pole, is completely 'imaged' along the slit, and presents a 'brightness profile', averaged over eight pixels across the slit, in Figure 3.

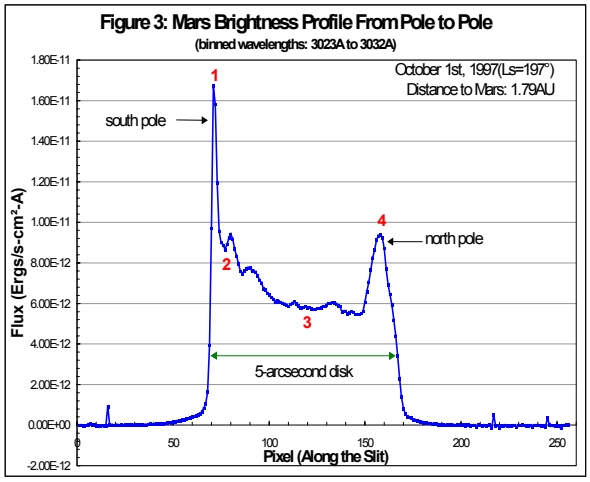

Four regions of interest are identified: the south pole (1), high latitude region close to south pole (2), equatorial region (3), and the north pole (4).

Spectra of Four Regions: UV Spectra, averaged over four pixels (along the slit), of the four regions of interest (as identified in Figure 3), are shown in Figure 4.

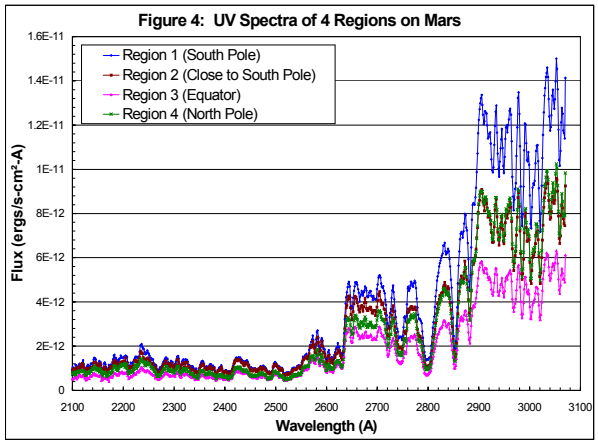

The spectra shown in Figure 4 (same observation, on October 1, 1997) have been corrected for the grating scatter effect. Spectral resolution is approximately 11A.

Analysis Plans: We plan to perform extensive analysis of the available spectral data of Mars, from both the STIS and NICMOS instruments on the HST. The spectra will be compared to the known absorption bands of CH_4 and SO_2. Adjacent spectra, along the slit, will be compared to each other, for any regional variations in the absorption features. A STIS spectrum of the Moon, taken with same instrument settings as the Mars spectra, will be used as a solar surrogate spectrum. This will produce Mars albedo spectra independent of any instrument aliasing effects that could occur when comparing spectra taken with different instruments. Figure 5 shows an image of the Moon taken by the HST, contemporaneous with the STIS spectral data.

Figure 5: HST Image of Moon (1999)

We will correlate any evidence of the signature gases found during the analysis with the available high-resolution images of Mars taken by the Mars Global Surveyor (MGS) during the observation runs.

Detailed Observations in the Future: Even if no conclusive evidence of CH_4 and H_2S is found, the HST spectral data will improve the upper abundance limits on these gases. The STIS exposure time calculator will be used to estimate possible improvements in the data with the STIS MAMA detectors, which have higher sensitivity and do not suffer the grating scatter effect in the UV region.

References:

[1] Malin, M.C. and Edgett, K.S. (2000) *Science, 288,* 2330-2335

[2] Korablev et al. (1993) *Plant. Space Sci., 41*, 441-451

[3] Wong, A.-S., Atreya, S.K. and Encrenaz, T. (2003) *J. Geophys. Res., 108(E4)*, 5026, doi: 10.1029/2002JE002003

[4] Maguire, W.S. (1977) *Icarus, 32*, 85-97

Further Information:

Please contact Tatiana Ouvarova by email: tats000@yorku.ca

PRESERVATION OF ANCIENT GLACIAL ICE BELOW SUBLIMATION TILL IN THE DRY VALLEYS OF ANTARCTICA: IMPLICATIONS FOR MARS. A. V. Pathare[1], D. R. Marchant[2], and J. W. Head[3], [1]Division of Geological and Planetary Sciences, California Institute of Technology (avp@gps.caltech.edu), [2]Department of Earth Sciences, Boston University (marchant@bu.edu), [3]Department of Geological Sciences, Brown University (James_Head@brown.edu).

Introduction: Recent observations of circumpolar Martian terrains by the Gamma Ray Spectrometer are most consistent with the presence of widespread water ice in the uppermost meter of the near-surface blanketed by a thin dusty mantle [1]. A key question for Martian climatology concerns the stability of this buried ice: most models presume that the rate of exchange with the atmosphere is primarily a function of near-surface and atmospheric temperatures [e.g., 2].

However, the preservation of buried glacial ice in the dry valleys of Antarctica suggests a more complex mantle-dependent process. Within Beacon Valley, a thin till layer known as "Granite drift" that is less than one meter thick overlies stagnant Miocene glacier ice, the minimum 8.1 Ma age of which is derived from $^{40}Ar/^{39}Ar$ analyses of volcanic ash deposits within Granite drift that appear to lie conformably above the ice [3]. Furthermore, the concentration of cosmogenic ^{3}He in dolerite cobbles within the till exhibits steadily decreasing values that are most consistent with drift formation via sublimation of underlying ice [4].

If Granite drift is a layer of sublimation till, then the Antarctic paleoclimate has likely been relatively stable for several million years, since any significant climatic fluctuations would probably have melted the underlying remnant ice. Moreover, the long-term stability of Antarctic ice would suggest that much colder Martian ice could persist beneath similarly thin layers for even longer periods of time. Thus it is important to fully understand the reasons for Antarctic ice stability.

Sublimation of ice through an overlying mantle can be expressed as a combination of Fickian diffusion of concentration gradients and pressure-driven Darcian transport [5]:

$$q_v = -bD\phi\frac{\partial C}{\partial z} + \frac{k}{\mu}\frac{\partial p}{\partial z}C$$

where q_v is the vapor flux, C is the gas concentration, D is the diffusion coefficient, ϕ is the porosity, b is the tortuosity (which provides a measure of the complexity of transport paths within the mantle), k is the permeability, μ is the viscosity of the atmosphere, and p is the atmospheric pressure. Boundary conditions at the ice- mantle interface can be derived from saturation vapor pressure curves, while those at the surface are dictated by atmospheric humidity.

Hindmarsh *et al.* [5] showed that for typical Antarctic ice and till conditions, the sublimation flux into a dry atmosphere is $q_v = 10^{-3}$ m/yr, which is three orders of magnitude greater than the 10^{-6} m/yr required to preserve Miocene ice in Beacon Valley. They also showed that the near-saturation conditions proposed by [3] to inhibit sublimation should result in water ice condensation throughout the overlying till layer; such widespread icing is not observed in Granite drift [4]. Therefore, Hindmarsh *et al.* [5] concluded that the ice beneath Granite drift could only be over 8 Myr old if the porosity or tortuosity of the till layer is significantly lower than the combined value of $b*\phi = 0.2$ suggested by laboratory analogues.

Salinity: We propose that the presence of salts—which are particularly prominent in Antarctic soils [6]—may reduce sublimation rate in the dry valleys. Salt has two potential inhibiting effects, both related to brine formation due to the lowering of the melting point. First, the saturation vapor pressure of a solution decreases linearly with salt content as per Raoult's Law (indeed, this decrease is what lowers the melting point). Secondly, tortuosity varies inversely with liquid water content; hence, formation of thin briny films at temperature well below the pure ice melting point could greatly impede water vapor flow.

We will test this hypothesis by incorporating the effects of salt solutions into a finite difference vapor transport model similar to that of Hindmarsh *et al.* [5], and comparing our results to profiles of salt content through Granite drift that we obtained earlier this year in Beacon Valley.

Martian Implications: Interestingly, Mars may also provide a test of our hypothesis, for if the Gamma Ray Spectrometer detects a correlation of near-surface water ice content to the constitiuent elements of salts suchs as sulfates and nitrates, then this would strongly suggest that a common process is occurring in both Mars and Antarctica. GRS correlations observed in equatorial regions would be especially important, since the stability of non-polar ice deposits is difficult to explain with standard Martian diffusion models [2].

References: [1] Boynton W. et al. (2002) *Science, 297,* 81. [2] Paige D.A. (1992) *Nature, 356,* 43. [3] Sugden D.E. (1995) *Nature, 376*, 412. [4] Marchant D.R. (2002) *GSAB, 6,* 718. [5] Hindmarsh R.C. et al. (1998), *Geog. Ann*., *80A*, 209. [6] Claridge, G.G. et al. (1977), *Soil Sci.*, *123*, 377.

ELECTROMAGNETIC PROPAGATION MODELLING FOR GPR EXPLORATION OF MARTIAN SUBSOIL. E. Pettinelli[1], P.Burghignoli[2], A.Galli[2], A.R.Pisani[1], F. Ticconi[2], D. Del Vento[3] and A.Cereti[3], [1]Università Roma Tre - "E.Amaldi" Physics Department - Via della Vasca Navale, 84 00146 Rome, Italy, e-mail: pettinelli@fis.uniroma3.it, [2]Università La Sapienza – Electronic Engineering Departement – Via Eudossiana, 18 00184 Rome, Italy, [3] IFSI-CNR, Via del Fosso del Cavaliere, 100 00133 Rome, Italy.

Introduction: The use of GPR for Mars exploration has been suggested by several authors in the past ten years [1-5]. Some of the instruments proposed in the late 90s were designed to investigate the subsurface at great depth (thousands of meters)[1,2,4] and therefore implemented a measurement technique quite different from traditional GPR [6,7]. The interest toward a detailed investigation of the first few meters of Mars subsurface, linked to the exploration of past or present life on the planet, requires, however, the use of such a traditional technique, which is well established and has been widely applied on the Earth [7].

It is well known that GPR performance is maximized when it is applied in a very 'resistive' environment, like that expected in a cold and dry planet. Very little is known on the electromagnetic properties (permittivity, permeability, and conductivity) of the Martian soil [8], but the absence of liquid water on surface and in the shallow subsurface should in principle assure a good penetration of the signal.

Both Viking and Pathfinder missions have shown, however, that strongly magnetic mineral phases are present in the Martian dust [9,10] and therefore highly magnetic phases are also expected in the soil. Moreover, measurements from the Gamma Ray Spectrometer (GRS) experiment onboard the *Mars Odyssey* spacecraft [11-13] support the existence of significant quantities of shallow subsurface water ice in certain parts of the planet. The highest concentrations occur pole-ward from about 60° N and 60° S, as interpreted on the basis of the specific patterns of detected neutrons and spatial correlations with regions where ground ice has been predicted to be stable. The presence of both icy soil and magnetic materials may significantly affect the attenuation values and thus the achievable GPR penetration depth.

The main scope of the present work is to predict GPR propagation and attenuation features at 225 MHz and 900 MHz in Martian-like materials on the basis of the electromagnetic parameters measured in the laboratory, and also to evaluate the effect of volumetric scattering for possible in homogeneities (intrusions) in the planetary subsurface.

Laboratory measurements Dielectric measurements on different soil samples and mixtures have been performed in the frequency domain (20 *Hz* – 1 *MHz*) using a capacitive cell [8], while magnetic measurements have been performed in the same frequency range using a toroid. Table 1 summarizes the results at 1 *MHz* for the materials used in the simulations.

Note that CO_2 powder and CO_2 powder plus volcanic sand have also been included because they are common materials in the Martian polar caps, whereas the sample with magnetite has been considered in order to investigate the effect of a soil having a high iron oxide content.

Table 1

Martian soil simulants	ε'	ε"	μ'	μ"	σ (*S/m*)
CO_2 Powder	1.4	0.002	1.0	-	$1.0x10^{-7}$
CO_2 Powder+Volcano Sand	2.1	0.018	1.0	-	$1.0x10^{-6}$
Dry Volcano Sand	3.0	0.018	1.01	0.00056	$1.0x10^{-6}$
Icy soil (20% wt ice)	5.0	0.540	1.0	-	$3.0x10^{-5}$
Basalt	6.2	0.026	1.0	-	$1.0x10^{-6}$
Glass beads+Magnetite (15% wt)	4.54	0.043	1.3	0.006	$2.4x10^{-6}$

It should be underlined that the values at 1 *MHz* might represent an overestimation of both permittivity and permeability with respect to the values obtainable at hundreds of *MHz*, while the values for conductivity may be underestimated. However, these materials have shown a rather nondispersive behaviour at lower frequencies, and their values at 1 *MHz* were not very different from those measured at higher frequencies with a TDR (time domain reflectometry) technique [8].

Attenuation of GPR signals In order to evaluate the attenuation of the electromagnetic waves in the first few meters of the Martian soil, taking into account both the presence of the ice and the iron oxides, some calculations have been developed. Table 2 summarizes the attenuation and the skin depth obtained in the materials presented in Table 1 at two different frequencies.

Table 2

Martian soil simulants	**225 *MHz***		**900 *MHz***	
	Attenuation (*dB/m*)	Skin depth (*m*)	Attenuation (*dB/m*)	Skin depth (*m*)
CO_2 Powder	0.02	357.1	0.10	89.4
CO_2 Powder+Volcano Sand	0.51	16.9	2.06	4.2
Dry Volcano Sand	0.65	13.3	2.61	3.3
Glass beads+Magnetite (15 *wt%*)*	0.81	10.7	3.25	2.7
Magnetite grains (100%)*	5.51	1.6	22.06	0.4
Icy soil (20 *wt%* H_2O ice)	5.23	1.7	20.92	0.4
Basalt (dry)	0.21	40.6	0.86	10.2
*Grain size range: 200-500 μm				

In addition to the intrinsic attenuation of the involved media, the effect of scattering by small particles randomly distributed inside a host material has also been considered. In particular, a model of composite materials with spherical inclusions has been developed, and the resulting attenuation has been calculated on the basis of Mie theory of plane-wave scattering by dielectric spheres. Typical behaviours of total attenuation as a function of particle dimensions are shown in Figs. 1(a) and (b), for basalt spherical inclusions embedded in dry volcano sand and in CO_2 powder, respectively. It can be observed that maxima and minima may occur in the attenuation curve, especially at high frequencies, connected with free resonances of the inclusions.

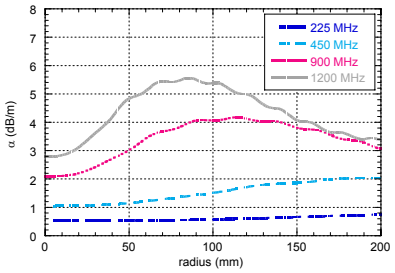

Fig. 1a

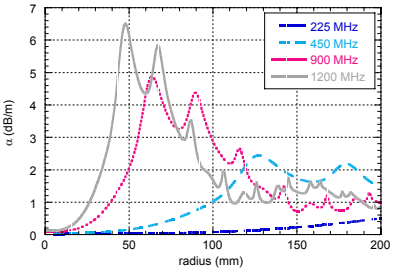

Fig. 1b

Maximum penetration depth The maximum depth of a detectable interface has been calculated using the radar range equation [6] and the *PulseEkko* Software version 4.2 (Sensors and Software Inc., Mississauga, ON, Canada). Table 3 shows the L values obtained for rough interfaces between different materials, where a two-layered soil model has been considered.

Table 3

Material interfaces	L_{max} (*m*) 225 *MHz*	L_{max} (*m*) 900 *MHz*
CO_2 Powder+Volcano Sand/ Volcano Sand	13.6	3.4
Glass Beads+Magnetite (15 *wt%*)/Icy soil	7.7	1.9
Magnetite grains (100%)/Icy soil	3.6	0.9
Icy soil/Basalt	2.7	0.7
Dry Volcano sand/Icy soil	12.5	3.1

Finally Figs. 2(a) and (b) show the maximum penetration depth achievable respectively with 225 and 900 MHz antennas as a function of the magnetite content (with a basalt as a bottom layer).

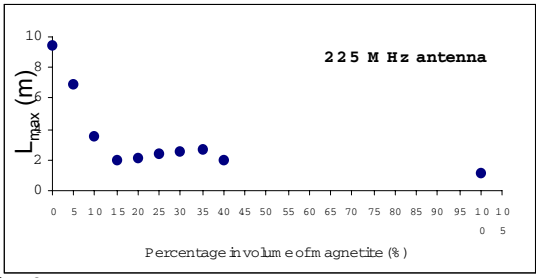

Fig. 2a

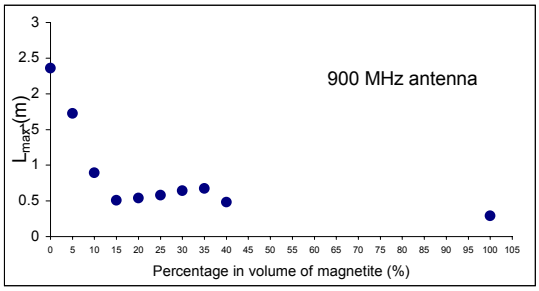

Fig.2b

References

[1] Barbin Y.et al., (1995*), JAG, 33*, 27-37
[2] Berthelier, J.J. et al. (2000), *PSP, 48,* 1161-1180
[3]Grant J.A. et al., (2003), *JGR, 108,* 1856-1865
[4]Berthelier J.J. et al., (2003) *JGR, 108*, 1866-1875
[5] Leuschen C. et al., (2003*) JGR, 108*, 1876-1885
[6] Annan A. P. (1992), Sens. and Soft., Canada
[7] Daniels D. J. (1996), Surface-Penetrating Radar
[8] Pettinelli E. et al., (2003) *JGR, 107*, 8029-8040
[9] Hargraves R.B. et al., (1979) *JGR, 84*, 8379-8384
[10] Madsen M.B. et al., (1999) *JGR, 104*, 8761-8779
[11] Boynton W. V. et al., (2002) *Science, 297,* 81-85
[12] Feldman W. C. et al., (2002) *Science*, *297,*75-78
[13] Mitrofanov I.et al., (2002) *Science*, *297,* 78-81

MODEL FOR FORMATION OF SPIDER PATTERNS IN THE CRYPTIC REGION. G. Portyankina and W.J. Markiewicz, Max Planck Institut für Aeronomie, Max-Planck-str., 2, Katlenburg-Lindau, 37191, Germany

Introduction: The cryptic region is one of the most dominant albedo features in data from Thermal Emission Spectrometer (TES) onboard of the Mars Global Surveyor (MGS). It is situated between latitudes 73°S and 81°S and longitudes 175°W and 225°W. Its main characteristic is that it remains cold well after it attains an albedo similar to the Martian soil. This low albedo is in contradiction with the low temperature that is close to that of CO_2 ice. One possibility to resolve this paradox is to assume that a large fraction of the solar flux passes through a surface layer of CO_2 ice and is absorbed by the dust underneath it. This is possible if the ice is slab CO_2 ice. Within this cryptic region Mars Orbiter Camera also onboard of MGS has taken images of radially converging dendritic patterns example of which is shown in Figure 1.

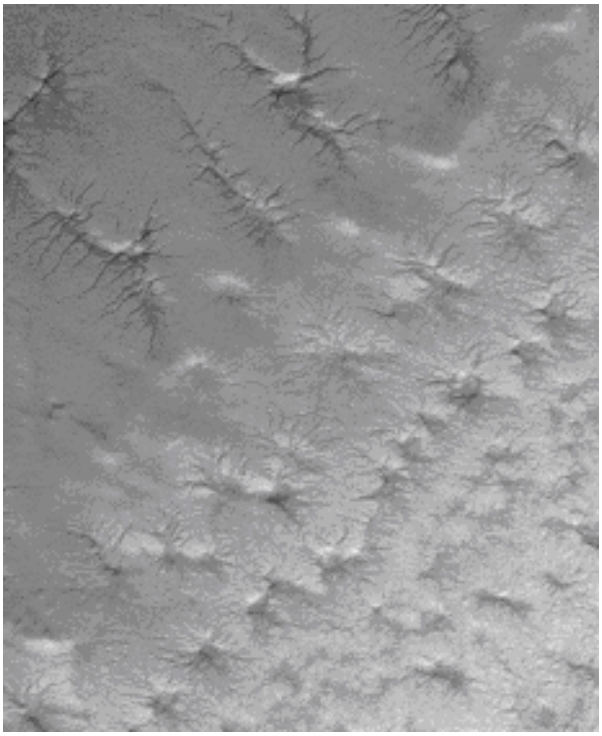

Fig. 1 MOC image showing an example of spider ravins.

These spiders are unique patterns of South Polar Regions. They have never been seen before neither in other regions on Mars nor on other Solar System bodies. A descriptive model for formation of such a patterns was proposed by [1]. The winter condensation of CO_2 includes atmospheric dust in roughly its average atmospheric mass fraction. The CO_2 slab ice is virtually transparent to solar radiation with 72% of solar energy reaching the bottom of a 1 metre thick layer [2]. Dust will modify the depth of penetration of sun light but can not influence the basic aspects of the model as long as the solar penetration is greater than the thermal flux attenuation length [1]. Dust grains embedded in the CO_2 slab will absorb solar radiation on a time scale of less than one second [3] and form individual gas pockets around themselves. The grains will rest in a gas layer, continue to sublime the ice underneath it, and "sink" downwards. Net result should be clean CO_2 ice with dust accumulating at the bottom. The transparent layer of the slab CO_2 ice will have low temperature and the underlying dust low albedo - the situation observed in the cryptic region. With increasing solar radiation flux during spring, the temperature of dust in and under the ice will increase raising the sublimation rate of CO_2 ice. The gas formed during sublimation at the bottom of the slab layer cannot diffuse through the CO_2 deposit and localized escape pathways should develop. Those of them large enough to carry adequate warm gas from the sub-layer to remain open will grow into vertical columnar vents. Mixture of fine dust grains and CO_2 gas can be ejected through them and redistributed according to wind direction to form patterns of spiders. In this model these patterns represent channels formed by sub-slab channelized flow of the sublimation gas towards the vents.

Model of cleaning CO_2 ice: The modeling of spiders' formation should include mechanism of cleaning dusty CO_2 ice to produce an ice slab transparent for most of the solar radiation that can reach the surface of Mars through its atmosphere. As a first step we calculated the timescale for this cleansing process. We consiered two types of shapes for dust grains: spheres and cylinders with the ratio height/radius = 1/10. Dust grains receive Solar radiation amount of which depends on time of day, season and and latitude of the place inside cryptic region. All radiation received by the dust grain is assumed to go into sublimation of the ice underneath it; the grain sinks to the bottom of sublimed volume – and in such a way moves downward inside the ice. Time needed for cleaning of 1-meter thick CO_2 slab ice by such a process was calculated for different particle shapes and orientations. Plots in Figure 2 show distance from the top of slab to the dust grain center (grain radius is 2.5 μm) versus time (starting with the southern spring at $L_s = 150^o$) for spherical grains and differently oriented cylinders. Curves are: cylindrical dust particle tilted by 10^o from vertical (1), 30^o (2), 60^o (3), 90^o (5), and spherical dust particle (4).

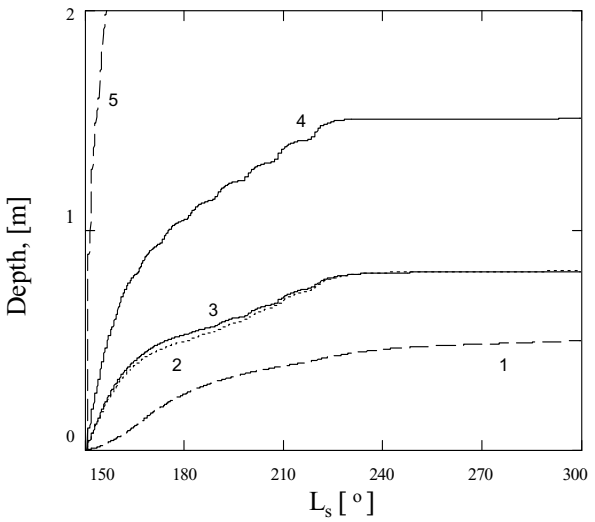

Figure 2 Depth to wich particles sink as a function of time

As the CO_2 ice evaporates, the boundary atmosphere-ice will move downward as well as dust particles. The comparison of the rates of two processes is shown at Figure 3. The dashed lines show the depth of boundary atmosphere-ice, curves are shown for several values of albedo, line 1 – depth of cylindrical dust particle tilted by 10^o from vertical and line 2 – depth of spherical dust particle.

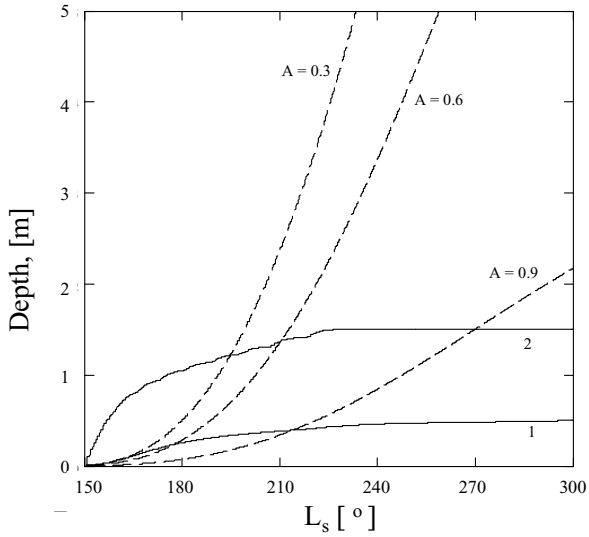

Figure 3 The comparison of particles sinking rate and the rate of ice sublimation.

Our initial estimates of the time scales critical for the cleaning process show that this aspect of the model is feasible.

Future work: We plan to create a physical model for the formation of spiders including elements such as: absorption of solar flux by dust imbedded in the CO_2 ice, sinking of the dust particles, and build up of pressure at the bottom of the CO_2 slab.

References:

[1] Kieffer, H.H. (2000) International Conference on Mars Polar Science and Exploration, p. 93. [2] Hansen, Gary B. (1997) *JGR, 102*, 21569-21587. [3] Kieffer, H.H. ; et al. (2000) *JGR, 105*, 9653-9699.

Martian North Polar Impacts and Volcanoes: Feature Discrimination and Comparisons to Global Trends. S. E. H. Sakimoto[1] and S. L. Weren[2,1], [1] GEST at the Geodynamics Branch, Code 921, NASA Goddard Space Flight Center, Greenbelt, MD 20771, sakimoto@geodynamics.gsfc.nasa.gov, [2]Geoscience Department, Franklin and Marshall College, P.O. Box 3003, Lancaster PA, 17604, serena.weren@fandm.edu.

Introduction: The recent Mars Global Surveyor and Mars Odyssey Missions have greatly improved our available data for the north polar region of Mars. Pre-MGS and MO studies proposed possible volcanic features [e.g., 1, 2] , and have revealed numerous volcanoes and impact craters in a range of weathering states that were poorly visible or not visible in prior data sets. This new data has helped in the reassessment of the polar deposits [e.g. 3, 4, 5] From images or shaded Mars Orbiter Laser Altimeter (MOLA) topography grids alone, it has proved to be difficult to differentiate cratered cones of probable volcanic origins from impact craters that appear to have been filled. It is important that the distinction is made if possible, as the relative ages of the polar deposits hinge on small numbers of craters, and the local volcanic regime originally only proposed small numbers of volcanoes. Therefore, we have expanded prior work on detailed topographic parameter measurements and modeling for the polar volcanic landforms [e.g. 6-10] and mapped and measured all of the probable volcanic and impact features for the north polar region as well as other midlatitude fields, and suggest that 1) The polar volcanic edifices are significantly different topographically from midlatitude edifices, and have steeper slopes and larger craters as a group, 2) the impact craters are actually distinct from the volcanoes in terms of the feature volume that is cavity compared to feature volume that is positive relief, and that 3) there are actually several distinct types of volcanic edifices present, and that 4) these types tend to be spatially grouped by edifice. This is a contrast to many of the other small volcanic fields around Mars, where small edifices tend to be mixed types within a field.

Approach: For topographic measurements, we use the released MOLA profiles to grid 30 degree regions at 128 pixels per degree longitude and 256 pixels per degree latitude (approximately 460 m/pixel by 230 m/pixel) using G. Neumann's crossover correction approach to gridding [11] and the publicly available GRIDVIEW software [12]. We measure parameters such as those in [13-14] and [6] for impact craters and volcanoes, respectively. For craters, this includes crater width, depth, rim height, ejecta thickness, rampart height, cavity volume, ejecta volume, etc… For volcanoes, this includes height, diameter, mean flank slope, max flank slope, crater depth, diameter, and volume, edifice volume, area, basal elevation, and locations. The volcano modeling includes the hydrostatic head models used in [7,8]. Examples of some of the features measured are shown in Figure 1 and include impact craters with a relatively fresh cavity, impact craters with filled cavities, cratered cones, steep near-polar cratered cones, and a field of steep cratered cones. The features in this region are compared to those in Tempe Mareotis, Syria, Tharsis, Elysium, the South Polar region, and others.

Figure 1. High resolution MOLA topography shown as shaded relief for A) a fairly fresh polar impact crater, B) a group of partially filled polar impact craters, a C) large cratered cone, D) a group of several near polar cap cratered cones, and E) A field of steeper cratered cones.

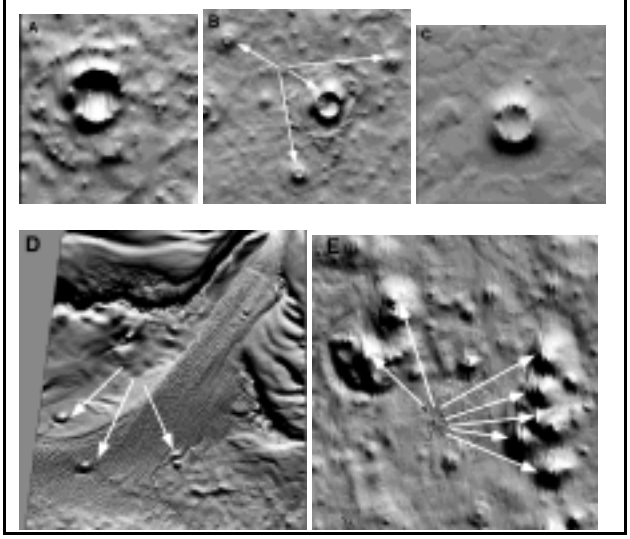

Results:

Polar and Mid-latitude differences. The higher resolution measurements support earlier conclusions that the polar volcanoes are systematically different than the midlatitude volcanoes in flank slope, crater sizes, and other parameters, and that their flank slopes as a group continue the global trend of increasing average flank slope with increasing latitude [e.g. 7, 8].

Impact Crater or Volcano?? While the cratered cones of presumed volcanic origin [e.g. 2, 6] have craters perched above the surrounding plains, local impact –craters with readily apparent ejects ramparts also have craters perched above the surrounding plains, and for those craters with minimal eject ramparts, the volcano/crater distinction is not always obvious in images or topographic grids. Additionally, the volume/diameter versus flank slope that helps differenti-

ate between volcano types sometimes yields overlapping impact and crater field plots (see Fig. 2).

Figure 2. This plot shows feature volume/diameter versus average flank slope in log-log axes for Tempe small volcanic features (in gray for comparison), polar small volcanic features (red triangles), and polar impact craters (blue circles).

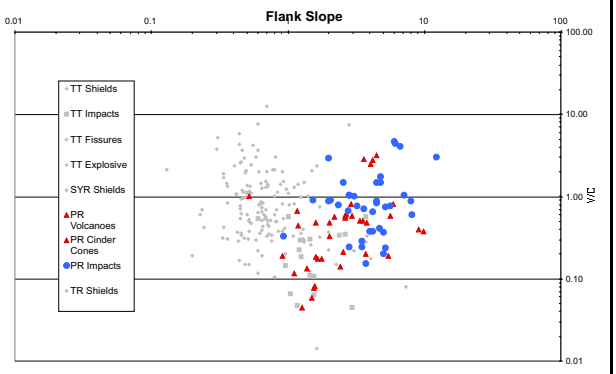

However, the readily identifiable impact craters with remnant ejecta blankets and topographically visible ramparts have a larger fraction of the landform occupied by the crater cavity than the features mapped as probable volcanoes do. We use this observation as the basis of plotting newly identified probable volcanoes and possible volcanoes with the impact craters in Figure 3, as crater cavity volume/edifice volume versus crater diameter. This plot tends to show fairly distinct impact and volcanism fields may hat help separate enigmatic features by most likely origins.

Volcanic Types and Origins. With the higher resolution topographic data, the prior suggestion of several different volcanic types within the polar volcanic landforms [e.g. 8, 10, 15] appears much more robust. The large cratered cones identified by several authors as probable volcanics are distinct from the steeper (< 7 degrees flank slope) cratered cones found closer to the polar cap, and these are also distinct from the cluster of steep cratered cones found directly between the polar cap and Alba Patera. The latter features overlap significantly, range in sizes, and are quite numerous within a defined region, while the near polar steeper cones tend to be more isolated, or are found in small groupings.

Conclusions: 1) Polar and mid-latitude volcanoes are fundamentally different in topography, thus and presumably eruption style, 2) Careful parameter measurements appear to assist in differentiating between impact and volcanic features, and there are several probable volcanic edifice types present in the north polar region, with the implication that eruption styles by sub-region tend to be distinct.

References: [1]Tanaka, K. L. and Scott, D. H. (1987) USGS Map I-1802-C. , [2] Hodges, C. A. and Moore, H. J. (1994) USGS Prof. Pap. 1534. [3] Tanaka et al., JGR-Planets, *108* (E4), GDS 24-1, CiteID 8043, DOI 10.1029/2002JE001908, 2003. [4] K.L. Tanaka, and E.J. Kolb, Regional Geologic History of the Polar Regions of Mars, *International Conference on Mars Polar Science and Exploration,*, p 168-169, 2000.[5] Plaut, J. J. et al. (1988) Icarus 73, 357-377. [6] Garvin J.B. et al., (2000), *Icarus*, 145, 648-652. [7] Sakimoto S.E.H. et al., (2002) *LPSC XXXIII*, Abstr.#1717. [8] Sakimoto S.E.H. et al., (2001) *LPSC XXXII,* Abstr.#1808. [9] Wong, M.P. et al., (2001) *LPSC XXXII,* Abstr.#1563. [10] Weren, S.L. and S. E. H. Sakimoto, Abstract #66446, submitted to GSA Fall meeting, 2003. [11] Neumann, G.A., et al., JGR, *106* (E10), p. 23573-23768, 2001. [12] Roark, J., et al., *LPSC XXI, Houston, TX*, *CDROM*, Abstract # 2026, 2000. 13] Garvin, J.B., et al., *LPSC XXI, Houston, TX*, *CDROM*, Abstract # 1619, 2000. [14] Garvin, J.B., et al., *Icarus*, *144* (April), 329-352, 2000. [15] Sakimoto, S.E.H., et al., *LPSC XXI, Houston, TX*, *CDROM*, Abstract #1971, 2000.

Acknowledgements: This research was supported in part by funding from the Mars Data Analysis Program and the MOLA Scence Team. Essential software support from J. Roark, helpful discussions and support from J. Garvin, and supplemental funds for S. Weren from H. Frey and Franklin and Marshall College are gratefully acknowledged. We thank E. King and J. Chadwick for assisting with collection of high-resolution mid-latitude volcanism data.

Figure 3. This plot shows crater cavity volume/edifice volume versus diameter for polar features. Polar impact craters (filled blue circles), large cratered cones previously mapped as volcanoes (large open red triangles), small cratered cones that are probable volcanis features (large filled red triangles) andsome enigmatic features that appear to be possibly volcanic (small filled red triangles) so far tend to be fairly distinct groupings. We are in the process of adding more complete data.

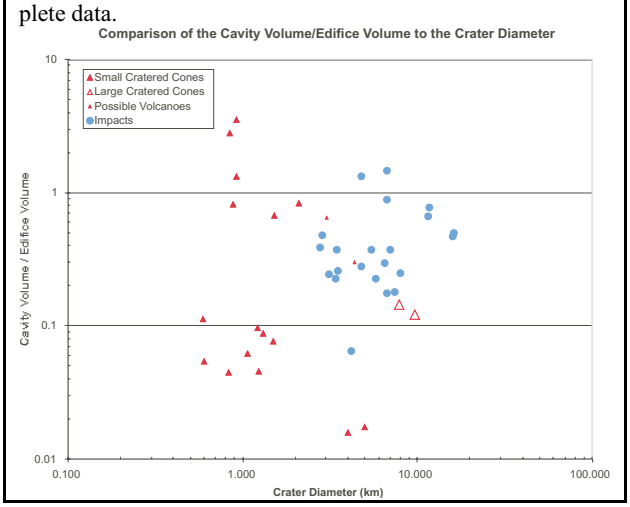

INVESTIGATION OF EXCHANGE PROCESSES IN THE MARTIAN WATER CYCLE. K. G. Schmidt, *Center for Planetary Science, University of Copenhagen, Denmark (kgs@gfy.ku.dk).*

Introduction

Water is found on Mars in the three reservoirs: The polar caps, the permafrost, and the atmosphere. We focus on the processes of mass exchange of water between the atmosphere and the polar caps as well as exchange with the regolith in order to investigate the relative importance of the two surface reservoirs to the present water cycle on Mars.

The polar caps of Mars are believed to consist mostly of water ice with large amounts of dust in both of them and some CO_2 ice. On images from space crafts stripes or layers are seen on the slopes of the polar caps facing the equator, which may be related to climate changes in the history of Mars, just as the climate history of the Earth is captured in the ice caps of Greenland and Antarctica.

A characteristic feature of the north polar cap is a spiralling pattern of scarps and troughs organised around the pole. Horizontal or north-facing areas appear white, while the scarps expose the dark layers. The alternating white polar ice and exposed layers suggest that the cap interacts with the atmosphere through deposition and sublimation processes and plays an active role in the current water cycle on Mars. The spiralling scarps and troughs are thought to be formed in a combination of sublimation, wind effects, deposition and ice flow [1,2].

In the northern summer, water may sublimate both from the North polar cap and from the northern lowlands, which were recently shown to contain large amounts of water beneath the surface [3]. This water may be stored as permafrost, adsorbed water, or water of hydration, depending on the latitude. However, a surface dust cover would protect subsurface ice from sublimating, e.g. as observed on terrestrial glaciers. The polar cap may thus be the dominant source of water vapour with its white surface and exposed ice deposits.

The spatial and temporal distribution of water vapour in the atmosphere has been measured by the Mars Atmospheric Water Detector (MAWD) on the Viking Orbiters [4, 5] and extracted from the Thermal Emission Spectrometer (TES) on the Mars Global Surveyor (MGS) [6].

Results

The model couples a simple atmospheric model with transportation of water by eddy diffusion and a sublimation and deposition model for the surface.

The sublimation rate of water from the ice surface is controlled by the saturation pressure of water vapour over an ice surface, which is a function of temperature, and the partial pressure of water vapour in the atmosphere, which varies in time. For the lower latitudes models for permafrost and adsorbed water are used.

Datasets for temporal and spatial water vapour abundance in the atmosphere and spatial distribution of water in the surface reservoirs are combined with model results in order to obtain understanding of the water exchange and circulation.

References

[1] Howard, A.D., et al., (1982). *Icarus*, 50, 161–215.

[2] Fisher, D.A. (1993). *Icarus*, 105, 501–511.

[3] Odyssey data: Boynton, W.V., et al., (2002). *Science*, 297, 81–85, (10.1126/science.1073722). Feldman, W.C., et al., (2002). *Science*, 297, 75–78, (10.1126/science.1073541). Mitrofanov, I., et al., (2002). *Science*, 297, 78–81, (10.1126/science.1073616).

[4] Farmer, C.B., et al., (1977). *JGR*, 82, 4225–4248.

[5] Jakosky, B.M. and C.B. Farmer, (1982). *JGR*, 87, 2999–3019.

[6] Smith, M.D., (2002). *JGR*, 107 (doi:10.1029/2001JE001522).

THE FORMATION AND DETECTABILITY OF CO_2 CLATHRATE HYDRATE ON MARS. B. Schmitt, L. Mulato and S. Douté. Laboratoire de Planétologie de Grenoble, UJF/CNRS, Bât. D de Physique, B.P. 53, 38041 Grenoble Cedex 9, France. E-mail: Bernard.Schmitt@obs.ujf-grenoble.fr

Introduction: CO_2 clathrate hydrate is suspected to be present near the surface of the south polar cap of Mars, and covered by seasonnal CO_2 frost during winter. After sublimation of this frost during summer times, it may be locally present at the surface where it may eventually decompose [see e.g. 1]. However there are currently no direct proof of its existence. Very limited laboratory spectral data are available in the mid-infrared and none in the near-infrared. Thermodynamical data on the formation, stability and decomposition rates are also sparse.

Clathrate Formation: Kinetic experiments have been performed on the formation of CO_2 clathrate by direct interaction of CO_2 gas with water ice grains at low temperature (195-213 K) [2]. We show the effects of several gas and solid phase parameters on the clathrate hydrate formation rates: temperature, pressure difference with dissociation pressure, specific surface area and surface stability of water ice, ... The stability of the CO_2 clathrate and its decomposition kinetics have been also studied. Microphysical mechanisms for both formation and decomposition processes are proposed.

CO_2 clathrate on Mars. The conditions for CO_2 clathrate formation and stability in the atmosphere and at the surface of Mars are discussed and the formation rates are estimated from the extrapolation of our laboratory data to the relevant Mars conditions.

Clathrate IR spectrum: We are currently performing laboratory experiments on the spectroscopic properties of CO_2 clathrate hydrate in the fundamental modes region (mid-infrared) and in the combination and overtone bands region (near-infrared).
We will present the result of this study focusing on the spectral signatures that may allow us to discern between pure CO_2 ice and CO_2 clathrate in the reflectance spectra of the polar caps.

Detectability of CO_2 clathrate. Using the optical constants of water ice [3], CO_2 ice [4] and those we expect to obtain for CO_2 clathrate hydrate we are performing radiative transfer calculations [5] to assess the detectability of CO_2 clathrate in reflectance spectra of Mars polar caps for different microphysical situations: 1) "pure" CO_2 clathrate; 2) mixed with CO_2 frost; 3) overlying water ice; 4) with a CO_2 frost layer on top; 5) thin water ice layer (from clathrate decomposition) overlying CO_2 clathrate. This study is performed at full spectral resolution (1 cm^{-1}) as well as at the resolution of the OMEGA spectro-imager (Mars Express mission).

References: [1] Kargel J. and Lunine J.I. (1998) *Solar System Ices,* Kluwer, 97-117. [2] Schmitt B. (1986) *Thesis, UJF-France,* 201-230. [3] Grundy W. and Schmitt B. (1998) *JGR E,* 103, 25809-25822. [4] Quirico E. and Schmitt B. (1997) *Icarus,* 127, 354-378. [5] Douté S. and Schmitt B. (1998) *JGR E,* 103, 31367-31390.

SUBLIMATION AND CONDENSATION FLOWS IN CHASMA BOREALIS: A SENSITIVITY STUDY USING A 2-D ENSEMBLE MESOSCALE CIRCULATION MODEL. T. Siili, *Finnish Meteorological Institute / GEO, FIN-00550 HELSINKI, FINLAND, (Tero.Siili@fmi.fi)*, A. Määttänen, *Division of Atmospheric sciences, FIN-00014 University of Helsinki, FINLAND*.

Introduction and background The University of Helsinki's 2-D Mesoscale Circulation Model (MCM) [1] has been adapted for Martian conditions in early 1990s [2] to create the University of Helsinki (UH), Division of Atmospheric Sciences (ATM) 2-D Mars MCM (MMCM). The model has since been used and developed at both UH/ATM and Finnish Meteorological Institute (FMI), Geophysical Research (GEO) to study a number of martian mesoscale circulations, especially so-called *surface-induced* phenomena. Among the forcing and circulation types are [2–5]:

- slope winds,
- (CO_2 and H_2O) ice edge winds,
- winds driven by horizontal variations in albedo, thermal inertia and horizontal dust optical thickness.

The model also incorporates a basic H_2O transport scheme, but no dust transport as of yet. A fairly comprehensive description of the model can be found in, *e.g.* [6].

Ensemble approach To our knowledge, until recently this and other MMCMs have been used in what might be called *single-forecast* mode, producing a single simulation result or a forecast from essentially a single set of initial and boundary conditions [7]. As those conditions are bound to have errors and the models are sensitive to initial conditions, *ensemble*-type approaches have, however, been and are being introduced to terrestrial operational numerical weather prediction systems in the recent years. In these approaches a set of simulations with varied and disturbed initial or boundary conditions is run and the forecast and a confidence estimate are derived from the set of results using, *e.g.*, statistical analyses. These approaches provide improved confidence in the range of and perhaps better robustness of the results obtained. Such multi-run approaches do multiply the requirements for computational resources and are hence in many cases prohibitively costly, even in terrestrial operational applications. For an introduction of the ensemble approaches, *see*, *e.g.*, the Web site (and links and references therein) of the European Centre for Medium-range Weather Forecasts (ECMWF) at `http://www.ecmwf.int/`.

For Mars research purposes the 3-D MMCMs are much more realistic, but at least in the near future probably remain computationally much too expensive for such systematical and more comprehensive statistical studies. The computational cost of the 2-D MMCM is only a fraction of a contemporary 3-D MMCM; hence a 2-D MMCM is a much more feasible tool for use in (at least initial) studies using ensemble approaches with reasonable set or sample sizes: in this early phase a typical sample size has been 5–50 runs.

At least two main sub-approaches to the ensemble approach can be identified: *parameter space mapping* and *Monte Carlo*-approach. Parameter space mapping implies a set of simulations run using, *e.g.*, systematically and deterministically varied initial or boundary values of some parameters (essentially using a parameter space grid) to investigate and analyse — also with statistical methods — the domain and range of the results. The Monte Carlo approach includes in addition or in stead introduction of (correlated or uncorrelated) random variations in selected parameters.

An environment enabling the use of an ensemble approach with the UH/ATM 2-D MMCM has recently been implemented and is currently being further developed at FMI/GEO. This environment comprises simulation preparation (including selection of variables to-be-perturbed as well as perturbation types and magnitudes) and statistical analysis tools — the latter providing statistical quantities such as pointwise set average, range, variance as well as distributions of the solutions included in a simulation set. Our first application of the system has been an idealised sensitivity study of mesoscale circulation and water transport phenomena occurring and emerging in a polar cap region where H_2O ice is being exposed in the springtime from under the wintertime CO_2 cover — perhaps in a patchy and irregular fashion [8].

Case study: influence of sublimation and condensation flows on regional circulation patterns in the Chasma Borealis area In this work we expand on earlier 2-D simulations of Martian winds across an idealised valley geometry. The geographical context is the northern polar terrain — especially the Chasma Borealis region and its section close to the pole. In this region the valley axis is directed approximately along a latitude circle. Our primary interest is in the interactions between the larger-scale sublimation and condensation flows and the regional flows up and down the valley walls, with secondary interest in the influence of the shape and dimensions of the valley cross section on the ensuing circulation patterns. In the geographical area of study the sublimation and condensation flows are expected to have substantial across-valley components.

In Chasma Borealis we have a varied topography due to the valley combined with seasonally varying coverages of H_2O and CO_2 ices. The topography drives slope winds and the ice coverage variations and the associated albedo and thermal inertia contrasts drive sea-breeze type thermal circulations. Hence, in a configuration and situation such as this a complex set of circulation patterns is expected to occur due to the combined slope, sea-breeze type and large-scale sublimation/condensation flow forcings. Since in our earlier works the large-scale influences have been studied less, we have here focussed thereon, corresponding to both spring/summer/sublimation as well as autumn/winter/condensation situations. Both parameter space mapping and the Monte Carlo approaches have been used.

Our goals here include: further testing of the feasibility of the ensemble approach as well as provision of improved (and perhaps more robust) insight into this type of regional features

of the Martian mesoscale circulations and the associated water cycle.

Funding for this work was provided by the Academy of Finland (project 51441) and is gratefully acknowledged.

References

[1] Alpert P, Cohen A, Neumann J and Doron E, 1982. A model simulation of the summer circulation from the Eastern Mediterranean past Lake Kinneret in the Jordan valley. *Mon. Wea. Rev.*, **110**:994–1006.

[2] Savijärvi H and Siili T, 1993. The Martian slope winds and the nocturnal PBL jet. *J. Atmos. Sci.*, **50**:77–88.

[3] Siili T, 1996. Modeling of albedo and thermal inertia induced mesoscale circulations in the midlatitude summertime Martian atmosphere. *J. Geophys. Res.*, **101**:14957–14968.

[4] Siili T, Haberle R M and Murphy J R, 1997. Sensitivity of Martian southern polar cap edge winds and surface stresses to dust optical thickness and to the large-scale sublimation flow. *Adv. Space Res.*, **19**:1241–1244.

[5] Siili T, Haberle R M, Murphy J R and Savijärvi H, 1999. Modelling of the combined late-winter ice cap edge and slope winds in Mars' Hellas and Argyre regions. *Planet. Space Sci.*, **47**(8-9):951–970.

[6] Siili T, 1999. *Two-dimensional modelling of thermal terrain-induced mesoscale circulations in Mars' atmosphere*. Ph.D dissertation, Helsinki University of Technology. Available as Finnish Meteorological Institute Contributions No. 27, Helsinki, Finland.

[7] Siili T, Savijärvi H, Määttänen A and Kauhanen J, 2003. Two-dimensional simulations of martian mesoscale circulation phenomena: a review and future role. In Desjean M C, Forget F, Lopez-Valverde M and Newman C, eds., *Proceedings of the workshop on Mars atmosphere modelling and observations*, pp. 6–4. Centre national d'etudes spatiales, European Space Agency, Instituto de astrofisica de Andalucia, Laboratoire de meteorologie dynamique / Centre national de recherches scientifiques, University of Oxford.

[8] Siili T, 2003. Simulations of mesoscale circulations and water transport in regions of water ice being exposed: first 2-D ensemble results. In *Proceedings of the 6th international conference on Mars*. Lunar and Planetary Institute, Houston, TX, USA.

THE APPLICATION OF THE ELECTRIC SOUNDING TECHNIQUE TO THE SEARCH FOR WATER AT SHALLOW DEPTHS WITH PLANETARY LANDERS AND ROVERS: A SURVEY OF THE RSSD-ESA ACTIVITIES

Fernando Simoes, Roland Trautner and Rejean Grard
Planetary Mission Division
Research and Scientific Support Department
European Space Agency
ESTEC, Keplerlaan 1, PO Box 299
2200 Ag Noordwijk, The Netherlands

The possible presence of subsurface solid or liquid water can be detected *in-situ* by measuring the electric properties of the soil. The Research and Scientific Support Department (RSSD) of the European Space Agency (ESA) has been engaged in the design of dedicated space instruments since 1990, when we first proposed a technique for measuring the complex permittivity of solid or liquid materials with multipolar arrays. In short, an alternating current is injected in the ground by means of two transmitter electrodes and the induced differential voltage is measured by two receiver electrodes. Information about the electric properties of the medium is derived from the voltage/current ratio, or mutual impedance of the quadrupole.

We shall review the specificity and complementarity of the various ongoing and planned activities, which form this line of research at RSSD in partnership with other laboratories.

(1) Laboratory characterization of the electric properties of water, and water mixtures, at low frequencies
The conductivity and permittivity of any material is strongly influenced by the presence of water and by temperature. This feature can serve as an indicator of water but is not well understood.

(2) Design and realization of space instrument concepts.
Prototype arrays with different configurations are designed and tested for specific applications and integration on platform, rover and drill systems.

(3) Laboratory and field tests:
The purpose of laboratory and field tests is twofold. They provide, on the one hand, information about possible planetary soil characteristics, e.g. the properties of Mars simulants as functions of temperature and water content. They serve, on the other hand, to validate the performances of candidate instruments in given environments.

(4) Numerical simulation and modeling.
The interpretation of results obtained with a mutual impedance probe in homogeneous media is rather straightforward, but deciphering the response of a layered or inhomogeneous environment is more intricate. A three-dimensional numerical code, presently under development, will simulate the response of composite terrains in general, and the effect induced by the presence of buried rocks and cavities, in particular.

(5) Experiment proposals and development of flight instruments:
Quadrupolar probes are parts of the scientific payloads carried by Huygens, which will land on Titan in January 2005, and the Rosetta lander, which will make contact with the nucleus of comet Churyumov-Gerasimenko in November 2014. Similar instruments have been proposed for Mars missions (e.g. Exomars).

INTERANNUAL COMPARISON OF WATER VAPOR IN THE NORTH POLAR REGION OF MARS. L. K. Tamppari[1], M. D. Smith[2], A. S. Hale[3], and D. S. Bass[3], [1]NASA Jet Propulsion Laboratory (4800 Oak Grove Drive, Pasadena, CA 91109 leslie.k.tamppari@jpl.nasa.gov), [2]NASA Goddard Space Flight Center (Michael.D.Smith.1@gsfc.nasa.gov), [3]NASA Jet Propulsion Laboratory (MS 264-235, 4800 Oak Grove Drive, Pasadena, CA 91109 amy.s.hale@jpl.nasa.gov), [4]NASA Jet Propulsion Laboratory (MS T1722, 4800 Oak Grove Drive, Pasadena, CA 91109 deborah.s.bass@jpl.nasa.gov).

Introduction: The Martian water cycle is one of the three annual cycles on Mars, dust and CO2 being the other two. Despite the fact that detailed spacecraft data, including global and annual coverage in a variety of wavelengths, have been taken of Mars spanning more than 25 years, there are many outstanding questions regarding the water cycle.

There is very little exposed water on Mars today, in either the atmosphere or on the surface [1] although there is geological evidence of catastrophic flooding and continuously running water in past epochs in Mars' history [2] as well as recent (within about 10,000 years ago) evidence for running water in the form of gullies [3].

The north polar cap region is of special interest as the residual cap is the main known reservoir of water on the planet today. The south polar residual cap may contain water, but presents a CO2 ice covering, even during southern summer. This hemispheric dichotomy is unexplained and is especially puzzling due to the fact that the Martian southern summer is much warmer (due to Mars' eccentricity) than the northern summer. Recently, water has been found in the top meter of the surface in both the northern and southern high latitude regions [e.g. 4-5] indicating an even greater amount of water on Mars than previously known.

Background: In order to better understand the current climate of Mars, we seek to understand atmospheric water in the north polar region. Our approach is to examine the water transport and cycling issues within the north polar region and in/out of the region on seasonal and annual timescales. Viking Mars Atmospheric Water Detector (MAWD) data showed that water vapor increased as the northern summer season progressed and temperatures increased, and that vapor appeared to be transported southward [6]. However, there has been uncertainty about the amount of water cycling in and out of the north polar region, as evidenced by residual polar cap visible brightness changes between one Martian year (Mariner 9 data) and a subsequent year (Viking data). These changes were originally thought to be interannual variations in the amount of frost sublimed based on global dust storm activity [5-7]. However, Viking thermal and imaging data were re-examined and it was found that 14-35 pr □m of water -ice appeared to be deposited on the cap later in the summer season [9], indicating that some water may be retained and redistributed within the polar cap region. This late summer deposition could be due to adsorption directly onto the cap surface or due to snowfall. We seek to understand what happens to the water on seasonal and interannual timescales. We address these issues by examining water vapor in the north polar region of Mars during the north spring and summer period from MGS TES data and by comparing these results to the Viking MAWD results.

Method:

Water vapor. Smith *et al.* [10] have performed retrievals for the column-integrated abundance of water vapor using the rotational water vapor bands at 220-360 cm^{-1}. Atmospheric temperatures are first retrieved using the 15-□m CO_2 band (Conrath *et al.*, 2000). Next, a forward radiative transfer computation is used to find the column-integrated water abundance that best fits the observed water vapor bands. At this time water is assumed to be well-mixed up to the condensation level and then zero above that. A total of six water vapor bands between 220 and 360 cm^{-1} are observed in TES spectra and the widths and relative depths of all six bands are very well fit by the synthetic spectra. Because the spectral signature of water vapor is spectrally very distinct from those of dust and water-ice, we can easily separate the relative contributions from each component (dust, water-ice, and water vapor) on a spectrum-by-spectrum basis.

Recent analysis with MGS TES data has shown evidence for water vapor "pulses" as the seasonal north polar cap sublimes [15]. This could be linked to the previous late-summer season deposition, discussed above. There appear to be significant differences in the details of the water vapor as a function of latitude and season between the Viking era and the current era (Figure 1). These differences may be a degree of interannual variability in the water vapor or a result of the coverage differences (Figure 2). Note that in Fig. 2, there are large differences in the MAWD coverage between the Ls=80°-95° bin (bin 7) vs. the Ls=95°-110° bin (bin 8). The TES coverage is much more uniform over time due to its orbit. An understanding of these possible interannual differences is important in several ways: (1) to understand the Martian climate, (2) to characterize the extent of interannual variability or lack thereof , and (3) to understand water-cycling within the north polar region and potentially in/out of the region. We will present our results of the investigation of the differences in these water vapor column amounts.

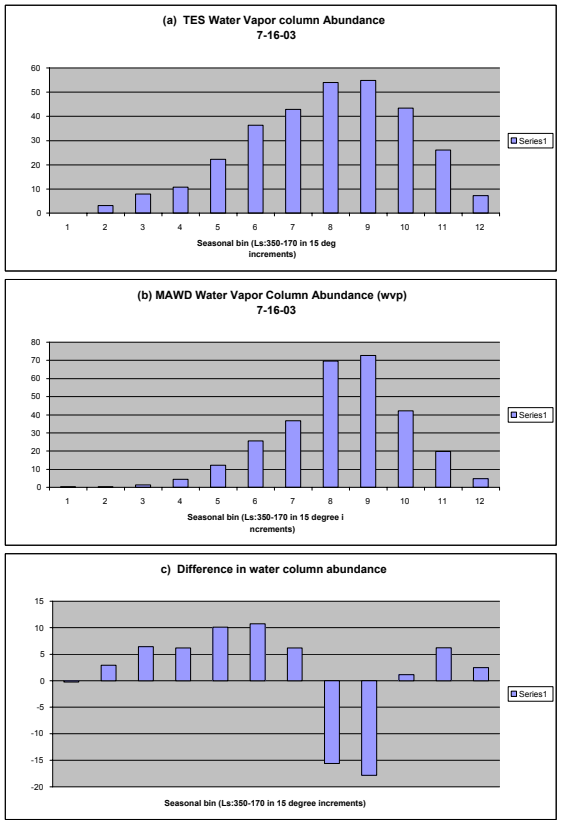

Figure 1. (a) TES water vapor column abundance in pr microns for the north polar region (60°-90°N). The seasonal binning is plotted Ls=15° increments, beginning at Ls=350° and ending at Ls=170°. Note that there is no TES data plotted for the first seasonal bin, Ls=350°-5°. (b) MAWD water vapor column abundance for same region and seasonal bins. MAWD data are shown for Ls=350°-5°. (c) The difference between the TES water vapor column abundance amount and the MAWD water vapor column abundance amount as a function of season.

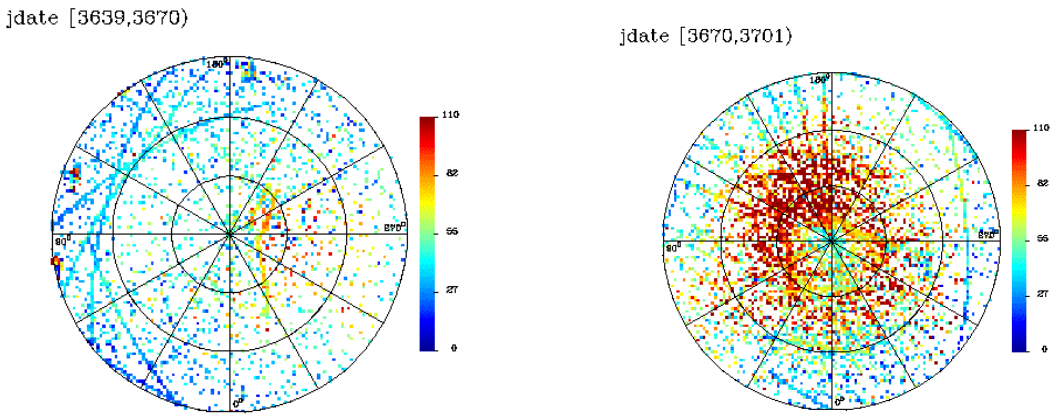

Figure 2. (Left) MAWD water vapor coverage shown for the Ls=80°-95° bin (bin 7). (Right) Similar for the Ls=95°-110° bin (bin 8). Note that the coverage near the cap center is much denser for the later season, possibly explaining the greater amount of water vapor measured during that season than in the previous season.

References: [1] Keiffer H. H. et al. (1976) *Science*, 194, 1341-1344 [2] Carr, M. H. (1998) *Water on Mars* [3] Malin M. C. and Edgett, K. S. (2001) *JGR* 106, 23429-23570. [8] Feldman W. C. et al., (2002) *Science* 297, 75-78 [4] Boynton W. V. et al., (2002) *Science* 297, 81-85 [5] Jakosky, B. M. (1985), Space Sci. Rev. 41, 131-200. [6] James P. B. and Martin L. (1985) *Bull. Amer. Astron. Soc., 17,* 735. [7] Kieffer H H. (1990) *JGR, 96,* 1481-1493. [8] Tamppari L. K. and Bass D. S. (2000) *2nd Mars Polar Conf.* [9] Tamppari L. K. et al. (2002) *Bull. 34th Am. Astron. Soc.,* 845. [10] Smith M. D. et al. (2000), *Bull. AAS*, 32(3), 1094.

DISTRIBUTION AND MORPHOLOGY OF POLYGONS, SOUTH POLAR REGION, MARS. S. van Gasselt, D. Reiß, R. Jaumann, *German Aerospace Center DLR, Institute of Planetary Research, D-12489 Berlin, Germany (Stephan.vanGasselt@dlr.de).*

Abstract: In this work we present a mapping of polygonal patterns at the south pole of Mars between 80°-90°S on the basis of all MOC narrow angle images (up to the current release of E18). We found 750 (out of 6000) MOC narrow angle images showing a variety of polygonal patterns resmebling terrestrial ice wedge polygons. They occur predominately inside circular depressions of the polar layered deposits, circum polar troughs and re–entrants or below slopes.

Introduction: Small–scale polygonal patterns have been observed in Viking Lander imagery [1]. Their morphology and development have often been ascribed to contraction cracking processes, analogous to terrestrial ice wedge polygons and are an indicator for the presence of subsurface water [e.g., 2]. With high resolution imagery from the Mars Orbiter Camera the features have been mapped and classified on a global scale by [3] and [4]. The main focus on analyzing the origin of polygonal patterns has been put on their distribution at southern and northern latitudes of $> \pm 40°$N. In this work we provide a detailed mapping of polygonal patterns at the south pole of Mars (s. fig. 2). The patterns are described on the basis of morphology and distribution.

We have mapped polygonal crack patterns on MOC narrow–angle imagery (up to E -18 release) and combined the results with color–coded MOLA digital elevation models superimposed on the MSSS MOC wide–angle MC–30 imagemosaics.

Geologic Setting and Observations: According to the geologic mapping of [5] the south polar region between 80°S and 90°S consists of the residual ice cap (Api) shifted towards longitudes between 0°W and 90°W. The remaining area is mainly covered by the Amazonian aged polar layered deposits (Apl) with small patches of non–polar related plains unit (s. fig. 1). At longitudes between 265°W and 90°W parts of the upper and lower Hesperian aged Dorsa Argentae Formation are exposed (Hdu, Hdl). The lateral distribution of this unit is equivalent to the area of low elevation (1200 m, blue color, s. fig. 2). At 10°W and between 70°W to 95°W remnants of the undivided Hesperian and Noachian material (HNu) which has undergone degradation processes by removal of ground ice, mass wasting and eolian removal occur.

We observe several regions (marked A–E, s. fig. 1) with clusters of polygonal patterns in MOC imagery. The distinct circum polar distribution (D) of polygonal patterns at 87°S is due to the dense coverage of imagery. The circum polar distribution at 87°S does not continue on the surface of the residual polar cap but spreads along circum polar troughs (C). Especially at longitudes >270°W the polygons are bound to the polar troughs, where (a) the trough material is older than the polar layers at the surface, (b) degradation and removal

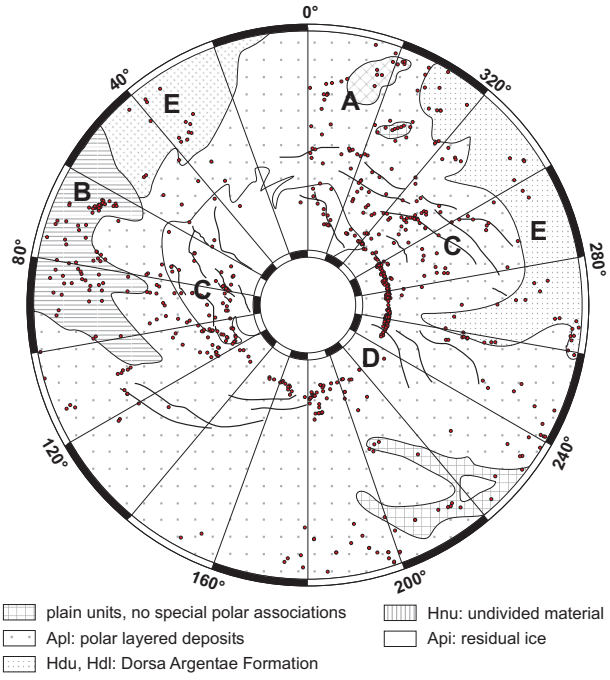

Figure 1: Simplified geologic map of the south polar region between 80°S and 90°S (after [5]) with polygonal crack patterns outside the polar cap. Letters represent areas discussed in the text.

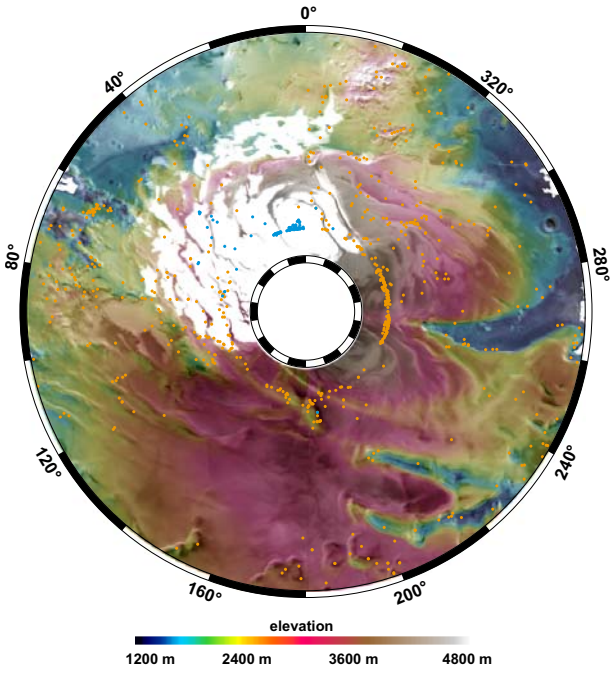

Figure 2: South polar topography and distribution of polygonal crack patterns at the south pole between 80°S and 90°S. Blue dots represent polygonal patterns associated with circular depressions [6] on the residual polar cap.

of material has not yet advanced as far as at the surface, and (c) only a few layers of the polar layered deposits show the typical polygonal pattern. The layers containing polygons are exposed at the Chasma Australe walls, the eastern chasmata, and inside depressions of the polar layered deposits at 180°W to 200°W. At 80°W the circum polar distribution furcates to the north and presents a large cluster of polygonal patterned ground in undivided Hesperian aged units (B).

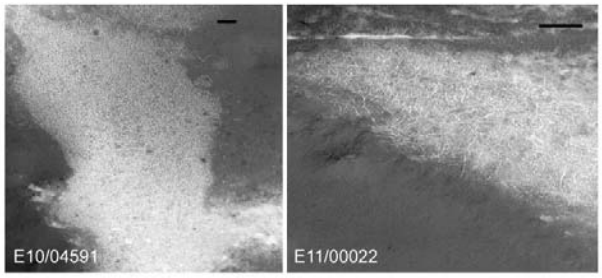

Figure 3: Plains units polygons at 80°S (A on fig. 2). The black bar represents 200 m, north is up. Polygons of the south polar plains units occur predominately in sheltered places at slopes and inside of depressions.

Small quantitites of polygonal terrain is visible on material of the Dorsa Argentae Formation (E), where it is bound to small depressions and rough terrain. Minor clusters of polygonal terrain is exposed adjacent to undivided plain units (A). Polygons related to plains units (A) are randomly orthogonal and highly complex shaped (s. fig. 3). They are degraded and occur south of sheltered slopes or inside depressions. Their diameter varies between 10 to 50 m but reaches up to 80 m. The polygonal troughs are filled with bright material, which might be associated with CO_2 frost [7]. Towards the pole polygons are orthogonal and their shape becomes more distinct with a preferred N–S direction. The polygonal troughs are filled with dark eolian material. Their diameter increase up to 100 to 200 m. Polar troughs related polygons (s. fig. 5) occur on the slopes and inside the troughs.

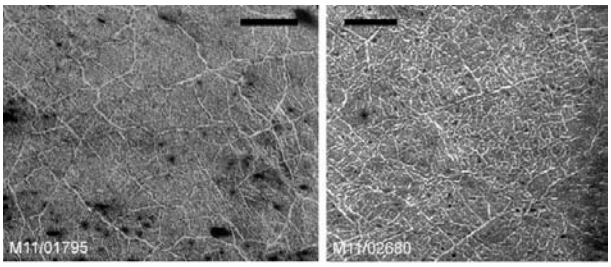

Figure 4: Randomly orthogonal and complex polygons of the Dorsa Argentae Formation (Hdl, Hdu) near 84°W and 80°S. The black bar represents 200 m, north is up.

They have an orthogonal shape and diameters between 10 m to 20 m. Outside the troughs the polygons dissappear below eolian material. Polygons of undivided material near 84°W and 80°S are, similar to the plains units, more complex shaped and randomly orthogonal (s. fig. 4). Polygons exposed at the eroded wall material of the polar layered terrain occur on a few layers only. These polygons are partly degraded but show a distinct orthogonal pattern and sizes in a range of 20-40 m.

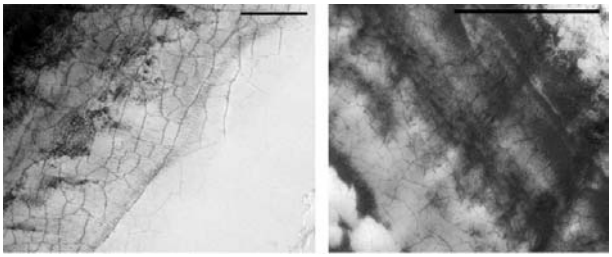

Figure 5: High resolution imagery of polar trough related polygonal networks near 85°W and 86°S. The black bar represents 200 m, north is up.

Conclusions: The distribution of south polar polygons is bound to circum polar troughs, polar re–entrants and depressions where polar layers are exposed (Apl). Polygonal patterns associated with circular depressions can be observed on the polar residual cap. Furthermore, clusters of polygonal patterns are distributed at undivided (HNu) and unclassified plains material. Polygons have a distinct shape and morphology according to their geologic and geomorphologic setting, although transitional morphologies occur in all units. As the distribution is not random at all, surfaces (especially few marker horizons of the layered terrain) showing polygonal patterns might have ages which are valuable to for implications on the past climate. Further research regarding ages is under way.

As far as insights have been provided by MOC, there are major dependencies on parameters like topography, homogeneity of (sub-)surface material, temperature changes, and exogenic degradation processes. Changes in these parameters will affect the growth, size, pattern and distribution of the polygonal networks [8]. Providing a complete coverage, color, and stereo information at high resolution, Mars Express will help to close the remaining gaps and to determine surface and morphologic properties to rule out some of the unknown parameters.

References: [1] T. A. Mutch et al. (1977), *J. Geophys. Res.*, **82**, 4452-4467. [2] M. T. Mellon (1997), *J. Geophys. Res.*, **102**, 25617-25628. [3] R. O. Kuzmin and E. V. Zabalueva (2003), *Lun. Planet. Sci. Conf.*, Houston, #1912. [4] N. M. Seibert and J. S. Kargel (2001), *Geophys. Res. Let.*, **28**, 899-902. [5] Tanaka K. L. and D. H. Scott (1987) *US Geolog. Surv.*, Map 1-1802-C, Washington D. C. [6] Thomas et al. (2000), *Nature*, **404**, 161-164. [7] K. J. Kossacki and W. J. Markiewicz (2002), *Icarus*, **160**, 73-85. [8] A. H. Lachenbruch (1962), *GSA papers*, **70**, New York.

THERMOPHYSICAL PROPERTIES OF MARS' NORTH POLAR LAYERED DEPOSITS AND RELATED MATERIALS FROM MARS ODYSSEY THEMIS. A. R. Vasavada[1], M. I. Richardson[2], S. Byrne[2], A. B. Ivanov[3], P. R. Christensen[4] and the THEMIS Team, [1]Department of Earth and Space Sciences, Box 951567, University of California, Los Angeles, CA 90095-1567, ashwin@ess.ucla.edu, [2]Division of Geological and Planetary Sciences, Mail Stop 150-21, Caltech, Pasadena, CA 90025, [3]Jet Propulsion Laboratory, Mail Stop 168-416, Pasadena, CA 91106, [4]Department of Geological Sciences, Arizona State University, Tempe, AZ 84287.

Introduction: The presence of a thick sequence of horizontal layers of ice-rich material at Mars' north pole, dissected by troughs and eroding at its margins, is undoubtedly telling us something about the evolution of Mars' climate [1,2]—we just don't know what yet. The North Polar Layered Deposits (NPLD) most likely formed as astronomically driven climate variations led to the deposition of conformable, areally extensive layers of ice and dust over the polar region. More recently, the balance seems to have fundamentally shifted to net erosion, as evidenced by the many troughs within the NPLD and the steep, arcuate scarps present near its margins, both of which expose layering.

Viking Orbiter imaging of the NPLD revealed that dark, dune-forming material is spatially associated with NPLD scarps [3]. This material may be liberated from an ice matrix by thermal erosion of the NPLD, either as sand particles or sand-sized aggregates of dust [4]. In either case, the NPLD seems to be a source of material similar in particle size and color to that present in the vast, circumpolar sand sea [3].

Recently, the stratigraphy of the NPLD has been subdivided into two distinct units [5-10]. The upper unit appears to consist of horizontal layers of water ice and a small fraction of dust. Layers are exposed within gently sloping, spiral troughs cut into the cap complex. The lower unit consists of thicker, darker layers with an irregular, platy appearance. It crops out near the margin of the NPLD and within Chasma Boreale. When troughs cut deeply enough to encounter the lower unit, the trough forms are replaced by steep, arcuate scarps. Edgett *et al.* attribute the change in morphology to a lower unit that is less resistant to wind erosion [7].

This stratigraphic sequence has been observed at widely separated locations within the NPLD [6]. If the layering is truly horizontal over the pole, such that the lowest portions of the stratigraphic column crop out in the marginal scarps, it suggests that the erosion of the platy unit uniquely contributes the dark, dune-forming material. Indeed, the platy unit may be an ancient sand sea now covered by the ice-rich, finely layered unit [6], although no bedforms have been found upon it [7].

Optical and thermal infrared (IR) measurements have been used to infer and compare the properties of the different polar materials. For example, Thomas and Weitz compared the color of the dark material near NPLD scarps to material within NPLD layers and within the circumpolar sand sea [3]. Herkenhoff and Vasavada used Viking IR measurements to determine the nature of the dune-forming material and its relationship to other dark, dune-forming materials at lower latitudes [4]. However, such investigations have been limited by the relatively low spatial resolution of Viking color imagery and IR data compared to the spatial dimensions of layers, troughs, scarps, and dune fields. We hope to take advantage of the unprecedented spatial resolution of Mars Odyssey Thermal Emission Imaging System (THEMIS) visible and IR imagery in order to make these inferences and comparisons with the highest possible accuracy (e.g., Figure 1).

THEMIS Observations: To address this science goal, we defined a number of Regions of Interest (ROI) for THEMIS to target as part of the Mars Odyssey Participating Scientist program. We gratefully acknowledge the THEMIS science team and operations staff for acquiring ~100 visible and IR image cubes during Mars' northern summer (L_s 110-160) as orbit tracks intersected our ROIs. The visible image cubes in our data set have five wavelength bands, along-track lengths of ~1000 pixels, and a spatial resolution of 19-38 m/pixel. The IR image cubes have ten wavelength bands and a spatial resolution of 100 m/pixel. The along-track footprint of the IR cubes often begins < 80° latitude, crosses the pole, and terminates < 80° latitude.

Visible Data Analysis: We use these THEMIS data in order to understand the morphology and color/thermal properties of the NPLD and related materials over relevant (i.e., m to km) spatial scales. We have assembled color mosaics of our ROIs in order to map the distribution of ices, the different layered units, dark material, and underlying basement. The color information from THEMIS is crucial for distinguishing these different units (Figure 1), which are less distinct on Mars Orbiter Camera images.

We wish to understand the nature of the marginal scarps and their relationship to the dark material. Co-registered Mars Orbiter Laser Altimeter (MOLA) data provides a measure of scarp morphologies and may help identify the process(es) eroding the NPLD (e.g.,

mass wasting, wind, sublimation). The dark material (or perhaps the platy unit in planar configuration) is present at the feet of many scarps, but does not express dune bedforms there. However, dark material has barchan-type formations when present tens of kilometers away from the scarps [3]. MOLA will help identify the relationship between the spatial distribution of dark material, the presence of bedforms, and the influence of topography.

Thermal Data Analysis: Our next, more ambitious goal is to derive the thermophysical properties of the different geologic materials using THEMIS and Mars Global Surveyor Thermal Emission Spectrometer (TES) data. Such analyses are complicated by the need for atmospheric correction (of both radiatively active CO_2 and dust) and accurate, representative surface temperatures. The latter may be compromised by the footprint size (compared to the areal extent of the material of interest), the influence of topography, and the absolute calibration of the measurement. However, the THEMIS data offer the promise of extending our previous analyses [4] to finer spatial scales and effort will be made to overcome these challenges. In order to derive thermal inertias and thermally derived albedos, we will employ a 1-D, radiative-convective thermal model of Mars surface, subsurface and atmosphere. The model will use simultaneous (or seasonally relevant) TES atmospheric dust opacities, and where possible, include the effects of surface slopes on insolation using MOLA topographic data.

Summary: We hope to understand the geologic evolution of the north polar region by studying the optical and thermophysical properties of polar materials. The primary questions include: what processes control the morphology of the troughs and scarps within the NPLD? What is the nature of the upper and lower NPLD units, as inferred from their thermophysical properties? And finally, what is the nature and source of the dark, dune-forming material?

References: [1] Murray, B. C. et al. (1972) *Icarus*, *17*, 328. [2] Cutts, J. A. (1973) *J. Geophys. Res*., *78*, 4231. [3] Thomas, P. C. and Weitz C. (1989) *Icarus*, *81*, 185. [4] Herkenhoff, K. E. and Vasavada A. R. (1999) *J. Geophys. Res*., *104*, 16,487. [5] Malin, M. C. and Edgett, K. S. (2001) *J. Geophys. Res*., *106*, 23,429. [6] Byrne, S. and Murray, B. C. (2002) *J. Geophys. Res*., *107*, 11-1. [7] Edgett, K. S. et al. (2003) *Geomorph*., *52*, 289. [8] Kolb, E. J. and Tanaka, K. L. (2001) *Icarus*, *154*, 22. [9] Tanaka, K. L. et al. (2003) *J. Geophys. Res.*, *108*, 24-1. [10] Fishbaugh, K. and Head, J. W. (2003), *6th Intl. Conf. on Mars*, abstract 3137.

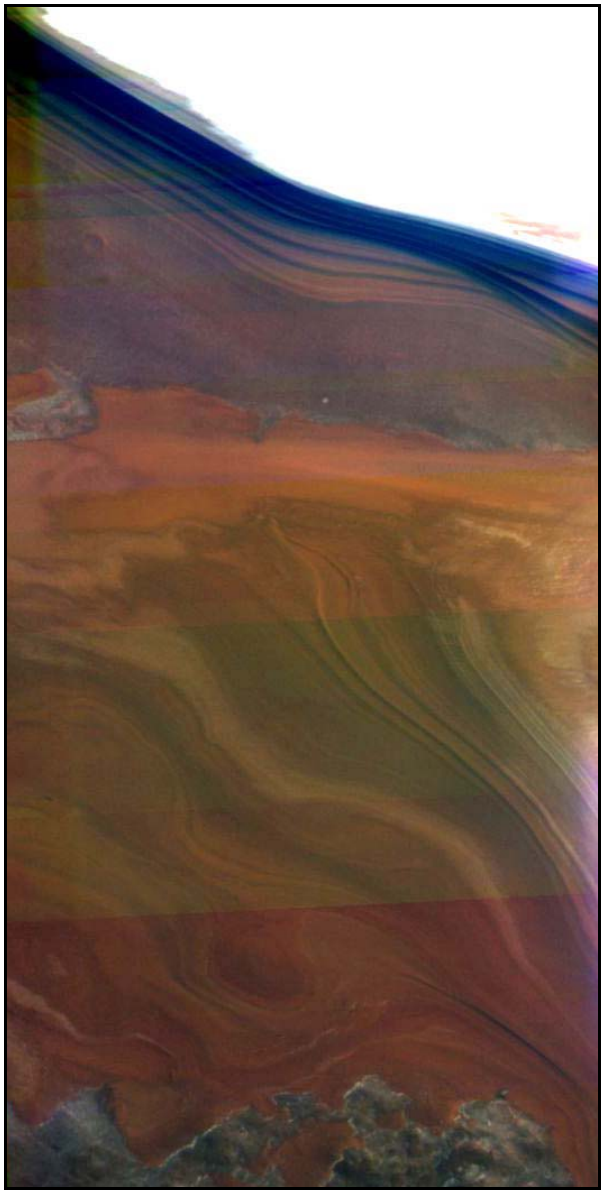

Figure 1. Color composite of THEMIS visible image data showing the north polar residual ice cap (top) and layered materials near the margin of the NPLD. Here the erosion of the deposits appears to "bottom out", exposing the basement terrain underneath the NPLD (best seen along the lower edge of the image). The color information greatly aids this interpretation.

LOW-TEMPERATURE, AQUEOUS ALTERATION OF SOIL IN WRIGHT VALLEY, ANTARCTICA, COMPARED WITH AQUEOUS ALTERATION ON MARS. S. J. Wentworth,[1] E. K. Gibson, Jr.,[2] and D. S. McKay[2], [1]Lockheed Martin Space Operations, C23, 2400 NASA Rd. 1, Houston, TX, 77058 (susan.j.wentworth@jsc.nasa.gov), [2]NASA Johnson Space Center, Houston, TX, 77058.

Introduction: The Dry Valleys of Antarctica are possibly one of the best analogs on Earth of the environment at the surface of Mars. Many types of research have been focused on the Dry Valleys, partly because of the potential application to Mars, and also because of the importance of the Dry Valleys in understanding the characteristics and development of terrestrial polar deserts. In 1983, we published a detailed study [1] of weathering products and soil chemistry in a soil pit at Prospect Mesa, Wright Valley, as a possible analog to Mars. Much more is now known about Mars, so we are re-examining that earlier work and comparing it with newer martian data. The Mars information most pertinent to this work includes (**A**) the strong evidence for recent aqueous activity on Mars reported by [2], along with more recent evidence for present-day, near-surface water ice on Mars [3, 4]; and (**B**) the identification of meteorites from Mars [5] and the subsequent, definitive proof that low-temperature, aqueous weathering has occurred in these meteorites prior to their ejection from Mars [6-8].

Soil column, Wright Valley: The samples used in the Dry Valleys study [1] were taken at irregular intervals from the soil pit shown in Fig. 1. The soil column consists of a permanently frozen zone below ~40 cm depth overlain by an active/seasonally frozen zone.

Results of the Wright Valley work seem to be consistent with what is now known or postulated about Mars. Orbital data indicate the presence of water ice just beneath the martian surface, especially at high latitudes [2, 3].

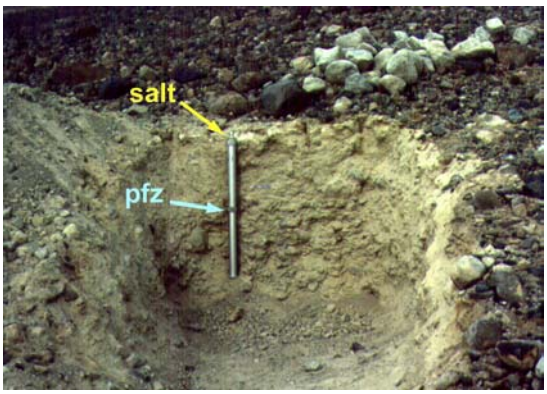

Figure 1: Soil pit, Prospect Mesa, Wright Valley, Antarctica. Drive tube=78 cm long. Yellow arrow points to salt-rich zone just beneath surface (~2-4 cm depth). Top of permanently frozen zone (pfz) is at ~40 cm depth; after [1].

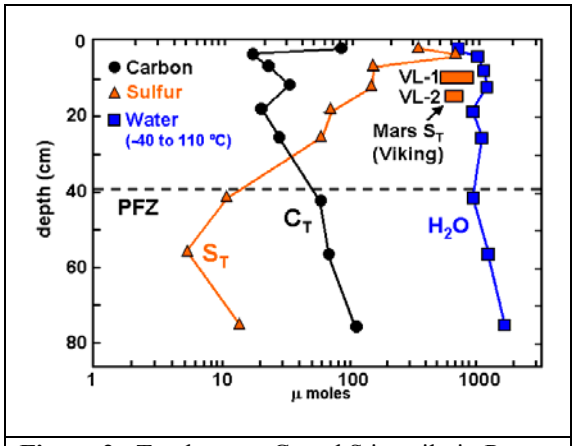

Figure 2: Total water, C, and S in soil pit, Prospect Mesa, Wright Valley; dashed line marks top of permanently frozen zone (pfz); after [1].

Similarly, Fig. 2 demonstrates that the water content (from -40 to +110 deg C) of the Wright Valley soil is much lower at the surface than at depth. This upward decrease in water occurs even within the permanently frozen zone.

In the Wright Valley soil column, water-soluble (salt-forming) species generally increase upward, with a salt-rich zone at ~2-4 cm depth and a dramatic decrease in salts at the surface of the soil (Fig. 3). Mars remote sensing data suggest that total amounts of alteration of original igneous rocks on Mars may be low [3]. The duricrust found just beneath the surface during Viking lander experiments, however, indicate that subsurface salts analogous to those in the Wright Valley soils are likely present on Mars although their possible abundance and distribution are unknown.

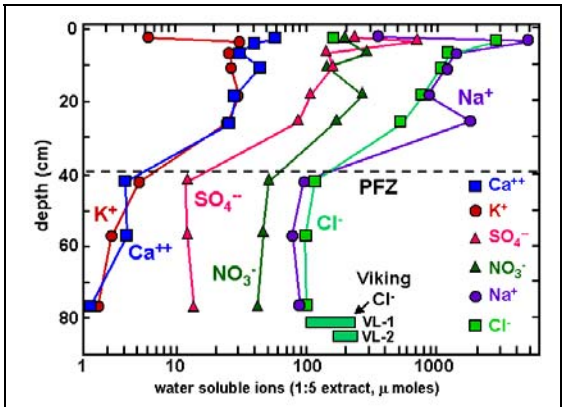

Figure 3: Water-soluble ions in soil pit, Prospect Mesa, Wright Valley; after [1].

Aqueous alteration and secondary phases: SEM studies of the Wright Valley soils [1] showed that aqueous alteration of detrital silicate grains and the formation of secondary phases occurred throughout the soil column, including the permanently frozen zone. Similar features are also present in martian meteorites, and various lines of evidence have shown that some of this alteration occurred on Mars [8, 9]. Examples of typical silicate dissolution in the Dry Valleys soil and a Mars meteorite (Shergotty) are shown in Fig. 4. These features are quite similar to each other. They are typical of chemical weathering of such silicates but are not diagnostic of the mode of alteration. Note that the Wright Valley grain (Fig. 4A) came from the permanently frozen zone of the soil, demonstrating active, although probably slow, alteration processes.

The Wright Valley soil (again, including the permanently frozen zone) and the martian meteorites also contain secondary salts. Secondary carbonates, Ca-sulfate, and halite are found in the Wright Valley soils and the martian meteorites, although not all the meteorites contain all these minerals. A martian origin has been well established for some, but not all, of the secondary phases in martian meteorites. Various means have been used to determine a martian origin for secondary phases; e.g., carbonates in meteorite ALH84001 were quantitatively identified as martian because of their ~3.9 Ga age (ALH84001 itself is 4.5 Ga old) [7]. The origin of many other secondary phases in other meteorites is less certain, however.

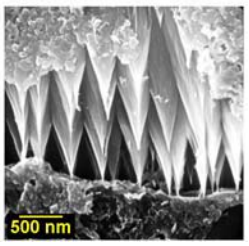

Figure 4A: SEM image of amphibole from Wright Valley soil pit sample WV-221 (permanently frozen zone) showing dissolution features typical for silicates; after [1].

Figure 4B: SEM image of pyroxene from martian meteorite Shergotty (observed fall) with dissolution features and incipient phyllosilicates.

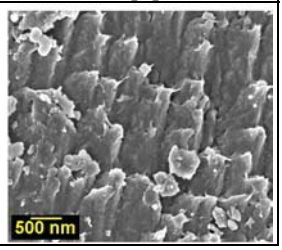

Recent orbital data have suggested the possible presence of a zeolite such as chabazite in Mars dust [10]. Chabazite is present as an authigenic mineral throughout the Wright Valley soil column (Fig. 5) in the Antarctic soil. This is consistent with the suggestion by [11] that chabazite may store water on Mars, especially near the equator. More work is needed to determine whether zeolites are not present in the existing martian samples, or whether they simply have not been found yet.

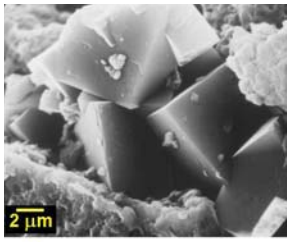

Figure 5: SEM image of authigenic chabazite in Wright Valley soil pit sample WV-221 (permanently frozen zone); after [1].

Conclusions: Aqueous alteration in Mars meteorites and the Wright Valley soil are quite similar with respect to type and degree of weathering of the primary silicates, and also to the nature and distribution of secondary phases. Alteration in the Dry Valleys soils occurs even in the permanently frozen zone, suggesting that similar alteration probably occurs on Mars. Alteration can occur gradually in permanently frozen material because of a liquid-like thin film of water that seems to persist at very low temperatures [12]. Freezing-point depression in brines could also cause weathering at low-temperatures; the salts in the Mars meteorites point to the existence of such brines. The low total amount of alteration of the martian meteorites, along with the presence of secondary phases only in trace amounts, seems consistent with such a process. Transient heating events (e.g., impacts and volcanic activity) have probably been responsible for some weathering on Mars. The Mars meteorites probably do not reflect strong heating events because significant alteration would be expected, at least in close proximity to the heated areas. The seasonal behavior of water ice at the martian poles and possibly elsewhere indicates that water (liquid or vapor) is available for periodic episodes of weathering, even if effects are concentrated mostly on wind-blown dust. Whether or not Mars was once wet and warm, or if it was always cold and dry as suggested by [13], it is clear that weathering and salt deposition have occurred in some form. If the cold, dry Mars model is correct, then the Dry Valleys of Antarctica may be a good analog for most of Mars for most of geologic history.

References: [1] Gibson et al (1983) Proc. LPSC 13, A912-A928; [2] Malin and Edgett (2000); [3] Boynton et al. (2002) Science 297, 81; [4] Christensen (2003) 6th Mars Conf. #3126; [5] Bogard and Johnson (1983) *Science*, 221, 651; [6] Gooding et al. (1988) *GCA* 52, 909; [7] Borg et al. (1999) *Science* 286, 90; [8] Wentworth et al. (2003) *Astrobio*, in revision; [9] Gooding et al. (1991) *Meteoritics* 26, 135; [10] Ruff (2002) *Eos* 83, 1059; [11] Bish et al. (2003) *LPS XXXIV*, 1786; [12] Anderson (1981) *NASA TM 84211*, 292.

LIFE IN PERENNIALLY ICE COVERED LAKES ON MARS - AN ANTARCTIC ANALOGUE

Alex T. Wilson Dept of Geosciences, University of Arizona, Tucson, AZ 86721, USA. (520) 298 5446, email atwilson@U.arizona.edu.

Introduction: As a past member of the New Zealand Antarctic Program, the author spent many summers studying the perennially ice covered lakes in the cold and arid regions of the Antarctic [1 – 5]. This presentation will review what is known about such lakes and conclude that versions of them may exist on Mars. If indeed this proves to be the case, they would be prime sites to look for life. They might also be suitable sites for the construction of a research base, since they would provide a good landing site, water and building material.

Fresh Water Perennially Ice Covered Lakes: It may come as a surprise that large bodies of fresh water can exist in regions where the mean annual temperature is –20 C and below. In the Antarctic, such lakes are possible because some water enters the perennially ice covered lake during a few days each summer. This water flows under an ice cover, which is many meters thick. Water can only be frozen on the bottom of the ice if its latent heat of fusion can be conducted through the overlying ice cover.

The water that enters the perennially ice covered lake flows into the lake and fingers into its appropriate density level. The maximum density for pure water is 4.1 C, which is the temperature of the bottom waters of many of these lakes. For a steady state situation, the amount of water in such lakes (on average) must equal the amount of water sublimed from the ice surface each year, or the lake level will rise or fall until it comes into balance.

During late winter, ice freezes onto the bottom of the perennial ice cover to replace the ice lost during the year. It follows that the thinner the ice, the more ice can freeze onto the bottom of the ice cover. In effect, the ice thickness is a measure of the aridity of the area. Thus the heat input to the perennially ice covered lake comes from the latent heat of fusion of the inflow water and from solar heating.

The very clear ice on perennially ice-covered lakes makes them appear blue. Such an unusual ice cover will give the lakes a low albedo and a "blue ice" color. The ice crystals in the ice cover have been growing for thousands of years. In the case of Lake Vanda [1], perhaps the most studied perennially ice covered lake, the ice crystals are 10 cm across and 3.6 meters long with the c-axis vertical. These crystals act as light pipes and allow the 12 ft ice cover on Lake Vanda to transmit 6% of the total incident solar energy [1]. Because of the unusual crystal orientation of the ice cover, it may be possible to develop methods to confirm the existence of perennially ice covered lakes on Mars.

Can Perennially Ice Covered Lakes Exist On Mars?: The situation on Mars is like the cold arid ice-free areas of Antarctica – only a more extreme version. The temperatures on Martian polar regions are clearly much colder but the relative humidities may be higher. The problem is to find a source of water for Martian perennially ice covered lakes which would replace the sublimation losses from the lake surface. One possibility would be the brine that would be flowing into the sides of the lakes – see discussion below. The origin of the brines entering Antarctic lakes will be discussed and is published [2] [3]. A saturated solution of sodium chloride has a freezing point of –20.7 C and an equilibrium relative humidity of 75%. A better candidate might be calcium chloride: a saturated solution has a freezing point of -50 C (223 absolute) and an equilibrium relative humidity of 45%. Of course in practice, any brine would be a complex mixture. However, it seems feasible to have a situation where in the warmer times of the annual cycle (or at some time in the past) salt brines would flow into a perennially ice covered lake and sink to finger into an appropriate density layer. During the late winter, relatively pure water would freeze onto the bottom of the ice to make up for sublimation from the ice surface. During the summer, the solar radiation would melt voids in the ice, particularly in places where any biological colonies intercept solar radiation. This happens on perennially ice covered Antarctic lakes - see for example references [4] and [5].

Origin Of Brine Needed To Feed The Ice Covered Lakes: The Northern Martian Ice Sheet has probably been in existence for a very long time. The surface of the ice sheet has been losing water by sublimation. This has been made up by the precipitation on the surface by ice crystals. This ice would not be pure water, but would contain small quantities of inorganic salts – e.g. calcium, magnesium and sodium chlorides. Where are these salts today? It is proposed that the more deliquescent of these salts have taken up water and have flowed down-slope into the topographically enclosed drainage basins associated with the ice sheet. Some of these might be expected to contain perennially ice-covered lakes. These lakes may have living things associated with their ice cover, since there would be relatively fresh liquid water at least for part of the annual cycle.

Direct Evidence Of The Existence Of Lakes Associated With The Northern Ice Sheet: Viking Surveyor color satellite photos will be shown (see below) in which a number of ice-blue lakes can be seen occupying the bottom of various enclosed basins. There may even be different kinds of Martian perennially ice covered lakes. For example, one lake appears to be a circular lake analogous to the lakes found on terrestrial icesheets and might be expected to have an ice bottom. Such a lake would be able to acquire water by melting the underlying ice and may contain fresh water. An interesting point is that there appear to be several lakes associated with the Northern Ice Sheet but none are observable in the South Polar Region.

[1]Wilson A.T. and H.W.Wellman Nature **196** 1171-1173.[2]Wilson A.T. Nature **280** 205-208.[3]Wilson A.T. J.Geoph. Rev.,D.V.D.P.,**33** 185-192.[4]Wilson A.T. Ecology **46** 376.[5]Wilson A.T. and H.W.Wellman Nature **196** 1773.

THE NORTHERN ICE SHEET OF MARS WITH FOUR OF THE LAKES ENLARGED

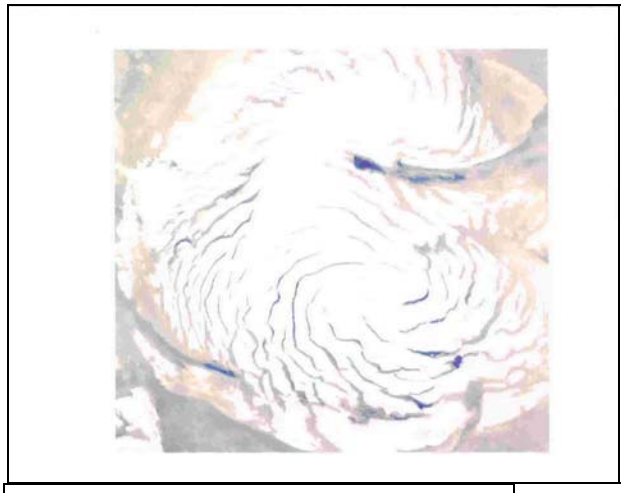

_____100 km_____

_____100 km_____

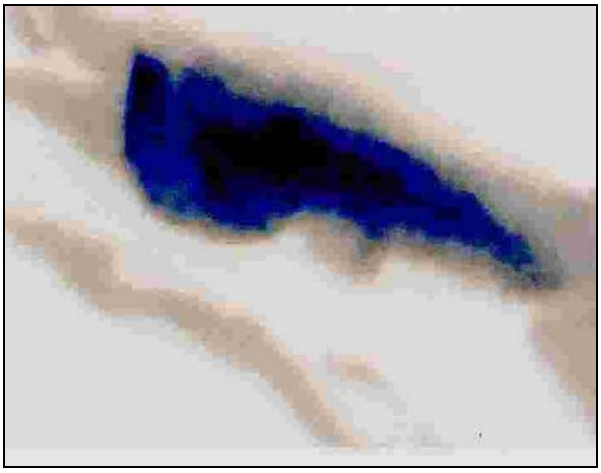

_____100 km_____

ICE KEEL SCOUR MARKS AND ICE FLOE GROUNDING STRUCTURES IN KASEI VALLES AND ECHUS CHASMA. Christopher Woodworth-Lynas and Jacques Yves Guigné, Guigné International Ltd. 685 St. Thomas Line, Paradise, Newfoundland, CANADA A1L 1C1 709 895 3819 chriswl@guigne.com

Introduction: We present further new observations from analyses of Mars Global Surveyor Mars Orbiter Camera images of surficial features interpreted to be the result of interactions between the keels of floating ice masses on submerged sediment [1]. The surface morphology of scour marks typically comprises a curvilinear trough from which seabed material has been ploughed to the sides by the entrenched, moving ice keel, to form two co-linear berms of excavated material.

Background: Scour marks are the seafloor tracks made by floating ice masses as their keels mechanically plough into soft sediments of lake, river or ocean floors. On Earth scour marks are ubiquitous features on the seafloors of the modern Arctic and sub-arctic regions and on the seafloor of the continental margin of Antarctica.

Scour marks commonly survive the transition from submergence to exposure above water level and ancient features are commonly seen, over large areas of southern Manitoba and parts of southern Ontario formerly occupied by glacial Lake Agassiz and glacial Lake Iroquois [2,3]. They are also found on several large islands of the Arctic Archipelago (e.g. King William Island, Victoria island) and are readily identified from aerial photographs. The relic Arctic features were formed in areas formerly submerged below sea level some 10,000 years ago. Scour marks preserved in Pre-Cambrian, Ordovician and Carboniferous/Permian age glacimarine sediments have also been identified on exposed bedding plane surfaces in several localities worldwide [4].

On Earth scour marks form today in water depths from < 5 - 500 m, and fall in the range < 100 m to several kilometers long, 5 - 100 m wide and < 1 - 5 m deep (exceptionally 25 m).

In a preliminary analysis [1] we examined several hundred high-resolution narrow angle images acquired by the Mars Orbiter Camera (MOC). We searched for ice keel scour marks to the margins of Chryse Planitia in the vicinity of an ancient shoreline, Contact 2, proposed by [5] and largely substantiated [6], and to the valley floor regions of the six great valley systems that empty into Chryse: the Mawrth, Ares, Tiu, Simud, Maja and Kasei Valles systems. We chose these regions because floating ice masses, either river ice from the valleys, or sea ice would likely ground and scour in the littoral waters of a river mouth and near-shore region, and that traces of this activity may be preserved on bedding surfaces.

Present work and description of Martian features: We have extended our analysis and interpretation to include much of Echus Chasma (Figure 1) where we have identified features interpreted as multi-keeled scour marks and in one place a zone of multiple, parallel scour marks related to the movement of ice keels locked in a floating ice canopy (Figure 2).

***Networks of Parallel sided Troughs with Berms*:** On the flat valley floor of Kasei Valles and in Echus Chasma we have found networks of curvilinear, intersecting, parallel-sided troughs that meander and intersect with no consistent orientation. The troughs typically are at least 1 km long and some exceed 3 and 4 km and range in width from 10 – 50 m. By observing sun shadows it is possible to distinguish narrow ridges, or berms, on one or both sides of most troughs. In places *multiple, overlapping sub-parallel trough*s coalesce into wide (100 - 300 m), irregular-sided grooved and ridged surfaces.

***Ridge-bounded regions*:** Associated with the troughs are poorly- to moderately well-defined irregular to rounded, smooth, low albedo regions, the margins of which are defined by low continuous ridges. These ridge-defined smooth areas range in size from 200 to 600 m, exceptionally up to 950 m. They may occur as solitary features, but more commonly occur in groups forming jig-saw-like ridge networks. In Echus Chasma these ridge-defined features are larger (in the range 0.5 to 1.0 km) and individual features may contain smaller, well defined jigsaw-like groups of sub-circular regions, that are also defined by ridges of a smaller scale than the larger feature in which they are contained.

In Kasei Valles the *parallel-sided troughs with berms*; the *multiple, overlapping sub-parallel troughs*; and smooth *ridge-bounded regions* are restricted in their occurrence to the lowest and flattest portion of the valley floor (Figure 1) and do not occur at or east of the vicinity of Sharanov crater and are not found on any of the elevated, older grooved surfaces of the Kasei system.

Ridge-defined smooth areas are considerably more common, and of larger scale, in the much wider, flat regions of Echus Chasma. Parallel-sided troughs with berms are less common but multiple troughs (Figure 2) and closely-spaced parallel troughs were found here.

Interpretation: We interpret the small-scale troughs on the floor of the Kasei Valles system as ice keel scour marks made by the bottom-touching keels of floating ice floes. We interpret the associated ridge-defined low albedo regions as grounding pits made by stranded tabular floes. The megaripple-like surfaces on

which the scour marks and grounding pits appear to have formed in the lower Kasei Valles during a period of strong unidirectional down-valley currents. There may have been floating ice present and ice scouring may have occurred during megaripple formation but all traces have been erased by the migrating ripples. As the strong currents associated with the megaripples waned, ice scour marks and ice floe grounding pits formed and were preserved. The meandering tracks of the scour marks point to a significant decrease in unidirectional flow, and suggest that winds may have played a significant role in driving the scouring floes.

We interpret the wide lanes of multiple, overlapping sub-parallel troughs as zones of linear shear in the ice canopy (Stamukhi zones), which are typically regions of intense ice keel scouring of the seafloor e.g. [7, 8].

Discussion and implications: The preserved traces of ice keel scour marks and ice floe grounding pits are restricted to the surface of stratigraphic Kasei unit 2. The scour marks are therefore of early Amazonian age. Scour marks demonstrate:

1. the former presence of a water body;
2. the water body must have been at least seasonally, or perhaps permanently, covered by ice floes;
3. the water area must have been large enough for wind and current to drive the floes forward during ice/seabed interaction.

References:

[1] Woodworth-Lynas, C.M.T. and J.Y. Guigné. 2003. Ice keel scour marks on mars: evidence for floating and grounding ice floes in Kasei Valles. 6th International Conference on Mars. Pasadena, July 20-25th.

[2] Gilbert, R.J., Handford, K.J. and Shaw, J., 1992. Ice scours in the sediments of glacial Lake Iroquois, Prince Edward County, eastern Ontario. Geographie physique et Quaternaire v. 46, 189-194.

[3] Woodworth-Lynas, C.M.T. and J.Y. Guigné. 1990. Iceberg scours in the geological record: examples from glacial Lake Agassiz. In, Glacimarine environments: processes and sediments (J.A. Dowdeswell and J.D. Scourse, eds.). Geol. Soc. Spec. Pub. No. 53: 217-233.

[4] Woodworth-Lynas, C.M.T. and J.A. Dowdeswell. 1994. Soft-sediment striated surfaces and massive diamicton facies produced by floating ice. In: Earth's Glacial Record (Eds. M. Deynoux *et al*.) Cambridge University Press: 241-259.

[5] Parker, T.J. , D.S. Gorsline, R.S. Saunders, D.C. Pieri and D.M. Schneeberger. 1993. Coastal geomorphology of the Martian northern plains. JGR, 98: 11061-11078.

[6] Ivanov, M.A. and J.W. Head. 2001. Chryse Planitia, Mars: Topographic configuration, outflow channel continuity and sequence, and tests for hypothesized ancient bodies of water using Mars Orbital Laser Altimeter (MOLA) data. JGR, 106 (E2): 3275-3295.

[7] Barnes, P.W., D.M. Rearic, and E. Reimnitz. 1984. Ice gouging characteristics and processes, In, The *Alaskan Beaufort Sea - Ecosystems and Environments.* Academic Press, Orlando: 185-213.

[8] Reimnitz, Erk, and P.W. Barnes. 1974. Sea ice as a geologic agent on the Beaufort Sea shelf of Alaska: In, *The Coast and Shelf of the Beaufort Sea,* edited by J.C. Reed, and J.E. Sater, Arctic Institute of North America, Arlington, VA: 301-351.

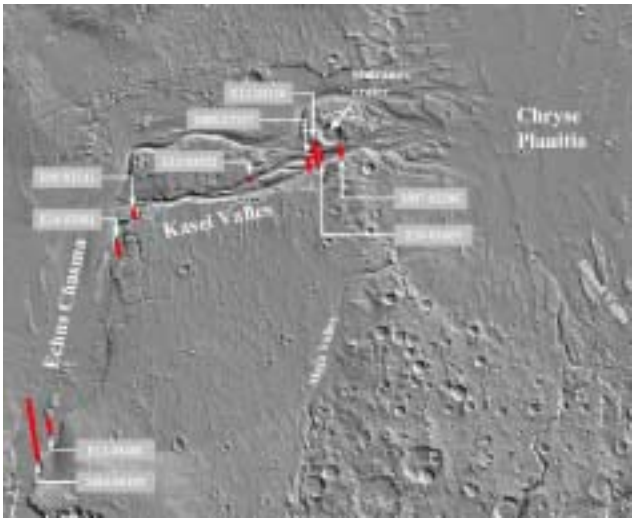

Figure 1 Relief map of Kasei Valles with location of selected MOC images that show ice scour marks and ice floe grounding pits. Context relief image from the Mars 2001 Odyssey THEMIS website (http://themis-data.asu.edu/).

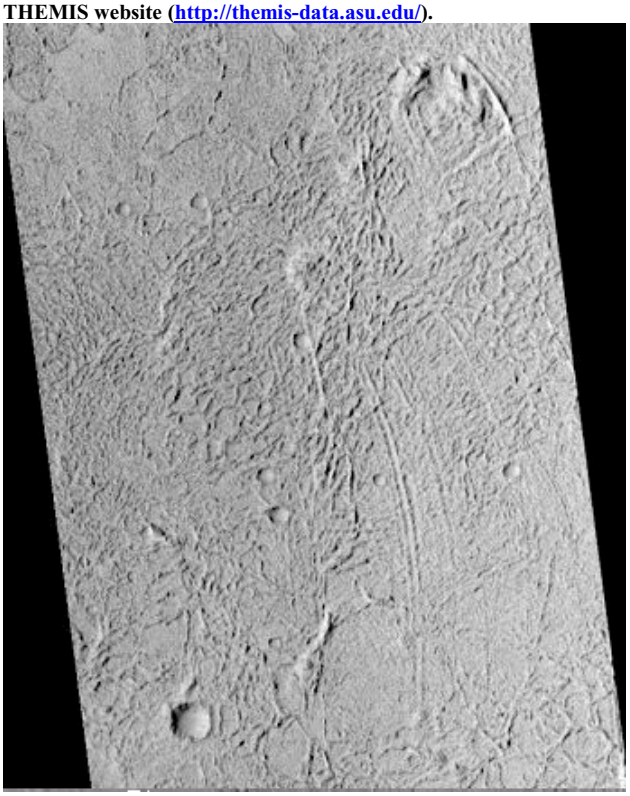

Figure 2 MOC image (southern Echus Chasma) of a 2 km-wide group of curved, wind-driven ice keel scour marks terminating in transverse ice-push ridges. MOC image M14-00193. Scaled pixel width: 11.6 m; Scaled image width: 2.96 km.

ORIGIN OF MGS-TES SURFACE COMPOSITIONS IN THE NORTHERN PLAINS AND POLAR REGION OF MARS. M. B. Wyatt[1] and K. L. Tanaka[2], [1]Department of Geological Sciences, Arizona State University, Tempe, AZ 85287 (michael.wyatt@asu.edu), [2]U.S. Geological Survey, Flagstaff, AZ 86001 (ktanaka@usgs.gov).

Introduction: The largest extent and highest concentrations of the MGS-TES derived Surface Type 2 (ST2) spectral unit, interpreted as an andesitic [1,2] and/or partly altered basaltic composition [3], are mapped in the low-albedo northern lowlands and circumpolar sand seas of Mars [1]. In this study, we examine the relationships between distributions of TES-derived surface compositions and mapped geologic units in the northern polar regions of Mars and integrate Viking, MGS-MOC and -MOLA and MO-THEMIS datasets to constrain theories of the composition, origin, and evolution of these materials.

MGS-TES Background: Studies of low-albedo regions on the martian surface using atmospherically corrected thermal emissivity data from the MGS-TES have identified two distinct global surface spectral signatures [1, 4-6]. The Surface Type 1 (ST1) spectral end-member has been interpreted as an unaltered basalt [1-2, 4], while the ST2 spectral end-member has been variously interpreted as an andesitic [1,2] and/or partly altered basaltic composition [3]. The ST1 surfaces roughly form an equatorial band, restricted to southern highlands and Syrtis Major regions and a few local depostis in the northern plains, capped with ST2 surfaces at mid-latitudes and high-latitudes [7,8]. The transition from ST1 to ST2 compositions at southern high-latitudes appears gradual with no obvious distinguishing boundaries, unlike the topographic dichotomy to the north where plains materials are dominated by ST2 compositions [8]. Detectable abundances of local hematite [e.g. 9], orthopyroxene [e.g. 10], and olivine [e.g. 10] have also been identified in equatorial regions where ST1 basaltic compositions dominate surface units. The mapped distributions of ST1 and ST2 materials indicate that surface compositions are not well correlated with crustal thickeness [8,9].

Northern Plains Geologic Relations: The ST2 surfaces in the northern lowlands correspond with the distribution of low-albedo surfaces, which surround Planum Boreum, cover vast expanses of Vastitas Borealis, and extend in some regions south of 30°N. These surfaces occur on a variety of geologic units, including the VBF, other plains materials, dissected and rugged volcanic flows of Tharsis and Elysium,and circumpolar dunes (Fig. 1).

Part of the ST2 signature in the northern lowlands may be related to chemical weathering caused by water at the surface during periods of high obliquity. The high southern latitudes of Mars (>30°S) also display ST2 materials and do not appear to be generally related to outcrops of volcanic rocks. The correlation with high latitudes may be indicative of modest chemical weathering of basaltic rocks (type ST1) in which liquid water has been present on and near the surface at least periodically, perhaps at times of high obliquity beneath snow packs [11]. The same explanation may hold true for basaltic rocks in the northern plains. However, the TES signature in the northern plains indicates a higher ST2 abundance than the south polar region. Given also the relative youth of northern plains surfaces vs. the southern highlands, it would appear that this obliquity-related mechanism cannot fully explain the northern plains ST2 signature.

In the plains surrounding Planum Boreum, Viking and MOC images show low-albedo dune fields, including the vast Olympia Undae (unit d in Fig. 1), and others near the mouth of Chasma Boreale. These dunes appear to originate from a dark unit containing uneven bedding that forms the base of Planum Boreum and has been interpreted as a sand sea deposit [12]. Geologic mapping of this Boreum unit indicates that it approaches 1000 m in thickness west of Chasma Boreale, was emplaced during the Early Amazonian, and was extensively eroded prior to emplacement of north polar layered deposits that bury much of the unit [13]. The original volume of the dark Boreum unit may have approached that of Planum Boreum, or ~10^6 km^3. If the Boreum unit consists of relatively unaltered andesite, this would suggest a highly eroded, andesite bedrock source. Maximum transport distances for basaltic sand grains on Mars based on models of abrasion and TES observations for saltating materials on Mars indicate maximum transport distances of a few hundred kilometers [8] (we also note that the dark ST1 dunes apparently derived from the ST1 Syrtis Major volcanic flows near Isidis Planitia have not produced a ST1 signature significantly beyond the occurrence of the flows).

The only major source of sand in the vicinity of Planum Boreum is the VBF and associated materials of the Scandia region (unit vb). The VBF materials are generally thought to be clastic sediments derived from catastrophic fluvial erosion of martian highland rocks, (unit f), perhaps emplaced within a temporary, plains-filling ocean [14-15]. Structures within the VBF and Scandia region, including polygonal troughs, pitted and pancake domes, terraces, and depressions, suggest reworking of the VBF materials by near-surface, volatile-driven processes [13]. Because the highland materials have a ST1 TES signature, it would appear that the Boreum unit's ST2 signature must originate by alteration of ST1 rocks, which is consistent with the apparent water-associated emplacement and reworking history of the VBF. The VBF also may likely be the

source of most of the ST2 material throught the northern plains (Fig. 1), because the limited eolian transport distances noted previously preclude an origin from potential dust-covered ST2 highland and volcanic rocks (units h and v) in surrounding terrains.

Early Amazonian volcanic outcrops with ST2 signatures in and near the northern plains include rugged flows in northern Amazonis Planitia that originated near Olympus Mons (unit fr in Fig. 1) and dissected flow deposits in central and eastern Utopia Planitia originating from the Elysium rise thought to be lahars [13,16]. Some have argued that the pitted cones that occur along the margins of the VBF may be silicate volcanoes [e.g., 17], but their geologic associations seem to be more consistent with a sedimentary volcanic origin [13]. In any case, these materials all could have interacted significantly with water during their formation, resulting in weathered basaltic material. Alternatively, the ST2 signatures could result from saltation of VBF fines onto the outcrops or from an original andesite composition for the material.

Origin of the ST2 spectra. The ST2 unit displays the highest concentrations in the northern lowlands regions of Acidalia Planitia and the circumpolar sand seas [1]. Alteration rinds or coatings (i.e., sheet silicates, palagonites, and zeolite) are probably too fragile to resist much eolian abrasion. Silica coatings, however, may be sufficiently resistant to mechanical weathering to survive as coatings or cementing agents that can account for the ST2 spectral shape. Recent work by [18 and references therein] summarizes evidence for the probability of sedimentary silica existing on Mars and emphasizes the highly mobile nature of silica during near surface alteration of basaltic rocks under a wide variety of temperature, pressure, and fluid conditions. Palagonitization is a commonly proposed alteration process for the martian surface and the production of palagonites and secondary clays, both of which have been shown to be spectrally similar to high-silica volcanic glass, result in a high degree of silica mobilization [18 and references therein]. The geologic context of the VBF within a sedimentary basin with either transported or indigenous materials having interacted with surface or near-surface volatile-rich materials [13-14] supports an altered basalt classification for the TES ST2 unit in the northern lowlands.

References. [1] Bandfield J. L. et al. (2000) *Science*, 287, 1626-1630. [2] Hamilton et al. (2001) *JGR*, 106, 14733-14746. [3] Wyatt M. B. and McSween H. (2002) *Nature* 417, 263-266. [4] Christensen P. R. et al. (2000) *JGR*, 105, 9609-9622. [5] Bandfield J. L. et al. (2000) *JGR*, 105, 9573-9587. [6] Smith M. D. et al. (2000) *JGR*, 105, 9589-9609. [7] Bandfield J. L. (2002) *JGR* 107 (E6), 10.1029/2001JE00151. [8] Rogers D. and Christensen P. R. (2003) *JGR*, 108, 10.1029/2002JE001913. [9] Christensen P. R. et al. (2000) *JGR*, 105, 9632-9642. [10] Hamilton V. E. et al. (2002) *LPSC XXXIII*, Abs #1937. [11] Christensen P. R. (2003) *Nature*, 422, 45-48. [12] Byrne S. and Murray B.C. (2002) *JGR* 107, 10.1029/2001JE001615. [13] Tanaka K. L. et al. (2003) *JGR* 108, 10.1029/2002JE001908. [14] Parker T.J. et al. (1989) *Icarus*, 82, 111-145. [15] Baker V. R. et al. (1991) *Nature,* 352, 589-599. [16] Christiansen E. H. (1989) *Geology,* 17, 203-206. [17] Frey H.V. and Jarosewich M. (1982) *JGR,* 87, 9867-9879. [18] McLennan S. M. (2003) *Geology,* 31, 315-318.

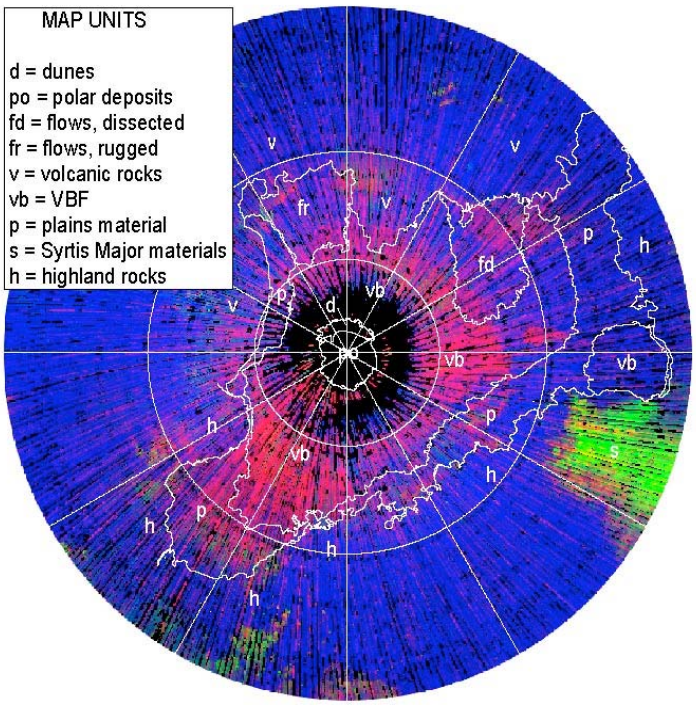

Figure 1. MGS-TES composition map of the northern hemisphere of Mars showing surfaces dominated by ST1 (green; basaltic spectra), ST2 (red, andesitic/weathered basalt spectra), and dust (blue). White lines outline geologic units described in text and generalized from [13].